X BAND TWO LAYER PRINTED REFLECTARRAY WITH SHAPED BEAM

A THESIS SUBMITTED TO
THE GRADUATE SCHOOL OF NATURAL AND APPLIED SCIENCES
OF
MIDDLE EAST TECHNICAL UNIVERSITY

BY

GÖKHAN ÜÇÜNCÜ

IN PARTIAL FULFILLMENT OF THE REQUIREMENTS
FOR
THE DEGREE OF MASTER OF SCIENCE
IN
ELECTRICAL AND ELECTRONICS ENGINEERING

OCTOBER 2011

Approval of the Thesis:

X BAND TWO LAYER PRINTED REFLECTARRAY WITH SHAPED BEAM

submitted by **GÖKHAN ÜÇÜNCÜ** in partial fulfilment of the requirements for the degree of **Master of Science in Electrical and Electronics Engineering Department, Middle East Technical University** by,

Prof. Dr. Canan Özgen _____
Dean, Graduate School of **Natural and Applied Sciences**

Prof. Dr. İsmet Erkmen _____
Head of Department, **Electrical and Electronics Engineering**

Prof. Dr. Özlem Aydın Çivi _____
Supervisor, **Electrical and Electronics Engineering Dept., METU**

Examining Committee Members:

Prof. Dr. Gönül Turhan Sayan _____
Electrical and Electronics Engineering Dept, METU

Prof. Dr. H. Özlem Aydın Çivi _____
Electrical and Electronics Engineering Dept, METU

Prof. Dr. Sencer Koç _____
Electrical and Electronics Engineering Dept, METU

Assoc. Prof. Dr. Şimşek Demir _____
Electrical and Electronics Engineering Dept, METU

Assoc. Prof. Dr. Vakur B. Ertürk _____
Electrical and Electronics Engineering Dept, Bilkent University

Date: October 31, 2011

I hereby declare that all information in this document has been obtained and presented in accordance with academic rules and ethical conduct. I also declare that, as required by these rules and conduct, I have fully cited and referenced all material and results that are not original to this work.

Name, Last name: Gökhan Üçüncü

Signature :

ABSTRACT

X BAND TWO LAYER PRINTED REFLECTARRAY WITH SHAPED BEAM

Üçüncü, Gökhan
MSc., Department of Electrical and Electronics Engineering
Supervisor: Prof. Dr. H. Özlem Aydın Çivi

October, 2011, 110 pages

X-band cosecant square shaped beam microstrip reflectarray is designed, fabricated and measured. Unit element of the reflectarray is in stacked patch configuration. With the aim of designing shaped beam pattern, phase-only synthesis method based on genetic algorithm is used. Phases of reflected electric field from antenna elements are adjusted by changing the dimensions of the patches. Unit cell simulations are performed using periodic boundary conditions and assuming infinite array approach to obtain reflection phase curves versus patch size. Then full reflectarray surface and its feed are designed and fabricated. Radiation patterns are measured in spherical near field range and results are compared with simulations. It is shown that the antenna is capable to operate in a band of 8.6 - 9.7 GHz.

Keywords: Reflectarray, Shaped beam, Cosecant square pattern, Broadband array, Stacked patch

ÖZ

X-BANT ÇİFT KATMANLI ŞEKİLLİ HUZMELİ BASKI YANSITICI DİZİ

Üçüncü, Gökhan
Yüksek Lisans, Elektirik-Elektronik Mühendisliği Bölümü
Tez Yöneticisi: Prof. Dr. H. Özlem Aydın Çivi

Ekim 2011, 110 sayfa

X-bandında çalışan kosekant kare şekilli huzmeli mikroşerit yansıtıcı dizi ve besleme anteni tasarlandı, üretildi ve ölçüldü. Yansıtma dizisinin birim elemanı olarak çift katmanlı yapı kullanıldı. Şekilli huzmeli örüntü elde edebilmek için genetik algoritma tabanlı sadece faz kullanılarak yapılan sentez kullanıldı. Antenlerden yansıtılan elektrik alanının fazları birim elemandaki yama anten boyutları değiştirilerek ayarlandı. Yama antenlerin değişik boyutlarında yansıtılan elektrik alanın fazlarının oluşturduğu eğrileri elde edebilmek için birim eleman benzetimleri sonsuz dizi yaklaşımı kabul edilerek periyodik sınır koşulları kullanılarak yapıldı. Sonrasında yansıtıcı dizinin yüzeyi ve dizinin besleme anteni tasarlanıp üretildi. Işınım örüntüleri küresel yakın alanında ölçüldü ve sonuçlar benzetim sonuçlarıyla karşılaştırıldı. Antenin 8.6 – 9.7 GHz bandında çalışabildiği gösterildi.

Anahtar kelimeler: Yansıtma dizisi, Şekilli huzme, Kosekant kare örüntü, Geniş bantlı dizi, Çift katmanlı yama

ACKNOWLEMENTS

I would like to express my gratitude to my supervisor Prof. Dr. Hatice Özlem Aydın Çivi for her supervision, guidance and support during the development of this thesis.

I would like to express my gratitude to M. Erim İnal, the administrator of Antennas Technologies Department at Aselsan for accepting me as an engineer in his squad, giving me the opportunity to improve myself and supporting me to do such a difficult and complicated thesis study.

I would like to thank Doğanay Doğan for his help at the beginning of this thesis and Can Barış Top for his invaluable support during the complicated situations in this study. He is a man who can open any doors which are sealed.
I would like to declare my gratitude to Erdinç Erçil, whom I think everyone can learn something from him.

I would like to thank Ahmet Muaz Ateş and Ozan Gerger for mechanical guidance and support they have provided me during this study.

I would like to thank also Nihan Öznazlı, for her support during my thesis review.

I would like to express my appreciations to Ali Günay Yıldız, the master of antenna measurement in Turkey, for his efforts to take me out of the endless and darkest roads and show me the complete truth.

I would like to thank also Özkan Sağlam, my roommate, who keeps his cool-head even in the worst situations, for his mental supports in my thesis.

A man can have many friends but few companions in this life. Ziya Şenbayrak is one these companions, provides me every support that he can have.

I would like to admire Erhan Halavut, who is sometimes a great mentor, sometimes a noble scientist, sometimes a perfect friend but always a closer person like an elder brother. Any words in any language can describe his greatness.

Without a real brother, my life during this thesis would become nothing but a boring study. Therefore, I would like to express my deepest appreciations to Egemen Yıldırım, for his support during thesis study and for our brotherhood.
I would also like to thank all of my colleagues in Antennas Technologies Department, from technicians to the administrator, whom train me in every single day in my career.

I specially thank to my father M. Cemal Üçüncü, my mother Pervin Üçüncü, my sister Gökçen Üçüncü, my grandfather Özcan Tüzüner and my grandmother Zikriye Tüzüner for teaching me to be not only a good scientist but also a kind person.

TABLE OF CONTENTS

LIST OF TABLES

LIST OF FIGURES

CHAPTER I

INTRODUCTION

In satellite and radar applications, usually high gain and high power antennas are required. Besides, in some satellite applications there may be a requirement for illuminating a certain area, such as a single country, a continent or a specific region on earth, which can be accomplished by using a shaped beam antenna [1] - [4]. Similarly, some radar applications may also require to utilize contoured beam antennas [5] - [7]. In order to meet all these requirements, reflector antennas with phased array feeds or phased arrays are used.

Although reflector antennas have been widely used in satellite applications, their bulky structures make it difficult to transport and deploy them in space [8]. Additionally, mechanical surface tolerances for a reflector dish becomes very critical, especially at high frequencies, which makes them harder to manufacture. Phased array antennas have also some disadvantages. They require complex and very expensive beam forming networks. Since microwave components with certain insertion losses, such as phase shifters, and switches are used, the overall efficiency is also reduced.

The printed reflectarray antennas appear to be a good choice for satellite and radar applications as they do not only meet the requirements but also eliminate the disadvantages of standard reflectors and phased arrays that have been discussed so far. A *Reflectarray* [11] is composed of a flat reflector (rather than a curved one), reflective unit elements on this flat structure, and a feed illuminating this reflecting surface. The basic principle of operation is that the incident field from the feed is reflected from the reflector and the phases of the

reflected electric fields are adjusted by the unit elements to form the desired beam. A generic reflectarray is shown in Figure 1.

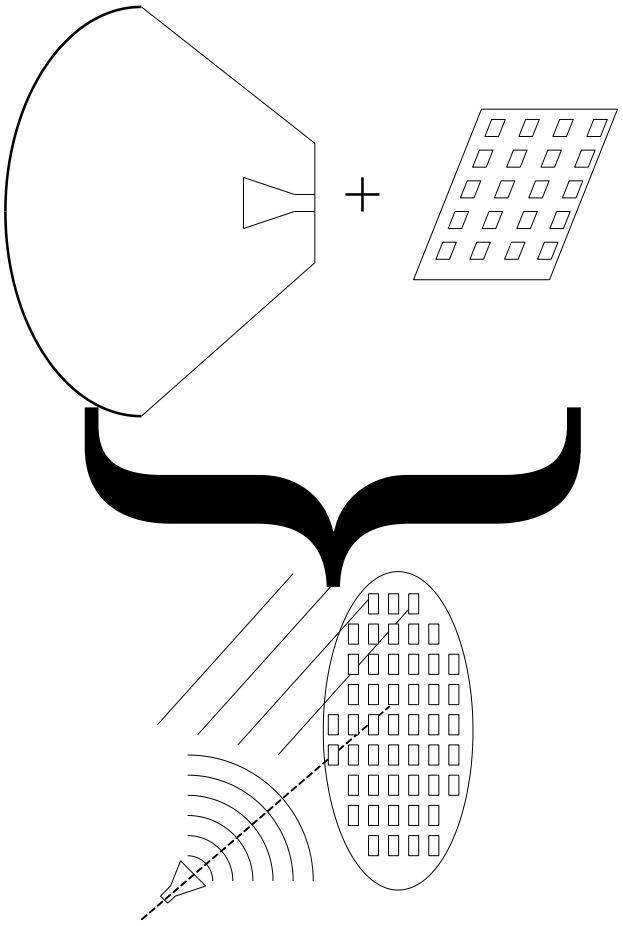

Figure 1 A generic reflectarray

The printed reflectarray can be designed to have high gain with relatively good efficiency. The main advantage of the reflectarray is its flat reflective surface, which makes it superior to standard reflector antennas, especially in space applications [1], [2], [3], [4], [5], [12]. When a large aperture satellite antenna requires a deployment mechanism, the flat structure of the reflectarray will allow a much simpler folding mechanism than the curved surface of a standard parabolic reflector. In reflectarrays, there is not any beam forming network; desired phase shifts can be introduced with unit cells. So this is an advantage of the reflectarray against phased array. Also using phase shifters and switches,

reflectarrays can be able to generate many combinations of different scan angles and different beam shapes as in phased arrays.

On the other hand, the main disadvantage of reflectarrays is their narrow bandwidth. There are two factors that limit the frequency bandwidth. In reflectarrays, resonant type antennas such as microstrip patches are generally used as unit elements. The fractional bandwidth of a regular microstrip patch antenna is nearly 3% but this value can be increased by multilayer designs or by using thicker dielectric substrates. The second disadvantage is the spatial phase delay from the feed to the flat structure of the reflector, which can only be compensated for narrow frequency bandwidths. However, in radar and satellite applications, generally narrow bandwidths are required, so reflectarrays attract more attention especially in these areas.

At this point it would be better to present the reflectarray concept and its development throughout the history. The term reflectarray was first used in 1963 by Berry, Malech and Kennedy [11]. This reflectarray is composed of open-ended waveguides as reflective elements, as shown in Figure 2.

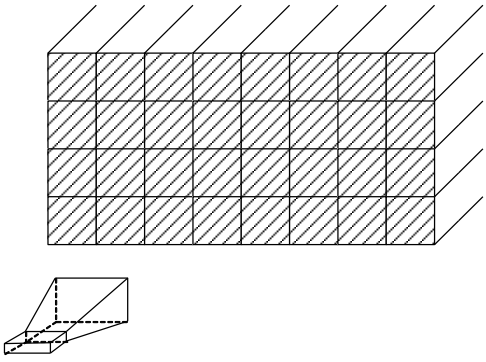

Figure 2 Waveguide reflectarray

Each of the open-ended waveguides has different length and all of them are terminated in short circuits. The coupled signal from the feed to waveguides travels in different path lengths in each waveguide and it is reflected from the short circuits. Therefore by adjusting the lengths of the waveguide sections,

desired phase shifts can be obtained. Beam scanning can also be done by introducing switching diodes in the waveguides between the short circuit termination and the aperture. In this configuration, when desired diodes are shorted, beam scanning is obtained. However, this structure is heavy, hard to manufacture and expensive due to the low frequencies studied in those years,. Thus, until 1970s, this concept was not studied too much. In 1977, "spiralphase" reflectarray [13] was introduced. It is composed of switching diodes connected to 4-arm spiral antennas to rotate the beam to wide angles with rotating the individual spiral element. This reflectarray element is given in Figure 3. In 1978 [14] the introduction of low cost, easy to manufacture, and low profile microstrip antennas made the reflectarray concept become very popular and several reflectarray structures have been studied thereafter till late 1980s.

Figure 3 A 4-arm spiral element with phase shifters [8]

Microstrip patches, dipoles, rings are some of the examples of printed reflectarray elements. Various types of such elements are shown in Figure 4.

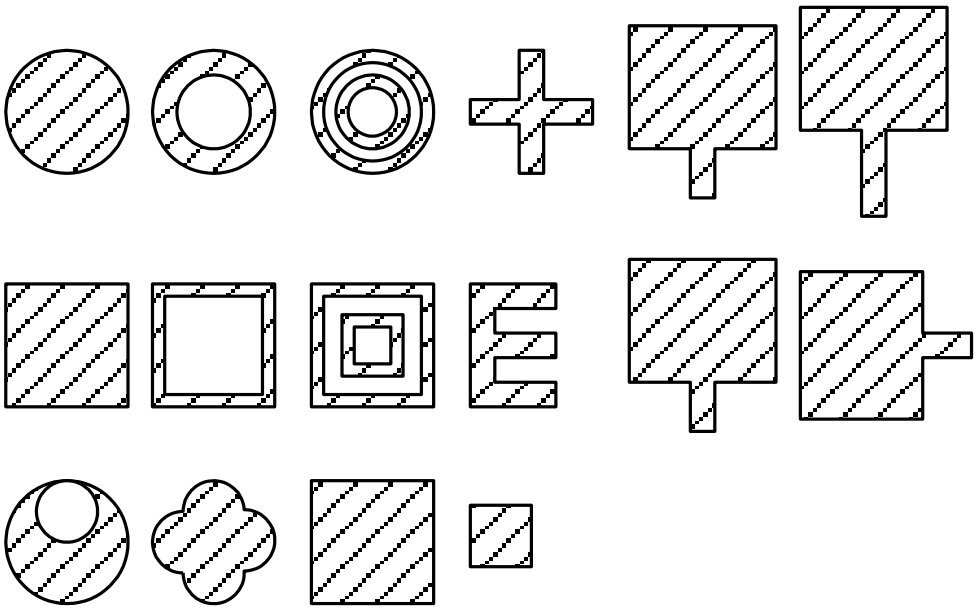

Figure 4 Microstrip reflectarray element types: circle, ring, annular ring, cross, identical patches with delay line, square, square ring, annular square ring, E-shaped, identical patches with rotations, crescent, petal and variable size patches

Each single reflectarray element reflects the incoming wave from the feed and the amplitude of the reflected wave depends on the feed pattern and the distance between the feed and the element. Therefore, generally it is not easy to control the amplitudes for each element. On the other hand, the phases of the reflected fields should be adjusted to form the desired pattern. In literature, various phase control mechanisms can be found. One of them is the patch rotation, where miniature motors are placed behind the patches so that required phase difference between elements can be achieved by rotating them [15]. This method can be used for circular polarization case. By using this method beam scanning can also be easily done without the need of additional phase shifters. In [16], square patches of equal dimensions are rotated to adjust phases. These patches also have delay lines to achieve circular polarization. Ring elements can also be used to have circular polarization and phase change is achieved by rotation of those elements [17]. Phases can also be controlled by changing the length of stubs loading identical patches. In this type of phase control, square or circular patches with the same dimensions and orientations are used and

depending on the polarization, delay lines are utilized [18, 19]. Another method to control the phase is to change the dimensions of the elements (variable size patches). In [21], length of the rectangular patches are changed to control phases while in [22] length of dipoles are modified. Similarly, square and ring elements are also used [23]. Switches can also be used on delay lines to make the antennas reconfigurable [26]. Additionally, for wideband applications, variable-sized multilayered stacked patch configurations [9], [24], [25], aperture coupled patches [20], [26], double cross loops [27], parasitic dipoles [28], and patches with attached stubs [29] are used.

The phase shift introduced by a patch changes as one geometrical parameter of the element such as patch length, delay line length or pitch angle changes. *The phase design curve* is the most important concept in reflectarrays, which shows the patch response versus changing dimension. It is the primary factor which determines the frequency bandwidth and the required manufacturing tolerances of the reflectarray. To form the desired beam, first the required phase of each element should be calculated. Then, using the phase design curve and the required phase information the dimensions of the elements should be determined. The desired pattern can be obtained by "phase only synthesis" method. With this method, beam shaping or beam scanning can be accomplished. It must be noted that the spatial phase delay taper caused by the feed pattern, which is shown in Figure 5, should also be compensated.

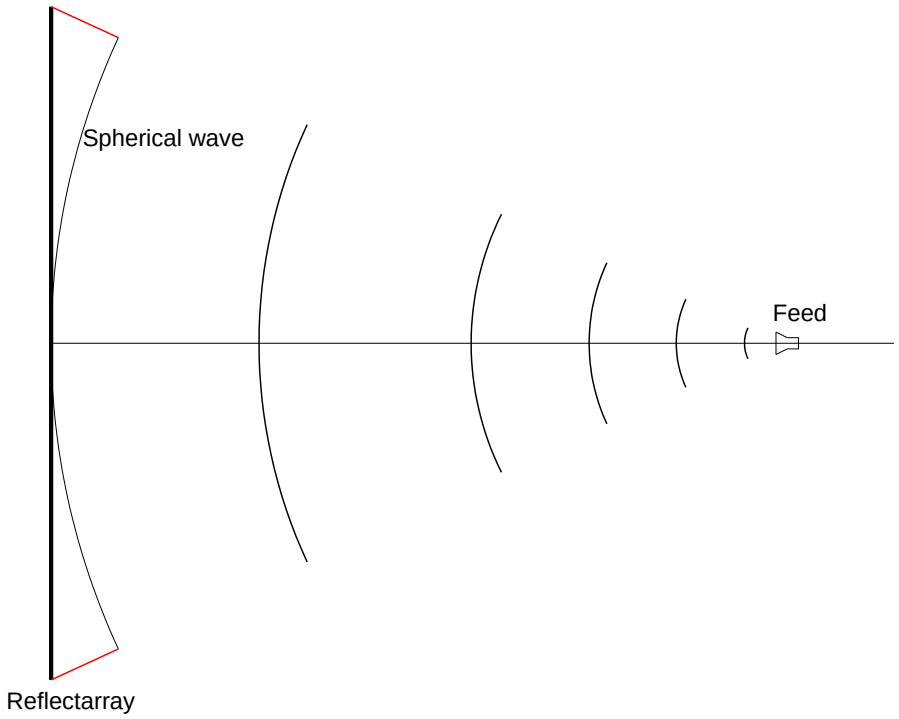

Figure 5 Spatial Phase Delay

In this thesis, X-band (9-10 GHz) cosecant square shaped beam microstrip reflectarray is designed, manufactured and measured. In order to design a reflectarray, first, initial unit cell dimensions are chosen according to the results of [1], [24] and [25]. In unit cell design, two layer stacked patch configuration is used to improve the bandwidth. Then, to find the best phase design curve, a parametric study is performed. The phase design curves are obtained by changing the dimensions of patches in stacked patch configuration in the operating frequency band [10]. Linear phase design curves show that over 400° of phase difference can be achieved, which appeared to be enough to design a reflectarray. After that the feed antenna is designed and the radiation pattern of the horn is used to find the magnitudes of the electric field over each patch. Then, a MATLAB code is developed to implement the phase only synthesis method based on genetic algorithm, and this code is used to calculate the required phases of each element to form the desired cosecant square beam. Also spatial phase delays are calculated and the phase compensation is performed. The required patch dimensions are determined from the phase

design curves for corresponding phases. Finally full reflectarray with its feed is simulated to obtain radiation pattern.

After this brief introduction about the reflectarrays, the organization of the thesis is given. In Chapter 2, the parametric study to observe the effect of each parameter on the phase design curve, which is performed by using simulation tools, is discussed. The simulation procedure and the simulation setup is also explained.

Chapter 3 presents the design procedure of the feed antenna. The results of the simulations and measurements are also compared. The mathematical expressions for the spatial phase delay caused by the spherical illumination are given. Additionally, the dimensions of the elements are optimized. Finally, the resulting reflectarray design is introduced.

The whole reflectarray simulation and measurement results are given in Chaper 4. Also the performance of the reflectarray is discussed. The manufacturing process is briefly explained at the end of this chapter.

The last chapter provides a brief summary of the results, and accomplished work along with the proposed subjects for future studies.

CHAPTER II

DESIGN OF THE UNIT CELL OF THE REFLECTARRAY

2.1 Reflectarray Unit Cell and Definition of Phase Design Curve

As mentioned in Chapter 1, unit cell is the building block of the reflectarray antennas. In this study, stacked patch configuration is chosen for unit cell structure to increase the operating frequency bandwidth. Variable size patch technique is used to obtain the required phase differences to design a shaped beam antenna. Bandwidth of the unit cell should cover 9-10 GHz band and maximum range of reflected field should be more than 360°.

In this chapter, parametric analyses are performed to observe the effects of each parameter in unit cell on the phase design curve. Performance parameters are introduced to compare and evaluate the results. Additionally, simulation tools are presented and brief information is given for the simulation techniques.

Unit cell is composed of a single or a multilayer microstrip patch. In literature, many unit cell patch types shown in Figure 4 (ring, square, annular ring, variable size patch, etc.) are introduced.

To obtain the phase of the reflected field, one parameter of the unit cell (patch dimension, delay line length etc.) is changed. Obtained phases of reflected fields are plotted versus the swept parameter value. The result is an S-shaped

curve, named *phase design curve*. A sample phase design curve is given in Figure 6.

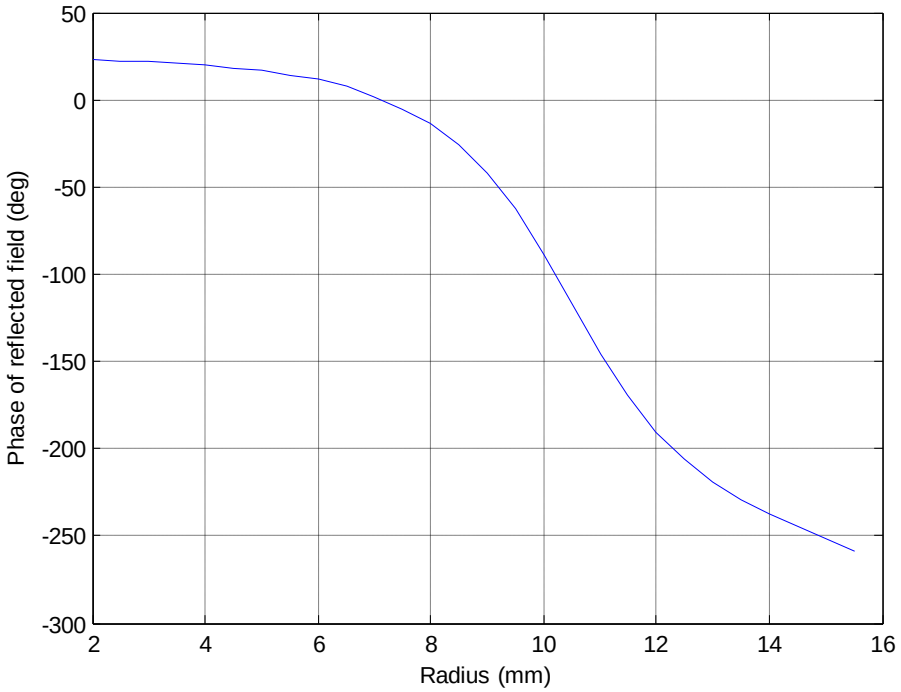

Figure 6 A phase design curve

As described in Appendix-1, phase design curves of multilayer unit cells are more linear than the single layer ones. So in this thesis multilayer unit cell design is carried out and used as the array element.

2.2 Reflectarray unit cell modelling and design

Since the overall characteristics of the reflectarray are directly depend on the performance of the unit cell, the modelling and the design of the unit cell must be carried out carefully.

There are many numerical methods to analyze reflectarray unit cell. Some of these methods are Finite Element Method (FEM), Method of Moments (MoM) and Finite Difference Time Domain (FDTD). Commercial software Ansoft

HFSS® [30] uses FEM, which assigns 3-D tetrahedral meshes to both dielectrics and metallic surfaces. Ansoft Designer solves integral equations to employ surface currents using MoM and only assigns meshes to surface of the antennas. CST Microwave Studio® utilizes FDTD, which benefits from square lattices to solve ***E*** and ***H*** fields [31]. In this thesis, simulations are performed by HFSS®.

Throughout the design, some of the features like infinite array approach, periodic boundary conditions, Floquet port, are used frequently. For the sake of completeness, these concepts will be explained briefly.

The behaviour of the antenna element in an array is different from its stand alone response due to the mutual coupling effects. Thus, unit cell simulations must be carried out in an array environment that includes mutual coupling effects.

In order to simulate arrays to observe mutual coupling effects, an approximation named infinite array approach, shown in Figure 7, is used. In this approach, periodic boundary conditions are applied to the boundaries of the unit cell. By doing so an infinite array is formed. There are two main drawbacks of this approach. Firstly all element dimensions are same, which is not a general case for reflectarrays. Secondly since all the elements are simulated in an infinite array the deviations of edge elements in a finite array are ignored. In these two cases, phases of the reflected field which are found by the simulations do not illustrate the real case. Infinite array approach gives some intuition about the behaviour of the elements rather than their exact response in array environment. This may cause some deviations in amplitude and phase, but does not affect the overall performance notably which proves that the infinite array approach is adequate.

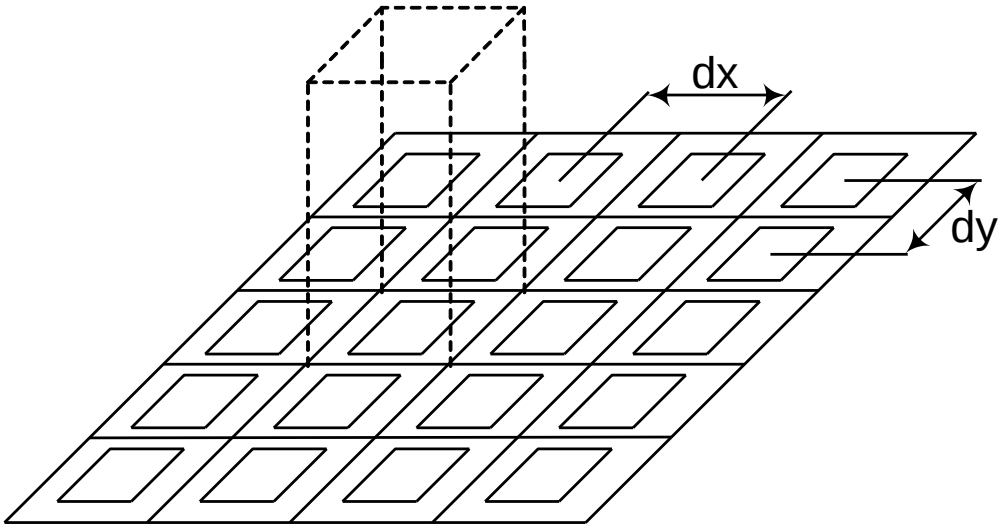

Figure 7 Infinite array approach. Unit cell treated as it is in an infinite array made with the same element

Second method is the waveguide simulator model [8], shown in Figure 8. In this model, in the case of normal incidence, perfect electric conductor (PEC) is assigned to walls where incident E-field is perpendicular and PMC is assigned where E-field is tangential. In fact, this approach looks similar to infinite array approach. The E-field repeats itself till infinity in the PEC boundaries and the same is true for the H-field in the PMC boundaries. This simulation setup can be called as PEC/PMC waveguide. A waveguide is terminated with this unit cell and the reflection characteristics (both amplitude and phase) are observed. Unfortunately, this simulation can be done only with normal incidence case. To measure the phase shift and the losses of the unit cell, in an array environment, rectangular waveguides loaded by unit cells are widely used. The fundamental TE_{10} mode of the rectangular waveguide can be considered as a superposition of the two plane waves with opposite angles θ° and -θ° relative to the waveguide axis. Then the measured reflection coefficient in TE_{10} mode excitation corresponds to that of a plane wave with incidence angle θ°. However, this method has some limitations. The angle of incidence is determined by the element spacing and the frequency, so that to measure

reflection coefficient of different incidence angles and frequency, waveguides with different dimensions should be manufactured.

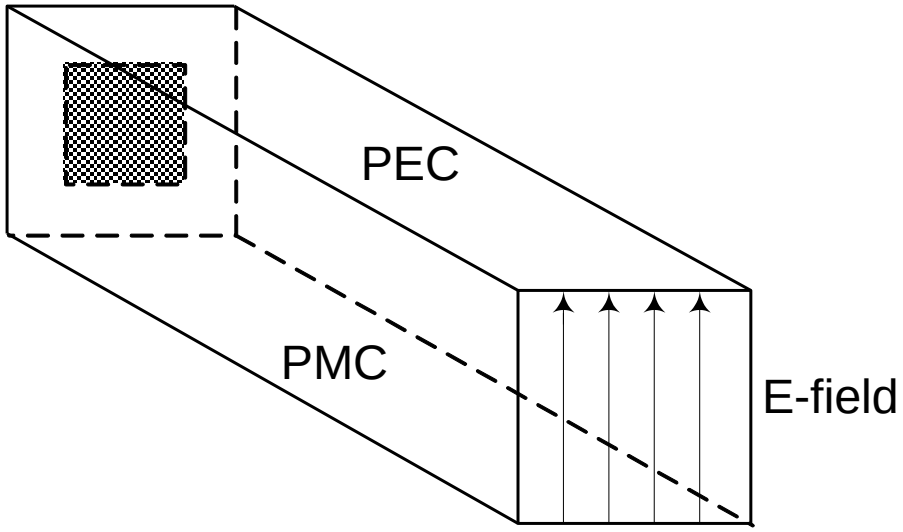

Figure 8 Waveguide simulator model

The first approach is chosen for simulations in this thesis. In order to get the phase and amplitude of the reflected field from the patch, plane wave excitation must be used. Thus, in HFSS®, Floquet port excitation, in which the plane wave is sent to patches, can be used. Floquet port uses Floquet modes and these modes can be explained with two indices. Fundamental mode is m=0, n=0 mode. With two polarization state, unit cell is illuminated with two orthogonal plane waves.

In HFSS®, any region or part which is not specified is treated as perfect electric conductor. Thus, a radiation box should be drawn around the antenna in all antenna designs. In order to see the response of the simulated patch without the radiation box, post processing should be used. In post processing, de-embed option is available, which transforms the port in simulation setup to just over the planar structure and gives patch's response. De-embed distance can be written manually or with "get distance graphically" option. In this option, user should define start and stop points of the de-embedding. Note that, positive

distance means from port to structure and negative distance means from structure to out of the port. In this setup, positive distance is used because the reflected field's response is needed on the patch.

Periodic boundary conditions must be imposed to constitute the infinite array. In HFSS®, master and slave boundaries are used to implement infinite array as shown in Figure 9. For normal incidence, phase difference between master and slave boundaries is set to zero. A phase shift, between master and slave boundary is applied to simulate the oblique incidence angles. In this process, master is taken as a reference and the shift is applied to the slave boundary. These boundaries are assigned with their own vectors, named u and v and their directions should be the same both in master and slave boundaries. These vectors can be expressed as a combination of x, y and z and used in the calculations during the simulations. Since the lattice shape is square in this study, u and v vectors do not have much importance but in other lattice types like parallelogram or triangle or circular, these vectors have high importance.

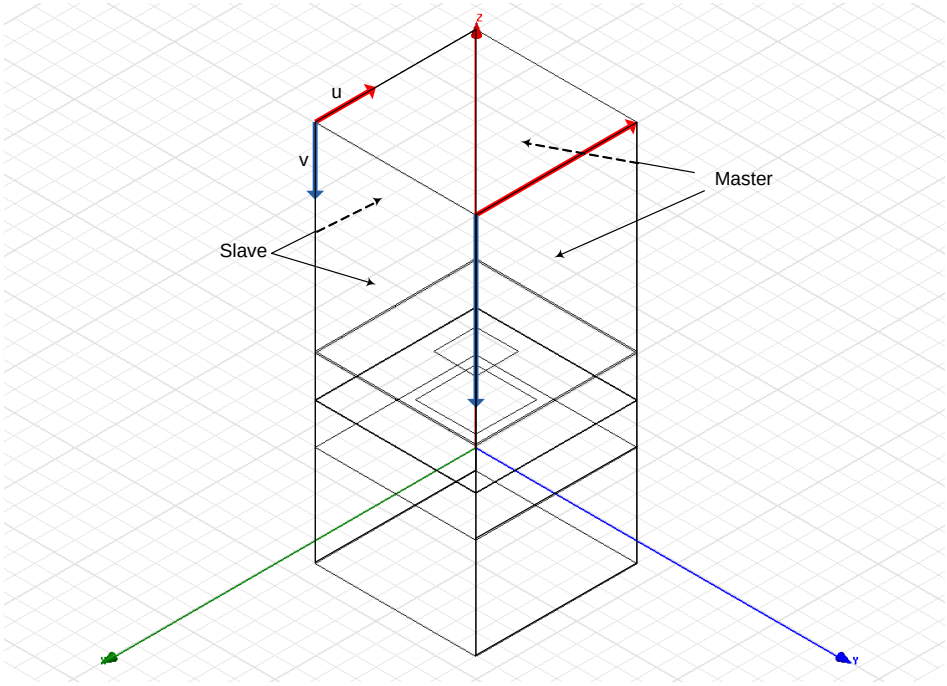

Figure 9 Master slave boundaries

2.3 Definition of performance parameters

Maximum range of reflection phase, sensitivity for mechanical tolerances, bandwidth, cross-polarization level and reflection loss are the parameters that determine whether the unit cell is an appropriate element for a reflectarray or not [33].

Maximum range of reflection phase is the difference of maximum and minimum reflection phases in phase design curve at chosen frequency. If the maximum range of the reflection phase is denoted as *R*, and ϕ_{min} and ϕ_{max} represents minimum and maximum phase shift values in the phase design curve, then maximum range of reflection phase is

$$R = \phi_{max} - \phi_{min} \tag{1}$$

Importance of this concept arises in all reflectarray configurations, because reflection phases which can differ from 0 to 360 can be required to obtain the shaped or steered beams and to compensate the phase delay due to the feed illumination.

Phase range for single layer substrate is approximately given as [32],

$$Phase = 360 * (1 - \frac{kh}{\pi}) \tag{2}$$

where k is the wave number in substrate and h is the substrate thickness.

From this approximation, it can be seen that thick substrates for a predetermined frequency or higher frequencies for a fixed thickness have smaller phase range. If single layer and multi layer unit cells with the same patch type are considered, it can be seen that multi layer structures offer wider phase range (Appendix-1).

The second parameter sensitivity, illustrates the maximum slope of the phase design curve. If sensitivity is denoted with s,

$$s = \max\left|\frac{\partial \phi}{\partial p}\right| \tag{3}$$

where p is the changing geometrical parameter (for instance delay line length, patch dimension). The unit of the sensitivity is deg/μm. This value determines whether the design is implementable or not. For the shaped beam and wideband reflectarrays, sensitivity is an important parameter due to the mechanical production tolerances because these antennas are vulnerable to small phase errors. As an example, if production tolerance is 10μm and sensitivity value for a unit cell is 1 deg/μm, then 10° of error can be introduced in manufacturing process and this error may cause antenna performance degradation.

Sensitivity parameter depends on the unit cell configuration. Parametric study on the dielectric thickness shows that thicker substrates are less sensitive than the thinner ones. From the studies on single layered configurations, it can be concluded that multi-layered structures are less sensitive than the single-layered ones.

Bandwidth is the third parameter, given by,

$$\beta = |f_1 - f_2| \tag{4}$$

f_1 and f_2 are the lower and upper bounds of the operating frequency where the slope of the phase design curves at those frequencies are in acceptable error bound compared to the slope at the center frequency.

Bandwidth definition is explained using Figure 10 and Figure 11.

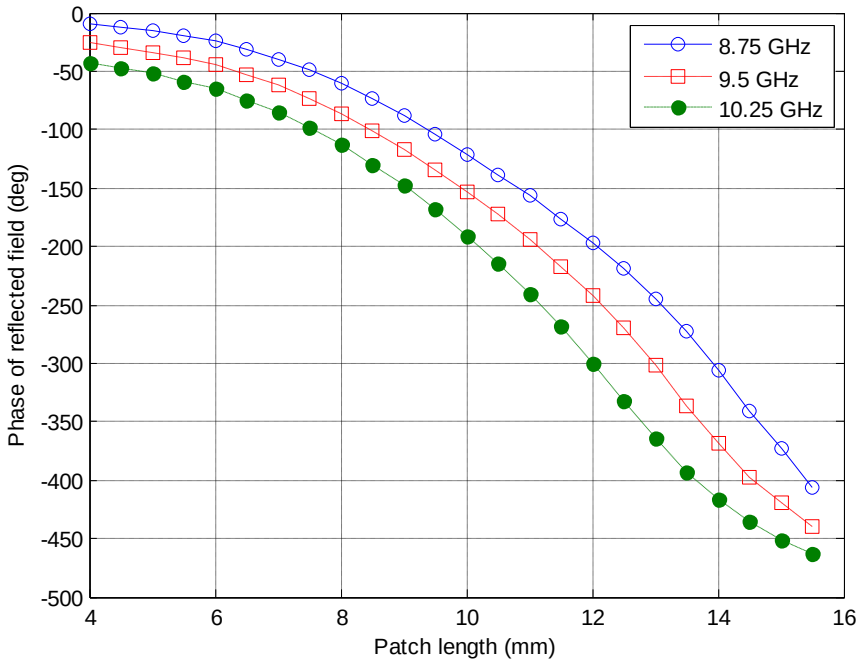

Figure 10 Phase design curves in three different frequencies

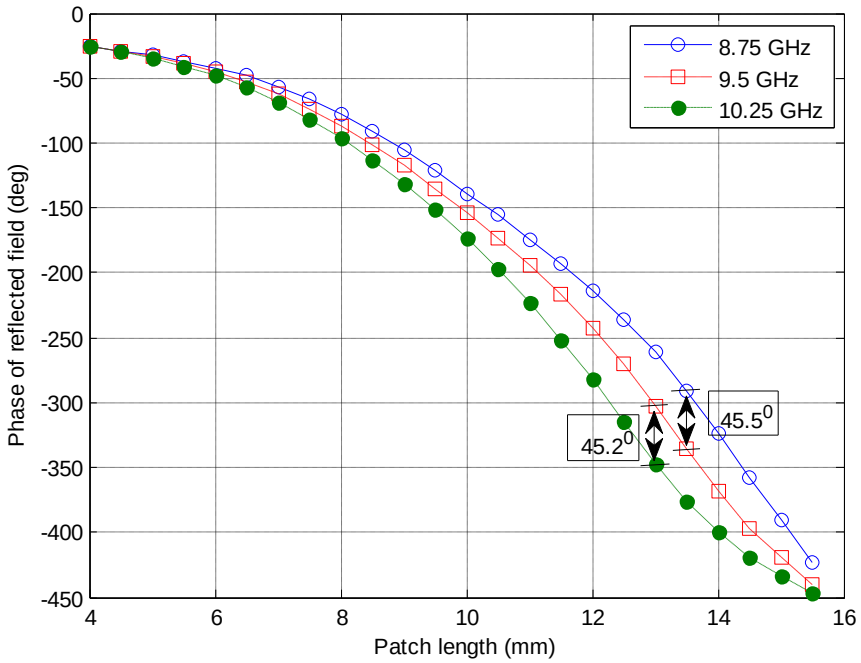

Figure 11 Normalized phase design curves

To calculate the bandwidth, first the phase design curves at different frequencies are normalized to the curve at the center frequency. Then for every patch size the phase differences are computed. If the phase differences are in the required error bound, it can be said that these frequency points are in the operating frequency band. In this thesis the error bound is taken as 45° [33].

Bandwidth of single layered configurations varies more rapidly than multilayered ones, which makes single layered arrangements to be narrowband (see Appendix-1 for single layer configuration simulations).

Fourth parameter is the cross-polarization level, showing the reflection coefficient amplitude of TM mode when TE mode is used as an excitation and vice versa and is shown by,

$$X_{pol} = max|\Gamma_{cross}| \tag{5}$$

where Γ_{cross} denotes the reflection coefficient of cross polarization and X_{pol} denotes the maximum of the magnitude of the reflection coefficient of the cross polarization.

Final parameter is the reflection loss, demonstrating the decrease in magnitude of co-polarized component of reflection coefficient in unit cell simulations. Since multilayered structures include multi conductor layers, due to metallic losses, reflection losses could be higher compared with single layered ones. But while the metallic losses are negligibly small compared with the dielectric losses, reflection loss of multilayer structure is nearly the same with single layered one with the same dielectric substrate height. If reflection loss is denoted with L, then

$$L = max|\Gamma_{CO}| \tag{6}$$

where Γ_{CO} denotes the reflection coefficient of co-polarization and L denotes the maximum of the magnitude of the reflection coefficient of the co-polarization.

Considering the performance parameters, for wide band application, two layer stacked patch configuration [8], [24], [25] is used for this design which offers relatively high maximum phase range of reflection phase, low sensitivity, wide bandwidth, low cross-polarization level and low reflection loss compared to the single layer case.

2.4 Parametric Study of Unit Cell

In this section, results of the parametric study of the unit cell are given. The aim of this study is to find the optimum unit cell dimensions and analyze the effect of various parameters (unit cell size, patch size ratio, thickness of the dielectric layers, dielectric constant and loss tangent, frequency sweep, incidence angle) over phase and amplitude of the reflected field.

The configuration of the unit cell used in the parametric studies is given in Figure 12 . In this thesis square shaped patches are used. W_1 and W_2 denote the width of the patches. h_1 and h_2 are the thicknesses of the foams, which are used as separators between the layers. t_1 and t_2 represent the thicknesses of the dielectric material that supports the patches. To reduce the number of unknowns, dielectric thicknesses and separator thicknesses are assumed to be the same ($h_1=h_2$, $t_1=t_2$). ROHACELL® HF71 foam is used as separator and ROGERS DUROID 5880™ is chosen as supporting dielectric material.

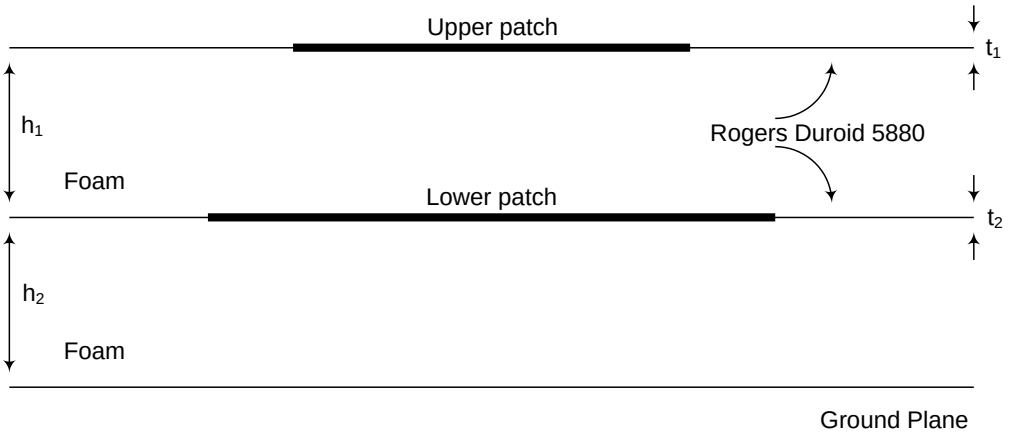

Figure 12 Stacked patch unit cell side view

In the simulations throughout this section, center frequency 9.5 GHz is used. Height of the dielectrics which support the patches are kept constant at 0.127 mm. Considering the parameter values (dielectric height, unit cell dimension) in [1] and [25], initial values are chosen for the unit cell. In [25], design frequency is 12 GHz, free space wavelength is 25 mm and unit cell dimensions are 14 mm x 14 mm, which are slightly larger than the half of the free space wavelength value. Therefore, initially, length and width of the unit cell are chosen slightly smaller than the half of the wavelength in free space at 9.5 GHz, heights of the separators are set 3 mm as in [25], and patch ratios ($\frac{W_1}{W_2}$) are selected as 0.7.

It should be noted that, since variable size patch technique is used, in all simulations, patch dimensions are swept for each parameter explained below. In each step, the best values found from previous steps are used and at the end, the best dimensions for the unit cell are achieved. Initial values of the parameters are presented in Table 1.

Table 1 Parameters of the unit cell and their initial values

$h_1 = h_2$	3 mm
$t_1 = t_2$	0.127 mm
$\frac{W_1}{W_2}$	0.7
f	9.5 GHz
d_x x d_y	15 mm x 15 mm

Note that 'patch length' on the graphs denotes the lower patch dimension. Since the upper and the lower patch lengths are related with $\frac{W_1}{W_2}$ ratio, the upper patch dimension is not mentioned throughout the study.

Simulated unit cell in HFSS® is shown in Figure 13.

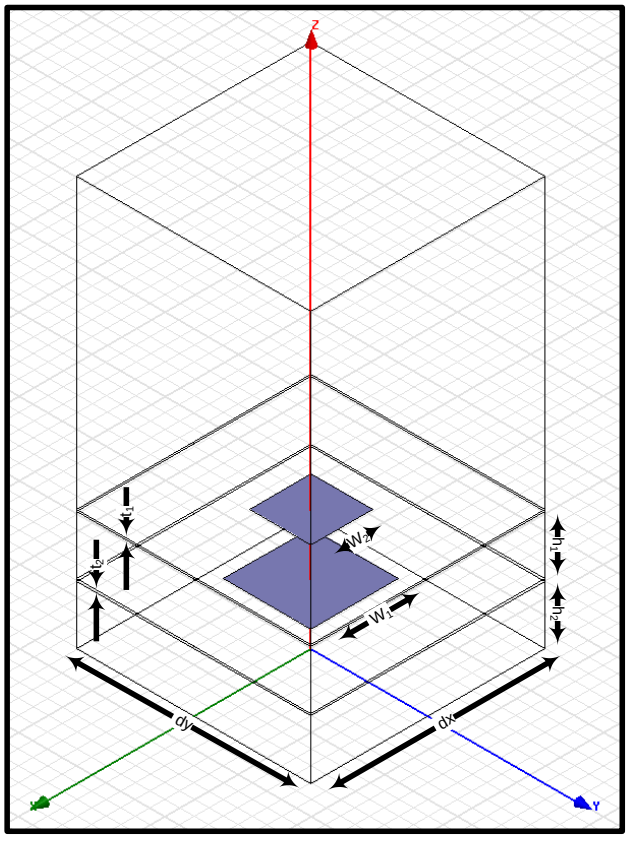

Figure 13 Simulated unit cell structure in HFSS®

2.4.1.1 Effect of the unit cell size on the phase of the reflected field

In this section, effect of the unit cell dimension on the phase of the reflected field is analyzed. Initial and swept parameters are presented in Table 2.

Table 2 Parameters in unit cell dimension simulation

$h_1 = h_2$	4 mm
$t_1 = t_2$	0.127 mm
$\frac{W_1}{W_2}$	0.7
f	9.5 GHz
$d_x = d_y$	$0.3\lambda \rightarrow 0.65\lambda$ with 0.05λ steps

Simulation results of the parametric study on unit cell dimensions are shown in Figure 14. It is observed that the smallest unit cell dimension should be 0.45 λ to cover at least 360° maximum range of reflection phase. In terms of sensitivity, unit cells with 0.5 λ to 0.65 λ dimension offers less and nearly the same slope so these dimensions are compliant with mechanical tolerances compared with smaller unit cells. Results of the parametric analysis with respect to performance parameters [33] are given in Table 3.

Table 3 Maximum range of reflected phase, sensitivity, cross polarization level and reflection loss versus unit cell dimension

d_x (λ)	R (°)	s (°/μm)	X_{pol} (dB)	L (dB)
0.3	238.18	0.0963	-43.86	0.055
0.35	278.7	0.0859	-54.83	0.04
0.4	274.84	0.0825	-28.15	0.05
0.45	365.15	0.0777	-35.32	0.06
0.5	401.44	0.0748	-40.66	0.07
0.55	411.79	0.068	-50.63	0.08
0.6	448.1	0.0641	-39.7	0.0892
0.65	441.24	0.0608	-43.36	0.0968

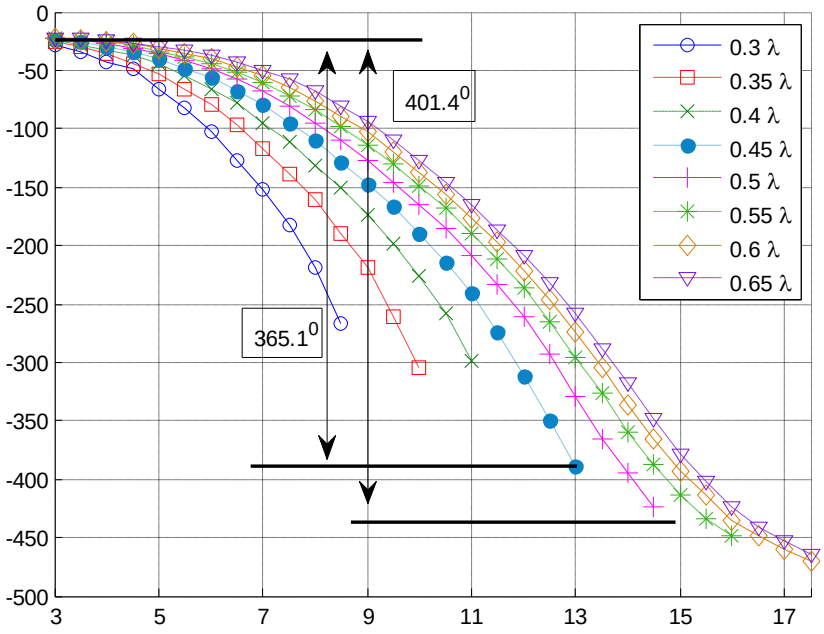

Figure 14 Variation of phase of reflected field with respect to patch length for different unit cell sizes at 9.5 GHz (normal incidence)

From Table 3, R values are seemed increasing with the increase in patch dimensions. But larger patches increase total antenna dimensions. Also

sensitivity values are very close to each other but these values are decreasing with increasing unit cell dimensions. Thus, to secure a 360° phase range and have good X_{pol} and s values, 0.5 λ (16 mm) unit cell dimensions are chosen. X_{pol} and L levels are very low so throughout the thesis these values are assumed negligible.

2.4.1.2 Effect of the patch size ratio over the phase of the reflected field

This section covers the effects of $\frac{W_1}{W_2}$ ratio variation on the phase of the reflected field. With all other parameters kept constant, only patch ratio is changed. In this section, 'r' is used to denote the ratio. Constant and swept parameters are shown in Table 4.

Table 4 Parameters in unit cell patch ratio simulation

$h_1 = h_2$	4 mm
$t_1 = t_2$	0.127 mm
$r = \frac{W_1}{W_2}$	$0.45 \rightarrow 0.9$ with 0.05 steps
f	9.5 GHz
$d_x \; x \; d_y$	16 mm x 16 mm

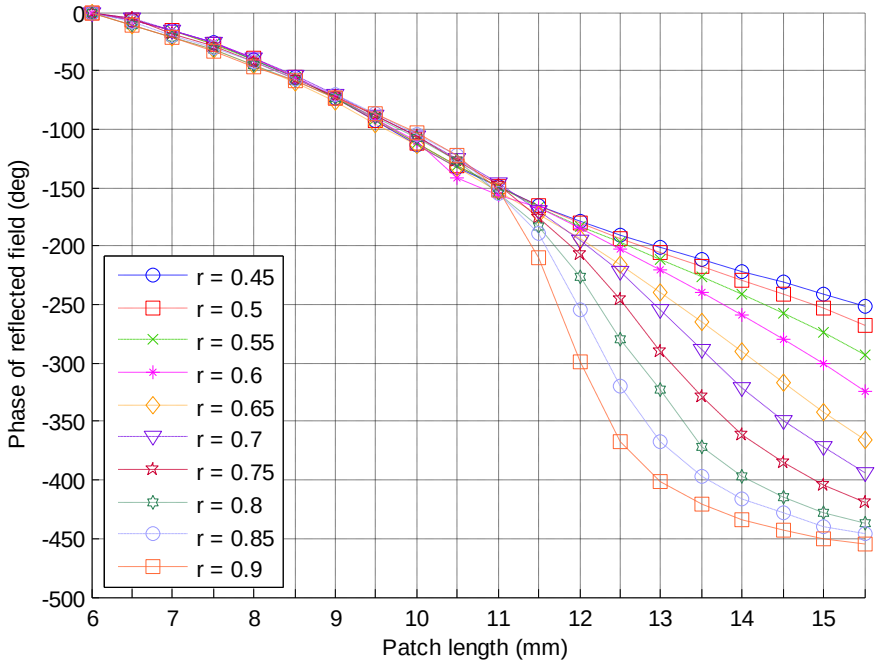

Figure 15 Effect of the patch size ratios over the phase of the reflected field (normal incidence)

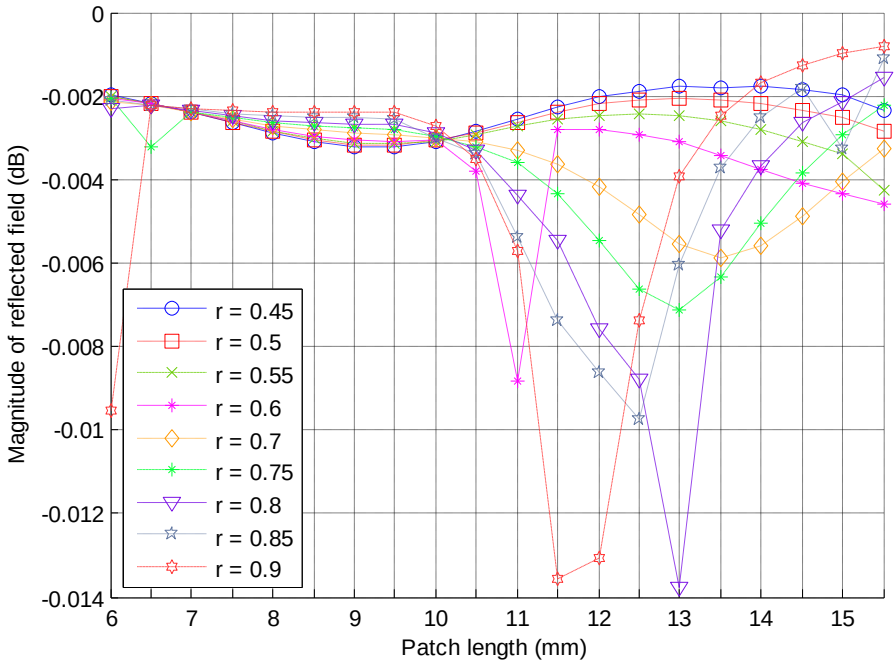

Figure 16 Effect of the patch size ratios over the magnitude of the reflected field (normal incidence)

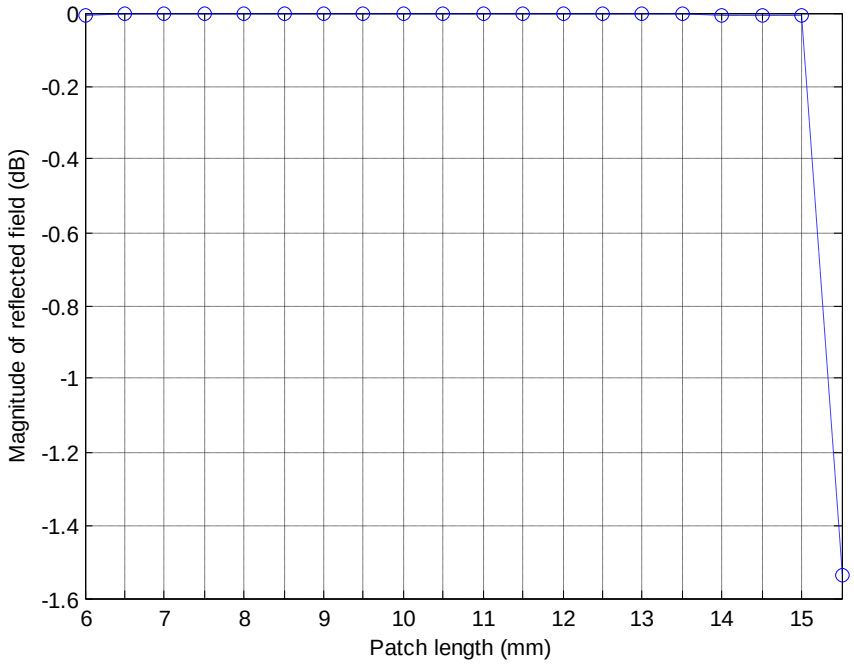

Figure 17 Effect of the patch size ratios over the magnitude of the reflected field for 0.65 patch ratio (normal incidence)

Table 5 R and s values for different patch ratios

r	*R* (°)	*s* (°/μm)
0.45	252.15	0.0399
0.5	267.31	0.0399
0.55	292.85	0.0395
0.6	324.39	0.0834
0.65	362.48	0.052
0.7	393.3	0.068
0.75	419.59	0.0883
0.8	437.58	0.1053
0.85	445.9	0.1309
0.9	455.45	0.1784

From Figure 15, as ratio increases, maximum range of reflection phase also increases but sensitivity decreases. The numerical results are presented in Table 5. Since sensitivity is primarily important, choices are reduced to 0.6-0.65 and 0.7 ratio values. From these three, most phase difference can be seen in 0.7 ratio, so this ratio is chosen for the design. As seen from Figure 16 and Figure 17, losses are negligible because the foam material has very low loss tangent and the main losses in reflectarrays caused by dielectric losses.

2.4.1.3 Effect of the height of the dielectric layers over phase of the reflected field

In this section, effect of the height of dielectric substrate over the phase of the reflected field is investigated. It is known that microstrip patch antennas operate in relatively wider frequency bands when dielectric substrate thickness is increased [35], and from (2), in single dielectric layer, maximum range of reflection phase is directly related with dielectric thickness. With those facts, effects of height to bandwidth and phase range are studied.

Parameters and constant values for unit cell simulation are given in Table 6. Phase and magnitude of reflected field simulations are presented in Figure 18 to Figure 24 for 9.5 GHz, 8 GHz and 10.5 GHz respectively.

Table 6 Parameters in unit cell substrate height simulation

$h_1 = h_2$	1 mm $\rightarrow$ 5 mm with 0.5 mm steps
$t_1 = t_2$	0.127 mm
$\frac{W_1}{W_2}$	0.7
f	9.5 GHz
$d_x = d_y$	16 mm x 16 mm

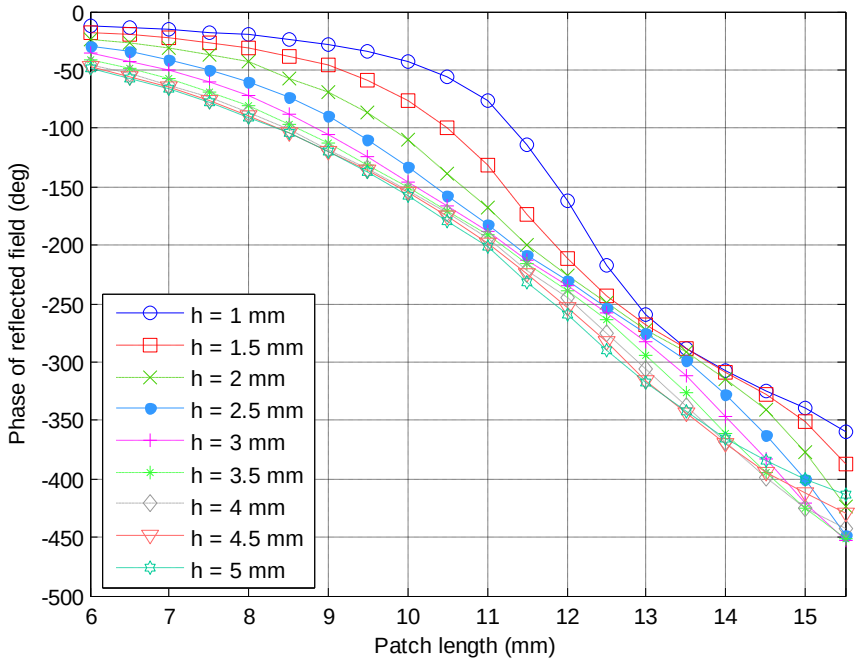

Figure 18 Effect of dielectric material height over phase of the reflected field (9.5 GHz, normal incidence)

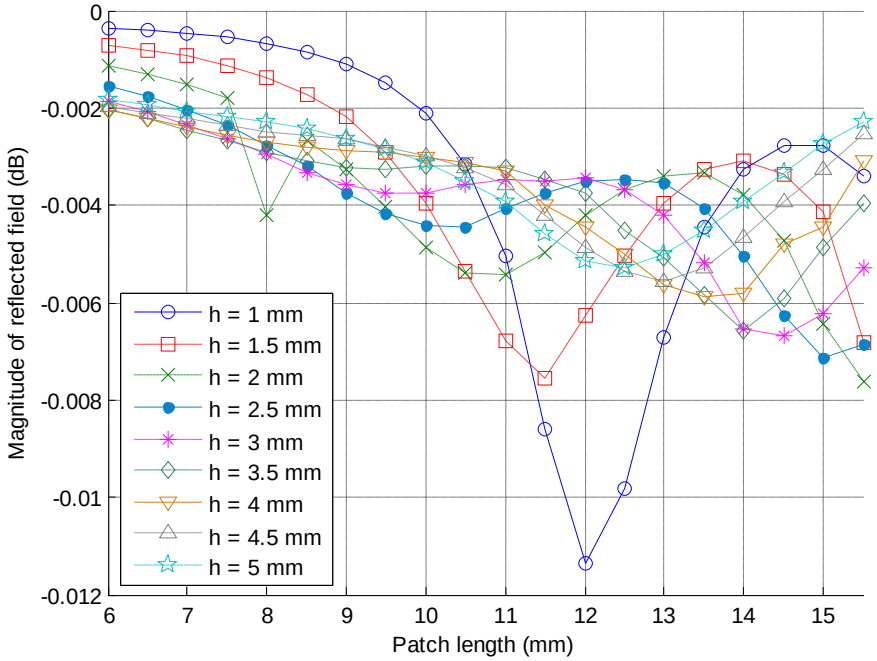

Figure 19 Effect of dielectric material height over magnitude of the reflected field (9.5 GHz, normal incidence)

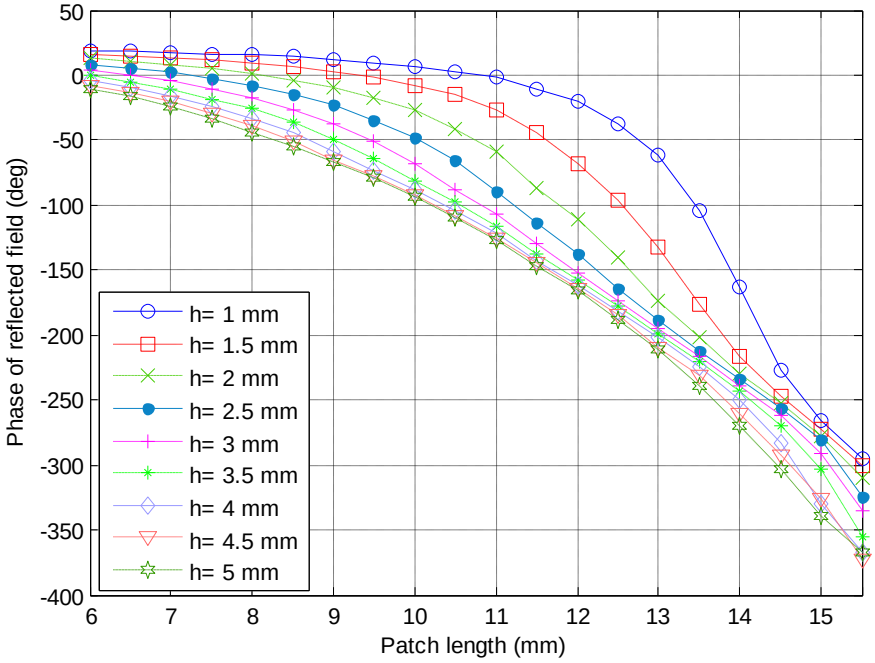

Figure 20 Effect of dielectric material height over phase of the reflected field (8 GHz, normal incidence)

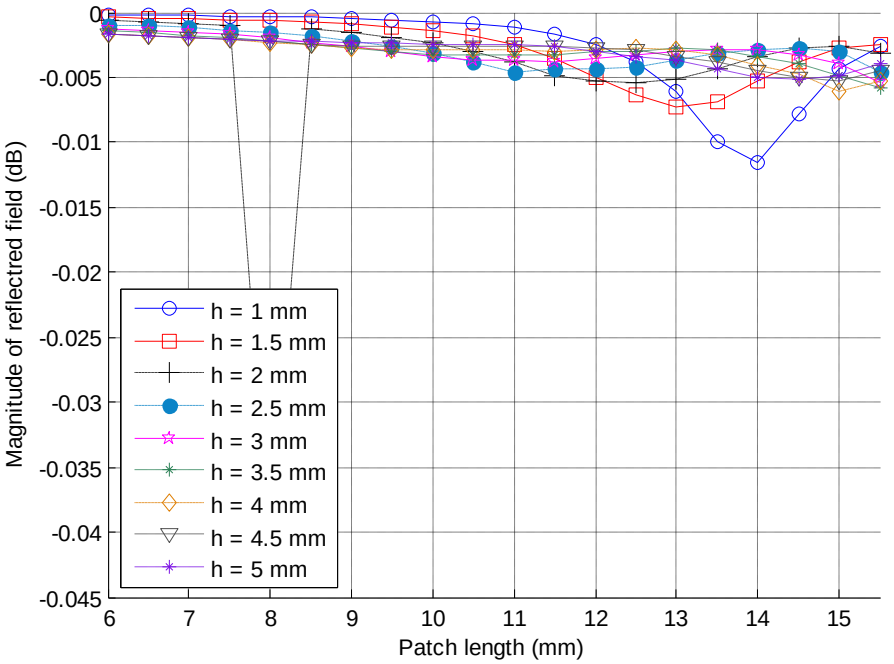

Figure 21 Effect of dielectric material height over magnitude of the reflected field (8 GHz, normal incidence)

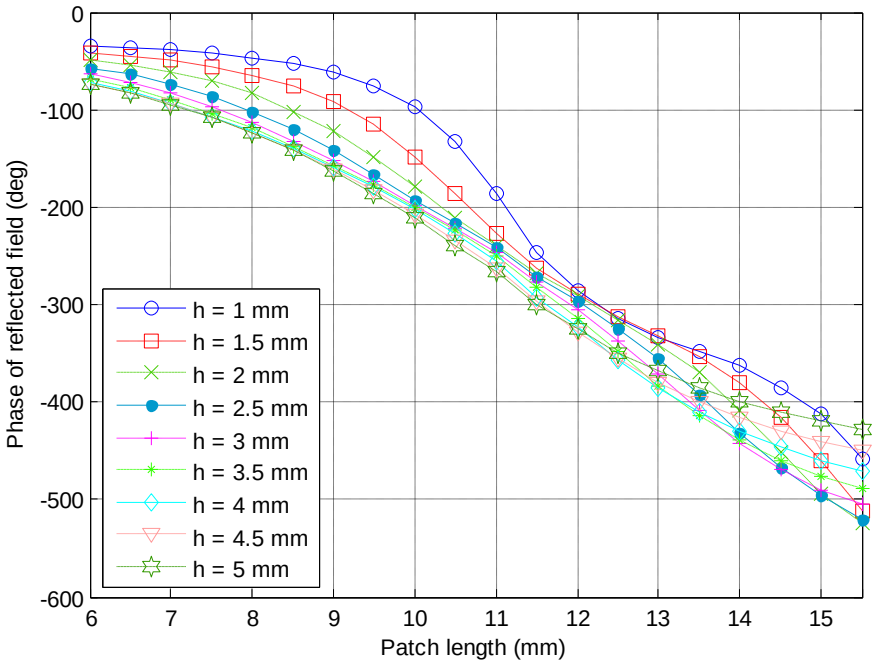

Figure 22 Effect of dielectric material height over phase of the reflected field (10.5 GHz, normal incidence)

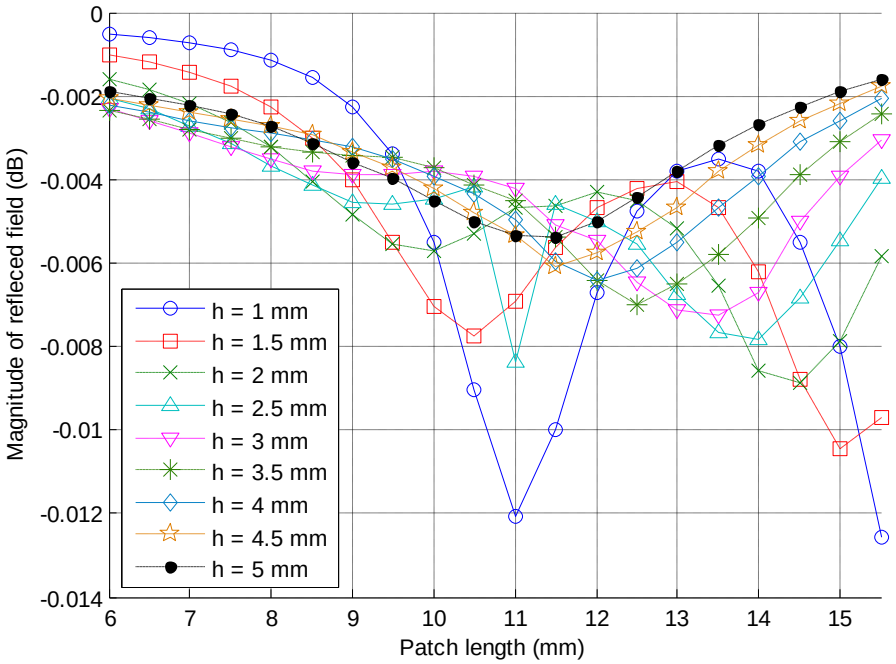

Figure 23 Effect of dielectric material height over magnitude of the reflected field (10.5 GHz, normal incidence)

The aim is to find the best unit cell which has the best performance parameters thus height should be chosen to satisfy both maximum phase range and sensitivity (since X_{pol} and L values are very low). For 9.5 GHz, maximum range of reflection phase for different foam thicknesses and sensitivity values are shown in Table 7. From this table, dielectric height between 2 mm and 4 mm seem suitable for the required phase range. The results also show that sensitivity is decreasing with increasing dielectric thickness. Considering the above two constraints 4 mm dielectric thickness is chosen for the unit cell.

Table 7 Difference of reflected phase of electric field of 15.5 mm and 6 mm patches at 9.5 GHz with corresponding foam heights

Height	R (°)	s (°/μm)
1 mm	346.54°	0.1104
1.5 mm	369.44°	0.0849
2 mm	399.7°	0.0918
2.5 mm	418.5°	0.0955
3 mm	416.98°	0.077
3.5 mm	410.27°	0.07
4 mm	397.12°	0.0655
4.5 mm	382.05°	0.0669
5 mm	364.43°	0.0603

In order to synthesize any desired pattern, 360° or more phase range is required. If 10% safety margin (considering mechanical errors) is added, nearly 400° of phase range is required. From Table 7, dielectric thicknesses of 2 mm to 4 mm are seemed suitable. On the other hand, sensitivity is decreasing with increasing thickness. Thus 4 mm dielectric thickness is chosen.

2.4.1.4 Effect of dielectric constant and loss tangent over frequency band and phase of the reflected field

In the previous sections, ROHACELL® foam material is used as separators. In this section, the effects of permittivity and loss tangent of the dielectric materials over phase design curve are investigated. To do so, different dielectric materials are used in HFSS® database.

Dielectric materials and corresponding permittivity and loss tangent values used in the study are listed in Table 8. Simulation setup values are given in Table 9. As a reference, vacuum is also included in simulations.

Table 8 Permittivity values of dielectric materials used in unit cell simulations

Dielectric material	Permittivity (ε_r)	Loss tangent (δ)
Vacuum	1.0	0
ROHACELL® Foam	1.05	0.0002
Rogers Duroid 5870™	2.33	0.0012
Rogers Duroid 5880™	2.2	0.0009
FR4	4.4	0.02
Rogers Duroid 6010™	10.2	0.0023

Table 9 Simulation setup values

$h_1 = h_2$	4 mm
$t_1 = t_2$	0.127 mm
$\frac{W_1}{W_2}$	0.7
f	9.5 GHz
dx x dy	16 mm x 16 mm

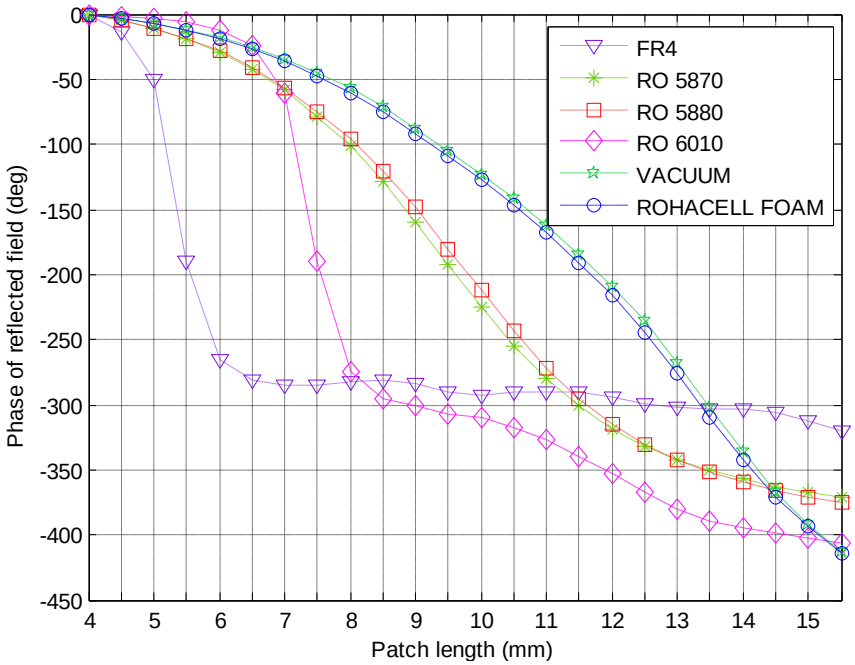

Figure 24 Effect of dielectric constant over phase design curve (normal incidence)

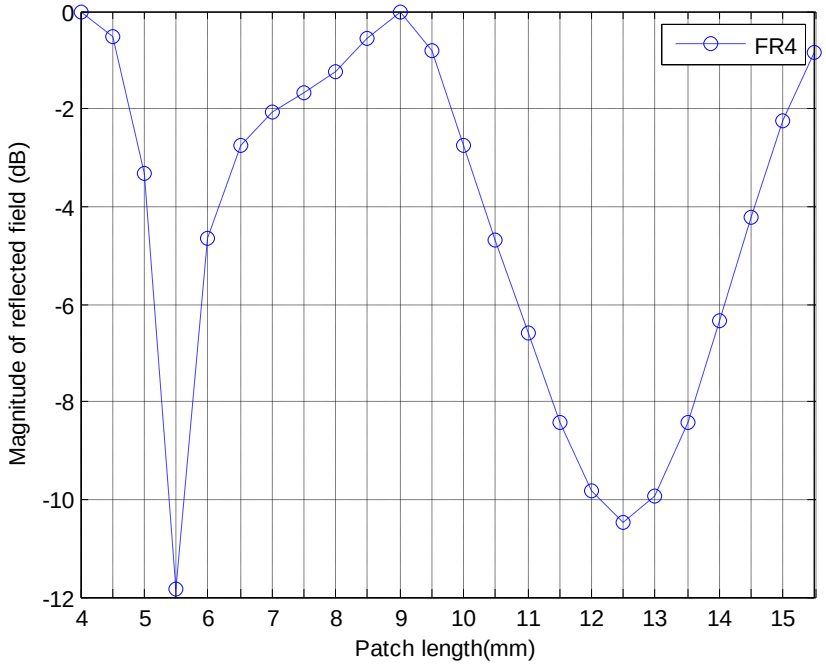

Figure 25 ***Effect of permittivity over reflected amplitude for FR4 (normal incidence)***

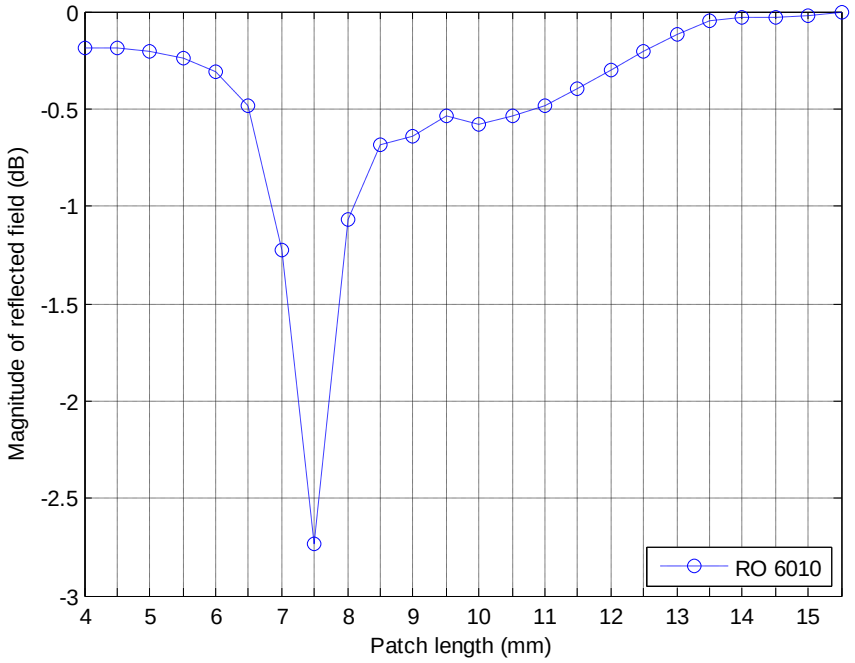

Figure 26 ***Effect of permittivity over magnitude of reflected field for RO6010 (normal incidence)***

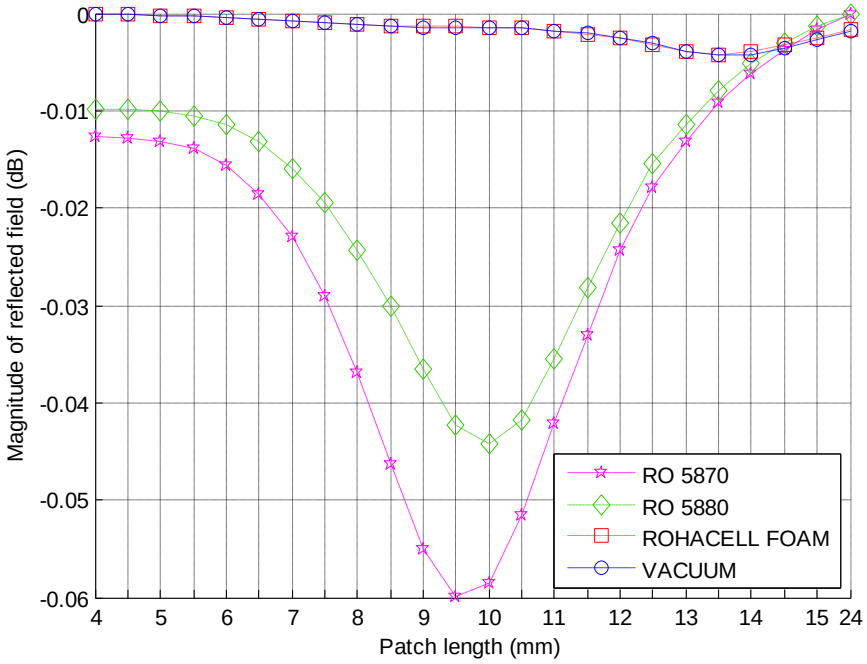

Figure 27 Effect of permittivity over reflected amplitude (normal incidence)

From Figure 24, with increasing dielectric constant, phase design curve becomes steeper and phase range becomes narrower. Comparing two layer unit cell with single layer unit cell (Appendix-1), all the dielectric materials show wider maximum reflection phase range except for FR4.

At first glance, it seems that higher permittivity means lower phase range when air, foam, RO 5880, RO 5870 and FR4 are compared but RO 6010 refute this idea. In addition, low loss RO 6010 material has nearly the same phase range with air and foam, but due to high permittivity, high slope can be seen around 7-8 mm, which results less sensitivity and there is no linearity over entire patch dimension range.

From Figure 25, Figure 26 and Figure 27, it can be seen that the efficiency of the unit cell reduces when FR4 is used. Efficiency means the ratio of the received power to the incident power. If loss tangent values are studied shown in Table 8, one can conclude that high-loss FR4 material is very poor in efficiency (both amplitude and phase) and gives very narrow phase range.
One more important concept that should be discussed in Figure 27 is, for air, there is a decrease in the amplitude of reflected field with respect to increasing patch size, which means that loss can be seen for larger patch dimensions. This is because of the numerical errors of HFSS®. In HFSS®, if PEC is used instead of lossy materials such as copper, this kind of numerical errors can be seen very often (efficiency of the antennas may be greater than 1).

To conclude, higher dielectric constant materials affect linearity negatively and low loss tangent values provide bigger phase range,[34].

2.4.1.5 Effect of the frequency sweep on the phase of the reflected field

In this section for the best patch size ratio, dielectric constant and unit cell size (i.e. the design with the most linear phase design curve with the largest phase coverage), the frequency swept analyses are carried. Results of the frequency sweep for different frequencies from 8 GHz to 12 GHz with 0.25 GHz steps are presented in Figure 28. Simulation setup values in this analysis are shown in Table 10.

Table 10 Simulation setup values

$h_1 = h_2$	4 mm
$t_1 = t_2$	0.127 mm
$\frac{W_1}{W_2}$	0.7
$d_x \; x \; d_y$	16 mm x 16 mm
ε_{foam}	1.05

From Figure 28, the difference of phases between two similar patches is greater for larger patches depending on frequency. However these differences can be acceptable and all of these lines can be assumed parallel to each other for narrow band applications. But this may cause serious phase errors in wide band applications or shaped beam antennas where small phase changes are very important and intolerable. Maximum differences of phases are calculated for the center frequency 9.5 GHz and presented in Table 11. As mentioned in section 2.3 the error bound is chosen as 45°, then 8.75 GHz – 10.25 GHz band is the operation frequency band for this unit cell.

Table 11 Bandwidth of the unit cell

β (GHz)	Phase difference (°)	β (GHz)	Phase difference (°)
8 - 9.5	84.06	9.5 – 10.25	44.71
8.25 – 9.5	72.48	9.5 – 10.5	58.84
8.5 – 9.5	59.22	9.5 – 10.75	72.04
8.75 – 9.5	44.98	9.5 – 11	83.47
9 – 9.5	30.78	9.5 – 11.25	95.16
9.25 – 9.5	15.51	9.5 – 11.5	105.6
9.5 – 9.75	15.43	9.5 – 11.75	115.78
9.5 – 10	30.62	9.5 – 12	127.63

Figure 29 presents the magnitude of the reflection coefficient in 8.5-10.5 GHz band. Magnitude of the reflection coefficient for all patch lengths is very close to 0 dB so it can be concluded that dielectric losses are negligibly small.

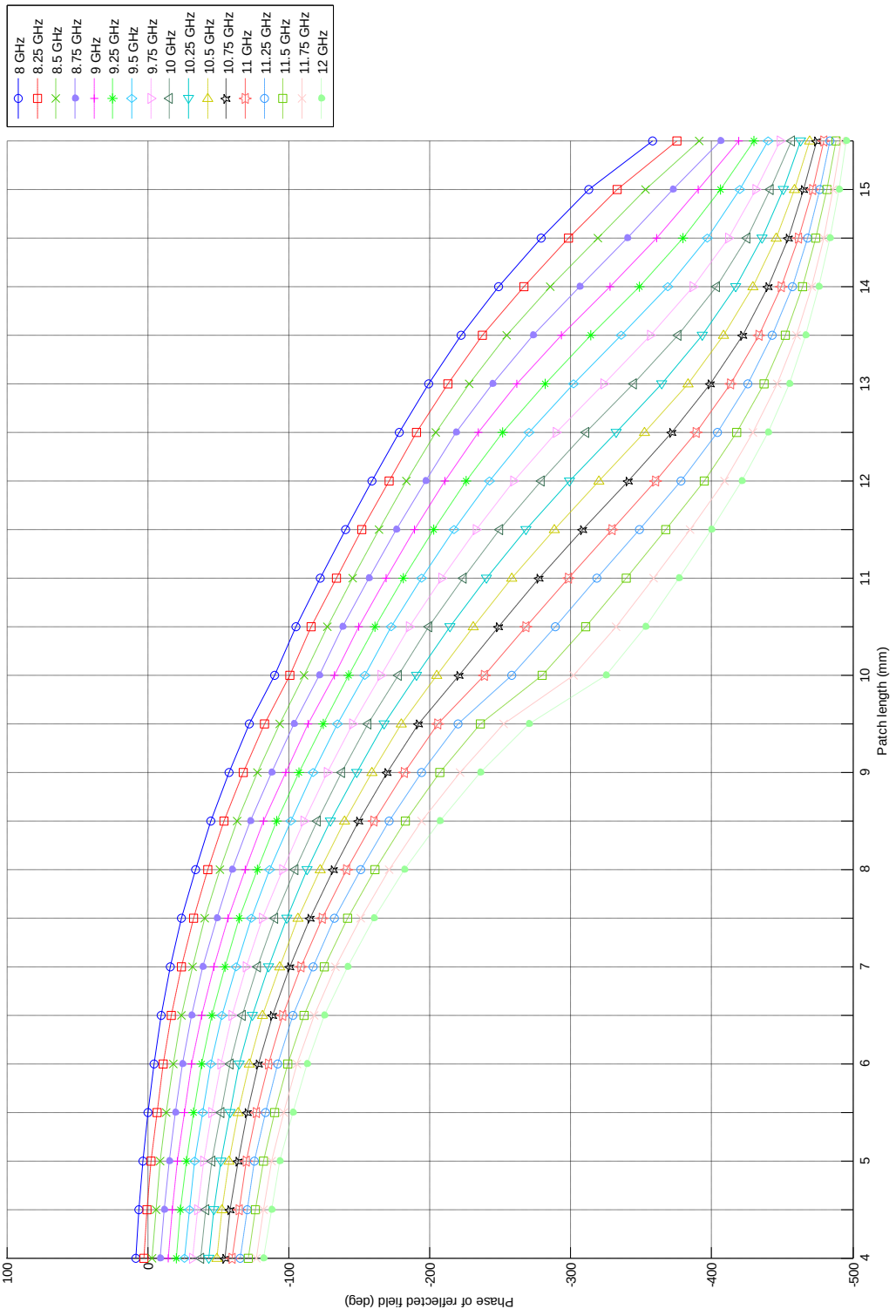

Figure 28 Phase design curves for different frequencies ranging 8-12 GHz

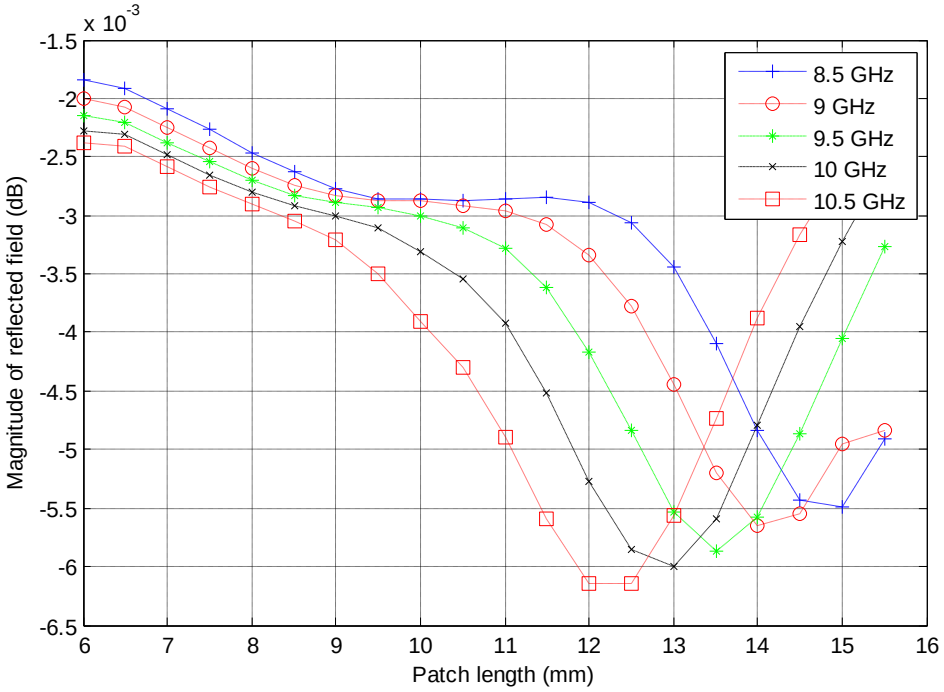

Figure 29 Magnitude of the reflection coefficient as a function of patch length for different frequencies at normal incidence

The analysis carried in Appendix-1 on the single layer patches shows that the resonance occurs where the phase design curve has the highest slope. A similar case also appears for multilayer configurations.

Curve of the phase differences for the consecutive patch lengths (ex. 8mm - 8.5mm, 8.5mm - 9mm, etc.), as in Figure 30, shows that with increasing patch length, the phase differences increase up to some value. After some point, the phase differences begin to decrease. With increasing frequency this point shifts to the smaller patch lengths as in Figure 31. The peak value of this curve occurs where the slope of phase design curve reaches its maximum. This is a similar situation that single layer patches show at the resonance. So one must avoid from using these patch sizes in a reflectarray design.

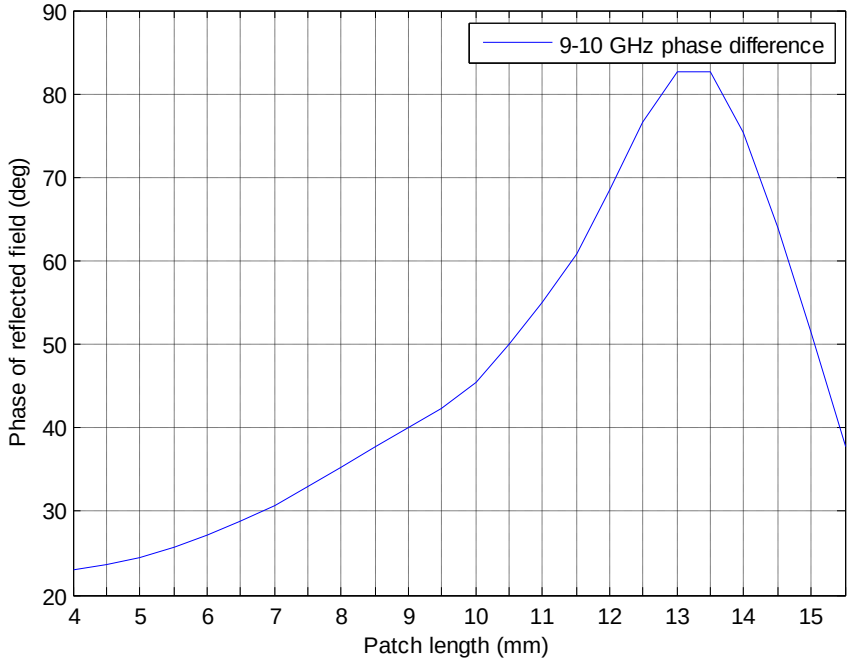

Figure 30 Phase difference between 9GHz and 10GHz unit cell patches versus lower patch size

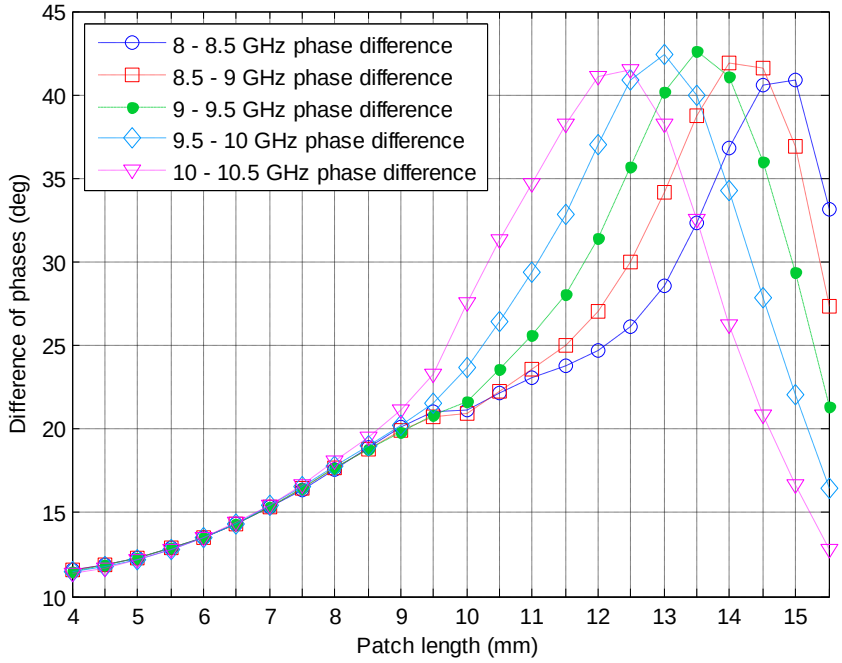

Figure 31 Difference of phases between 8 GHz- 10.5 GHz unit cell patches with 0.5GHz steps versus lower patch size

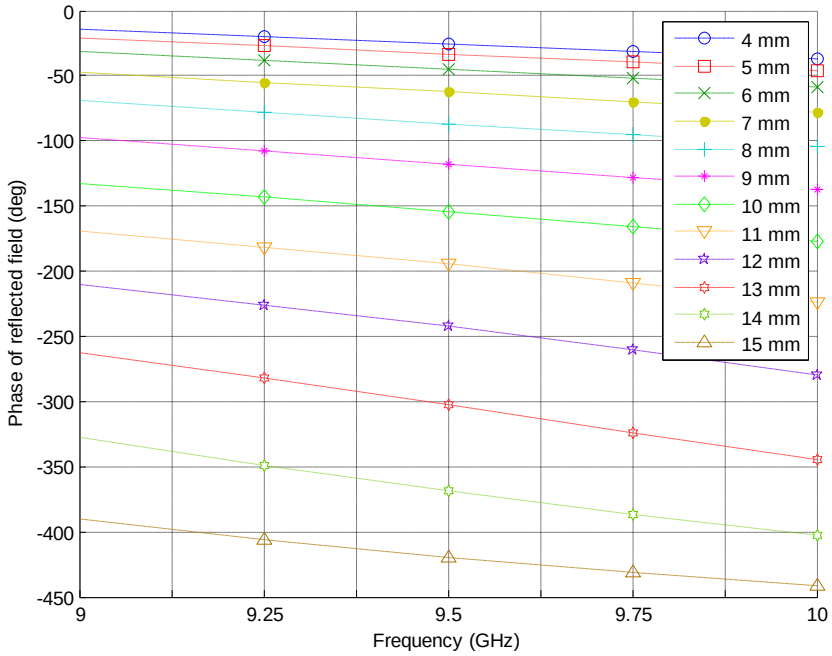

Figure 32 Phase design curves for different patch lengths ranging 4-15 mm as a function of frequency (9-10 GHz, normal incidence)

It is observed from Figure 32 that, with increasing frequency, phase change is increasing with increasing patch dimension for normal incidence. For this reason, smaller patches should be preferred at the center for reflectarray applications.

2.4.1.6 Effect of various incidence angles over the phase design curve

Due to the feed structure, the elements in the edge of the reflectarray cannot be illuminated at normal incidence. Therefore in this section, effect of different incidence angles over patch response is presented.

In this simulation, *x*-polarized plane waves with incidence angle θ (angle from *z*-axis) varying from 0° to 50° with 10° steps are used to illuminate the patches, amplitudes and phases of the of the reflected fields are observed.

These incidence angles are set by changing the phases of the slave boundary. De-embedding is done and results belong only to the unit cell, not including the air box where wave travels freely are calculated.

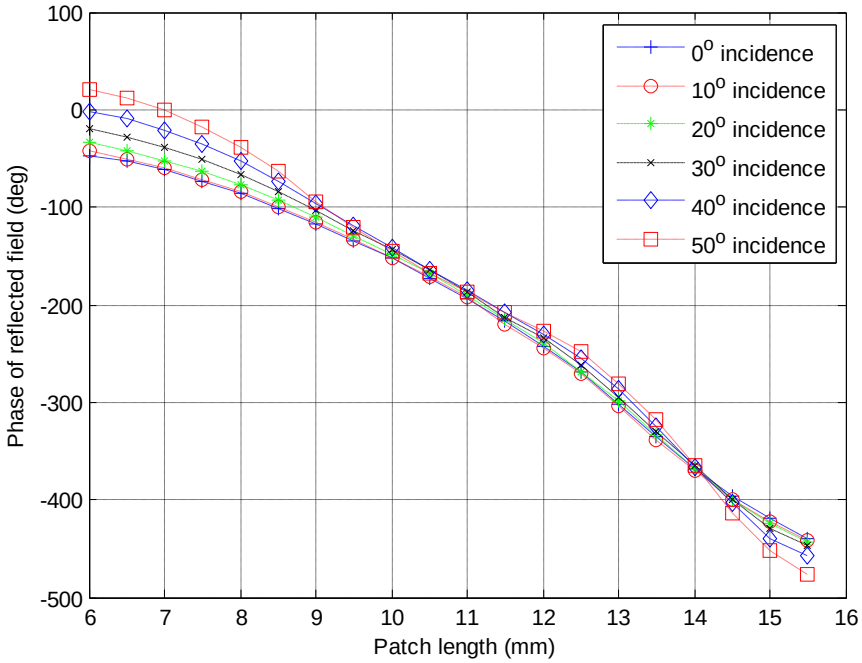

Figure 33 Effect of different incidence angles on phase design curve at center frequency (9.5 GHz)

From Figure 33, with increasing incidence angle, phase range is increasing but the shape of the phase design curve does not remain as smooth as normal incidence illumination. Also in the upper and lower bounds of the operating frequency, this behaviour gets worse.

Since the deviation of the phase design curve with respect to incidence angle becomes critical for 6-9 mm patches in center frequency, the elements with these patch sizes are used at the center of the reflectarray where the illumination can be considered as normal incidence.

2.5 Conclusion

Unit cell dimensions that are used in reflectarray design are determined using the results of the parametric analysis presented in this chapter. Dimensions of the unit element and the dielectrics (Rogers RO5880) which support patches are given in Table 12 and phase design curve of this cell at 9.5 GHz is presented in Figure 34.

Table 12 Dimensions of the unit element

$h_1 = h_2$	4 mm
$t_1 = t_2$	0.127 mm
$\frac{W_1}{W_2}$	0.7
f	9.5 GHz
$d_x \; x \; d_y$	16 mm x 16 mm
ε_{foam}	1.05
ε_{RO5880}	2.2

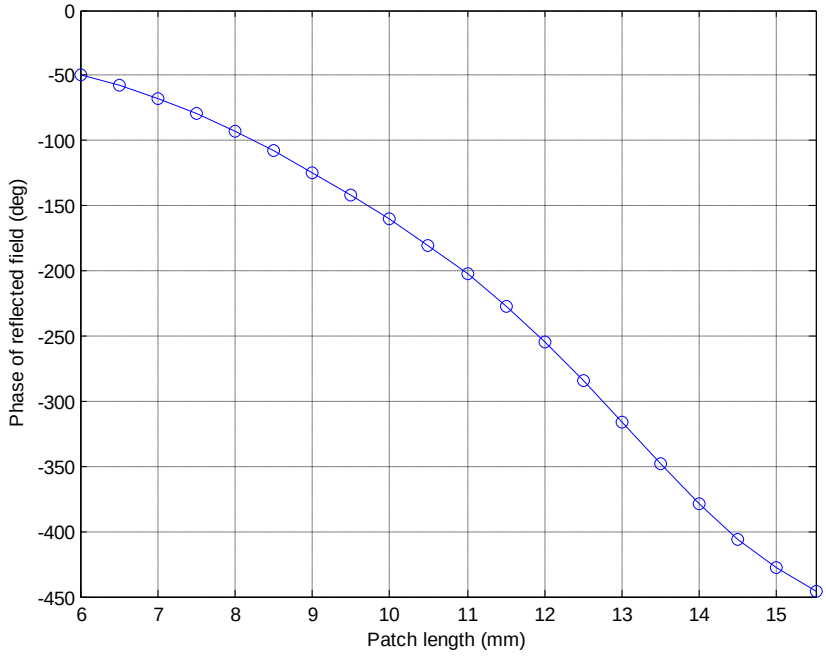

Figure 34 Phase of reflected field of the unit cell at 9.5 GHz at normal incidence

CHAPTER III

DESIGN OF THE REFLECTARRAY WITH SHAPED BEAM

3.1 Introduction

In this chapter, feed antenna of the reflectarray is designed by considering the antenna requirements. In order to illuminate the array, a horn antenna is theoretically designed and simulated. Also, horn antenna is manufactured and measurement results are compared with simulations. Two dimensional amplitude and phase graphs of the horn antenna are obtained in order to use for the final design of the reflectarray.

Phase compensation method, which is the most critical part in the design of the shaped beam reflectarray is investigated in this chapter. Also, phase only synthesis method based on genetic algorithm is explained and design procedure of the reflectarray is introduced.

Requirements of the shaped beam reflectarray antenna are given in Table 13. The most important requirement is to make the beamwidth of the reflectarray antenna as wide as possible. (BW>10%) By considering these requirements an appropriate feed antenna is investigated. The preceding sections mention the design, manufacturing and measurement procedures of the feed antenna.

Table 13 Final design requirements

Frequency range	9 GHz - 10 GHz (%10 Bandwidth)
Beam shape	Cosecant square in azimuth, pencil in elevation
Edge Taper	-10 dB in azimuth plane
Ripple in cosecant area	±1 dB
Side lobe level	< -15 dB
Azimuth plane dimension	30 - 40cm

3.2 Feed horn

Before starting the design of the reflectarray feed antenna, several horn antennas are considered. First of all, some commercial standard gain antennas are studied but these are not suitable as a feed of the reflectarray. For example, a standard gain (20 dB) horn antenna with 9 cm x 12 cm aperture has about 1.5 m far field at 9.5 GHz. At the far field, 10 dB beamwidth of the antenna corresponds to a circular region with 1m diameter and it is much larger than the size of the reflectarray. Therefore, it causes high spillover and reduces the efficiency of the reflectarray. On the other hand, low cross polarization levels are achieved with high gain antennas [8]. Since low cross polarization is not the primary target, using a horn antenna with smaller aperture is considered.

Thus, a feed horn is designed with wide beam and low gain to satisfy the predetermined amplitude taper over the reflectarray surface. Since all horn antennas have amplitude taper, only constraint in the design is to obtain the desired beamwidth.

For a good illumination of the designed reflectarray, a feed horn with 50° 10dB beamwidth and with a short far field distance is required. Also, to increase the

efficiency of the reflectarray, return loss should be minimized. In addition, in the operating frequency of the reflectarray, constant beamwidth and constant gain is expected. By considering all these requirements mentioned above, a rectangular horn antenna [35] is designed and fabricated. Dimensions of the horn antenna are shown in Table 14 and in Figure 35. The simulation result of the reflection coefficient is given in Figure 36. The feed antenna is fed with standard WR90.

Table 14 Feed horn dimensions

Aperture width (A)	30 mm
Aperture height (B)	30 mm
Antenna length (H_A)	70 mm
Input port width (a)	10.16 mm
Input port height (b)	22.86 mm

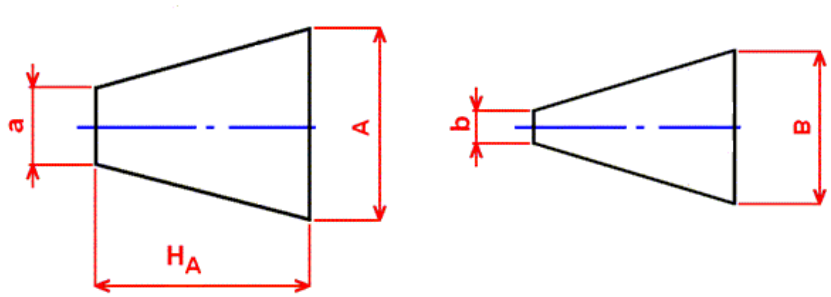

Figure 35 Feed horn dimensions

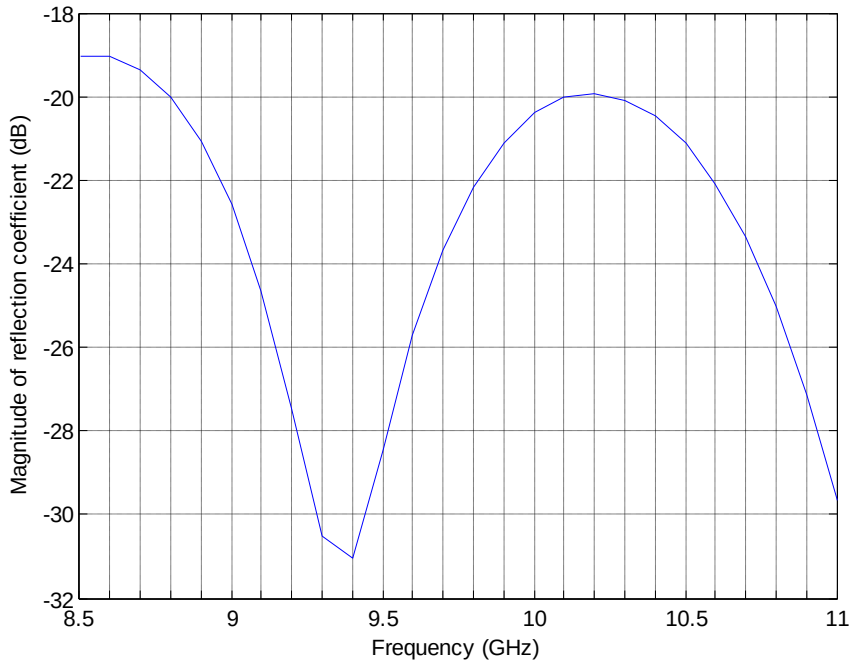

Figure 36 Magnitude of the reflection coefficient of the horn antenna versus frequency

Simulations and measurements of the radiation pattern of the feed antenna are shown in Figure 37 to Figure 41. Measurements have been performed in a tapered anechoic chamber. There are some notches seen on the main beam. These are the measurement errors and caused by the measurement program (Network analyzer missed the data). The shape of the main beam is exactly the same with the desired pattern, including 10 dB beamwidth. If the coordinate system in Figure 42 is considered, reflectarray is placed in the XY plane and cosecant square beam is synthesized in the YZ plane. Measurements of the YZ cut are presented in Figure 37 to Figure 41 ($\phi = 90°$ plane).

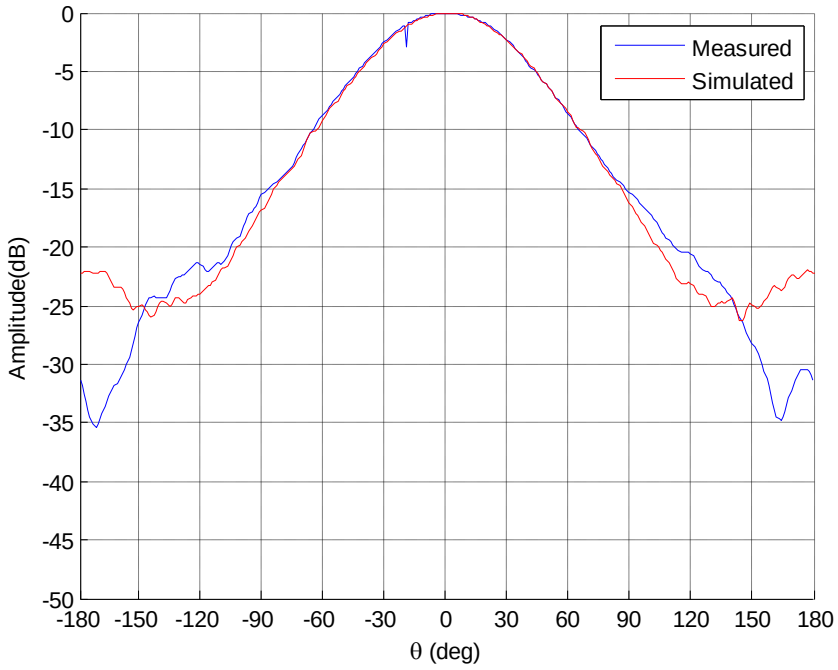

Figure 37 Normalized pattern of the feed antenna at 8.5 GHz

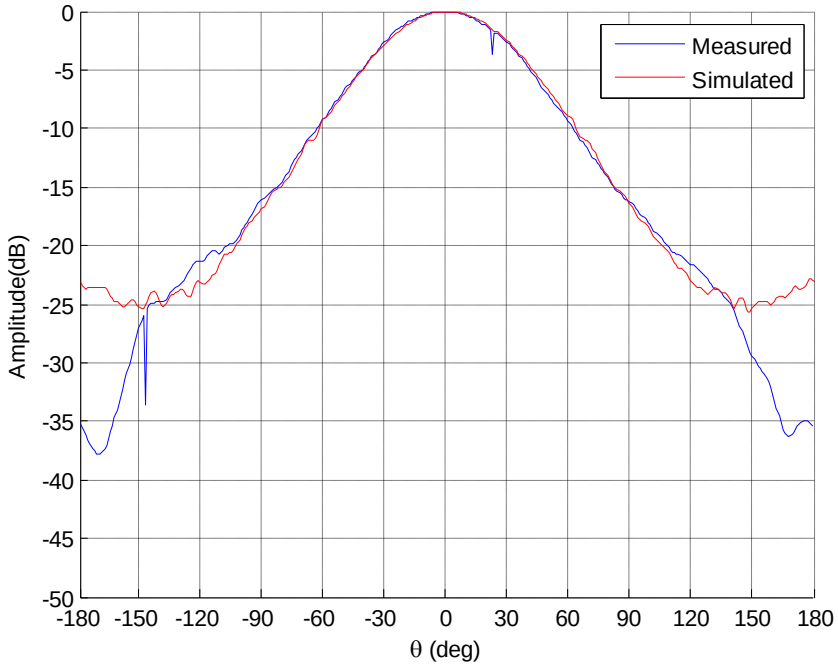

Figure 38 Normalized pattern of the feed antenna at 9 GHz

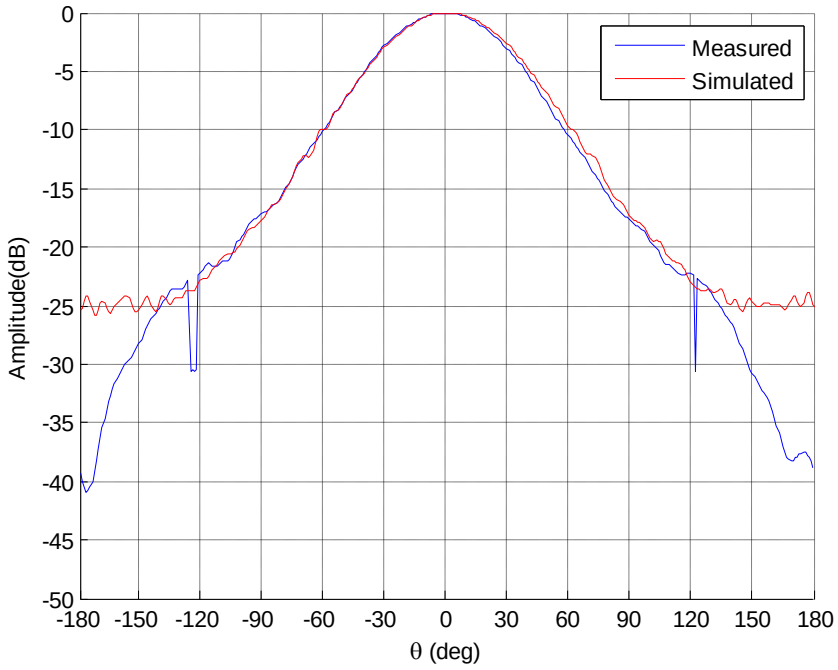

Figure 39 Normalized pattern of the feed antenna at 9.5 GHz

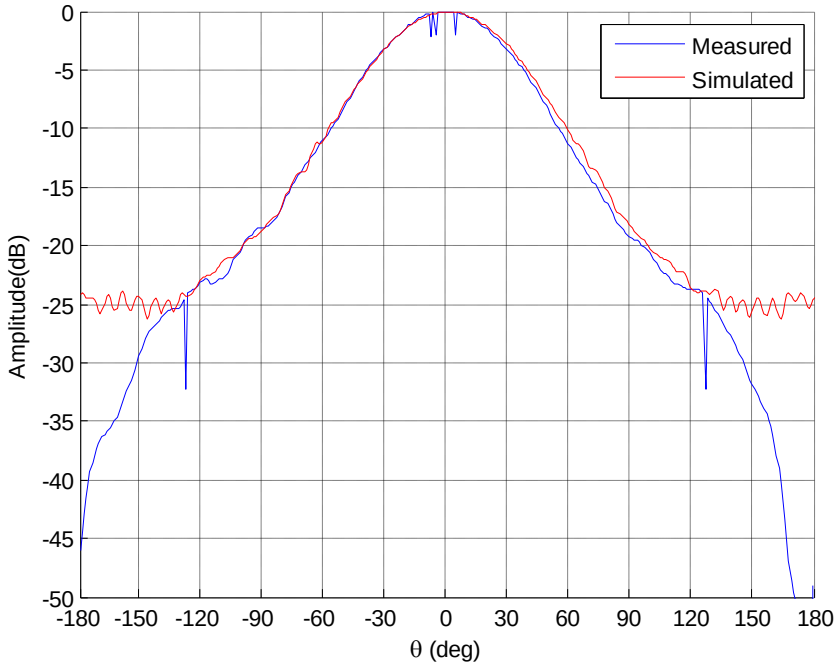

Figure 40 Normalized pattern of the feed antenna at 10 GHz

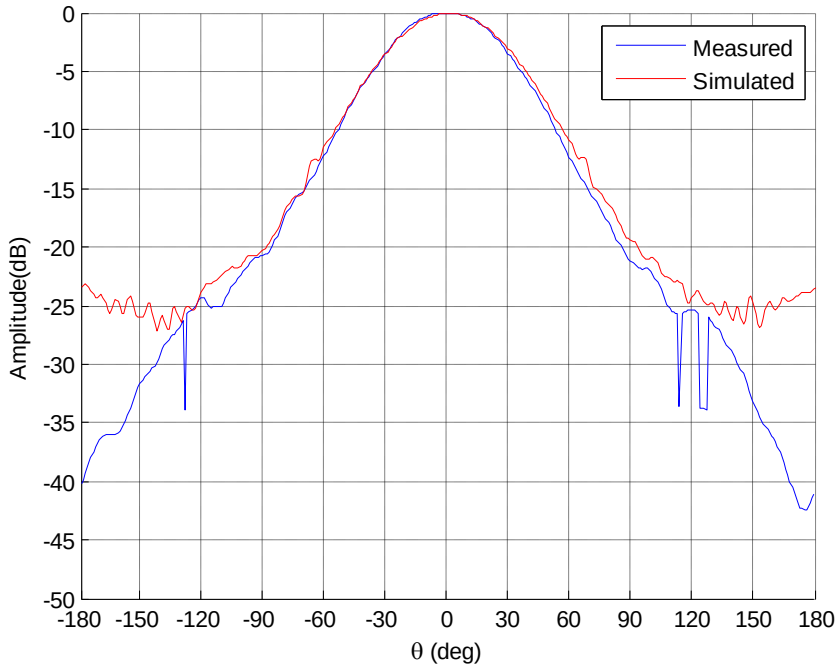

Figure 41 Normalized pattern of the feed antenna at 10.5 GHz

Considering the X-band waveguide dimension and the TE_{10} mode excitation, radiation box of the horn drawn as if there is a reflectarray in its exact position and that box covers the feed. Also due to the electronically large simulation setup, E-field symmetry boundary is used and all of the simulation setup is divided into two equal pieces. Simulation setup of the horn is shown in Figure 42. Simulation results of the horn antenna in ϕ=90° and ϕ=0° planes are shown in Figure 43 and Figure 44.

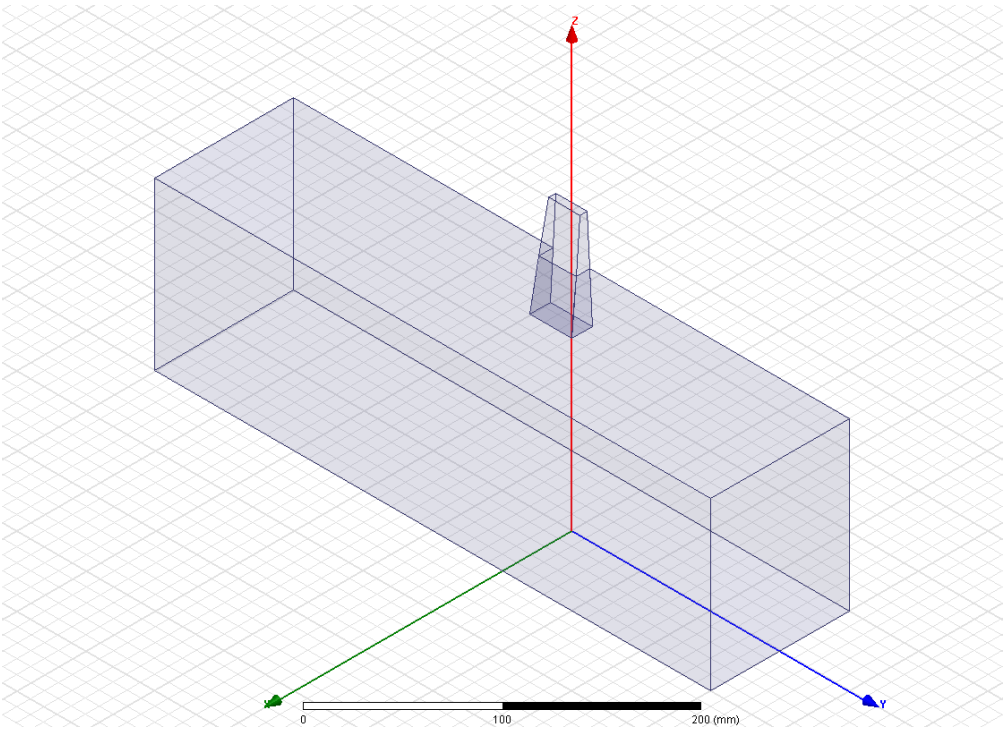

Figure 42 **Feed horn simulation setup**

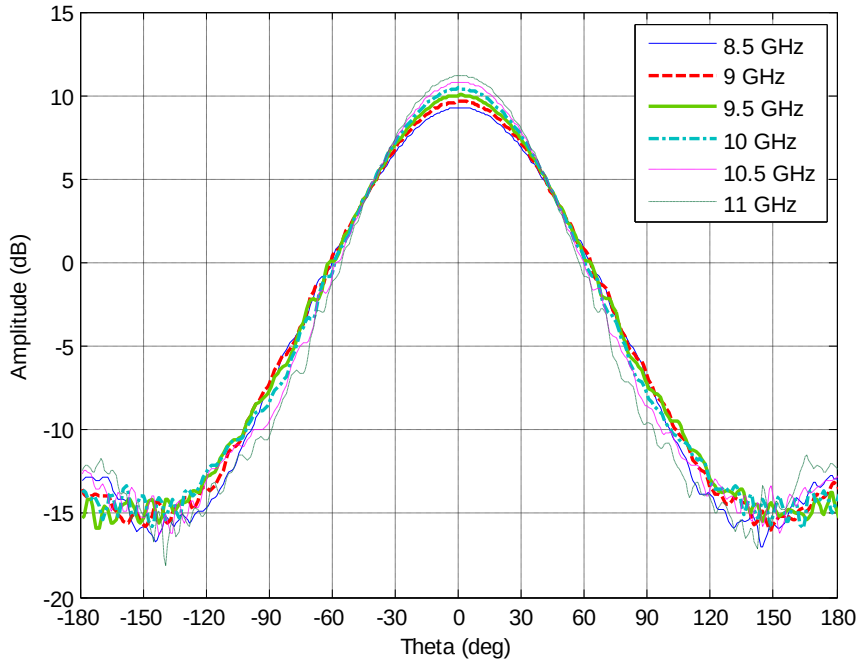

Figure 43 Far field radiation patterns of simulated horn antenna in ϕ=90° plane, between frequencies 8.5 GHz and 11 GHz with 0.5 GHz steps

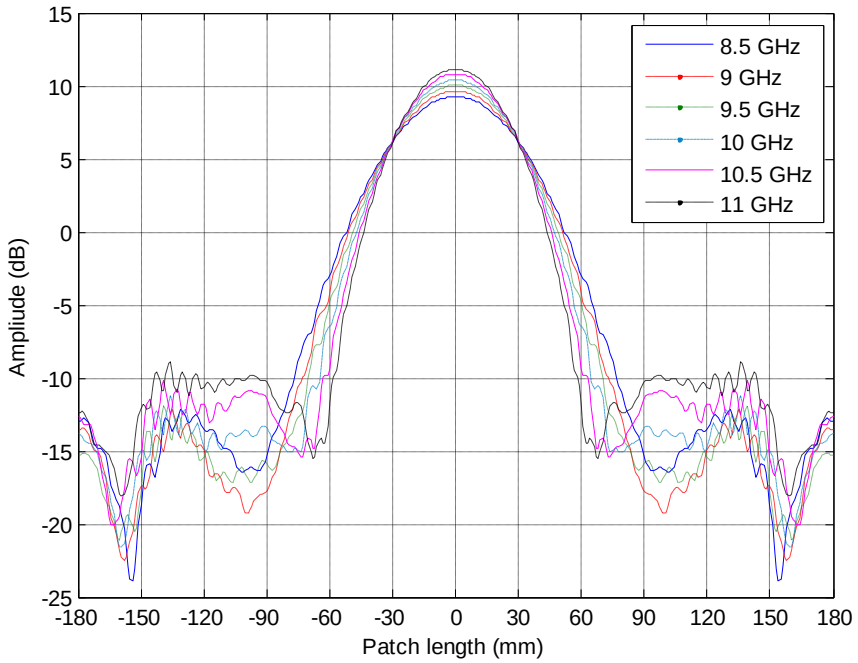

Figure 44 Far field radiation patterns of simulated horn antenna in ϕ=0° plane, between frequencies 8.5 GHz and 11 GHz with 0.5 GHz steps

It is observed from Figure 43 that, 10 dB beamwidths and gains do not change significantly throughout the operation band, which is presented in Table 15. Thus, this horn can be used as a feed in the reflectarray.

Table 15 10 dB beamwidths and gain values of the designed feed horn antenna

Frequency (GHz)	10 dB beamwidth at ϕ=0° cut	10 dB beamwidth at ϕ=90° cut	Gain (dB)	Cross-pol level (dB)
8.5	58.7°	65.3°	9.27	-42.8
9	55.2°	63.6°	9.64	-39.49
9.5	52.94°	62.4	10	-38.48
10	51.4°	60°	10.43	-36.77
10.5	48.87°	57.49°	10.78	-38.36
11	46.56°	55.86°	11.16	-35.23

3.3 Magnitude and phase distribution of the field on the reflecting surface

In reflectarrays, amplitude of the electric field on the reflecting surface, created by the feed antenna, should be calculated. Especially calculating the amplitude of the electric field is very important when 'phase only synthesis method' is used, because if the amplitudes are not correct, phases cannot be found accurately. For this reason, amplitudes should be determined with simulations.

First way of determining the amplitudes is using the far field data. In this way, far field pattern is calculated and amplitudes over individual patches are determined. But this method is not very suitable because although the distance between the feed and the array satisfies the far field criteria ($\frac{2D^2}{\lambda}$), the pattern at $\frac{2D^2}{\lambda}$ and at infinity may differ. Therefore, using the near field data of the feed horn gives correct results. For this reason, in this study, near field patterns are used. Amplitudes of the radiated electric fields of the feed antenna are

determined over the patches. These values are used in the phase only synthesis code. The amplitudes of the patches in the middle row are given in Table 16.

Table 16 Amplitude level of electric fields on the patches (V/m)

1st patch	0.18	***8th patch***	0.63	***15th patch***	0.91	***22nd patch***	0.33
2nd patch	0.21	***9th patch***	0.73	***16th patch***	0.82	***23rd patch***	0.26
3rd patch	0.26	***10th patch***	0.82	***17th patch***	0.73	***24th patch***	0.21
4th patch	0.33	***11th patch***	0.91	***18th patch***	0.63	***25th patch***	0.18
5th patch	0.4	***12th patch***	0.97	***19th patch***	0.54		
6th patch	0.47	***13th patch***	1	***20th patch***	0.47		
7th patch	0.54	***14th patch***	0.97	***21st patch***	0.4		

In Figure 45, 2D amplitude distribution of the feed horn over the planar array is shown. In this figure, each cell represents unit cell location; numbers below and at the left side represent column and row numbers, respectively. Coloured bar next to the figures shows the normalized amplitude distribution. As expected, amplitude values are much higher at the middle when compared to the ones close to the edges. Since the design requirement is to achieve -10 dB amplitude values at the edges of the array, rows and columns before 6^{th} and after 19^{th} can be omitted. This cancellation is done not only for the requirements; but also for the fact that the effect of those patches to reflectarray pattern is negligible. The synthesis code uses phase only synthesis method and is applicable for 1D arrays. In this synthesis method, it can be easier to find shaped beam pattern if there is amplitude taper over elements.

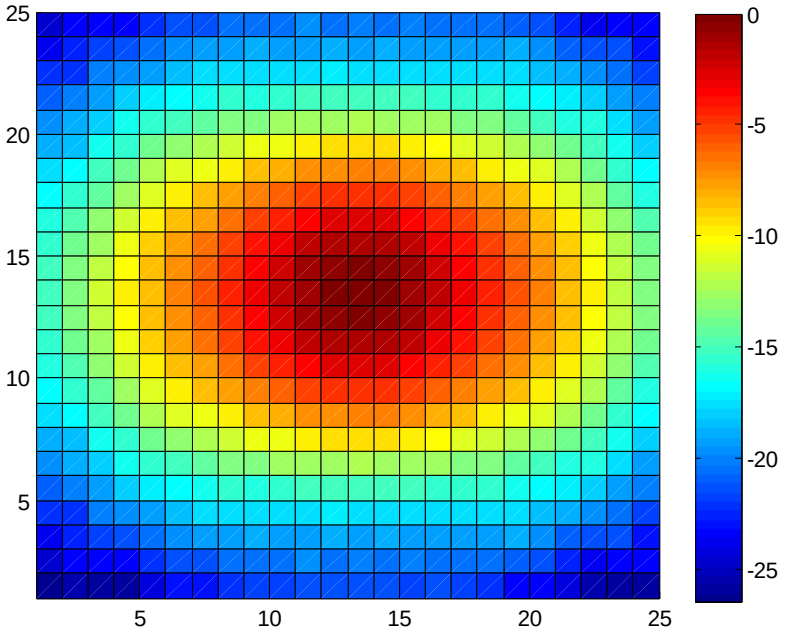

Figure 45 Normalized surface amplitude distribution of the feed horn over the planar array (x-axis directed)

Figure 46 shows the y-axis directed fields (cross polarization component). As expected, amplitude level of the electric field is very low in this region, because horn antenna has low cross polarization level in principal planes.

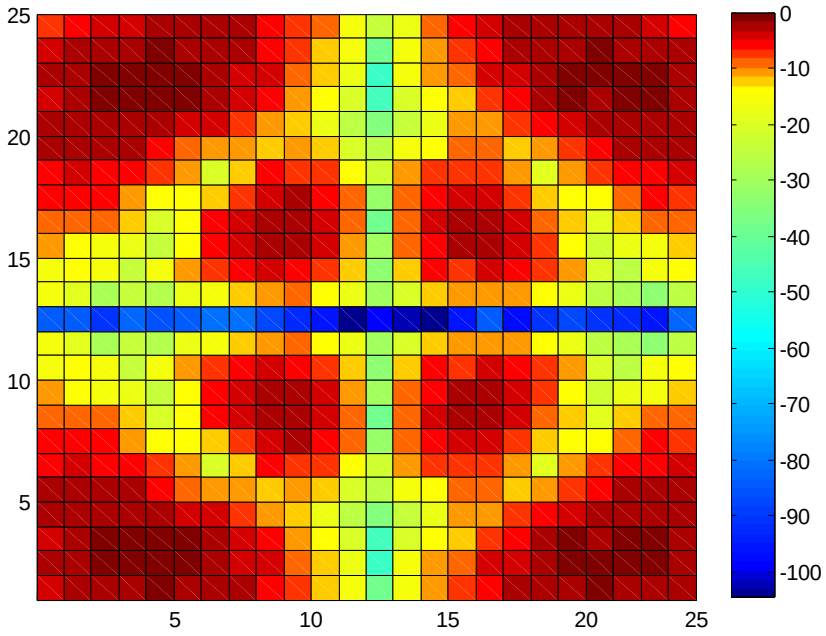

Figure 46 Surface amplitude distribution of the feed horn orthogonal to the previous one over the planar array (y-axis directed)

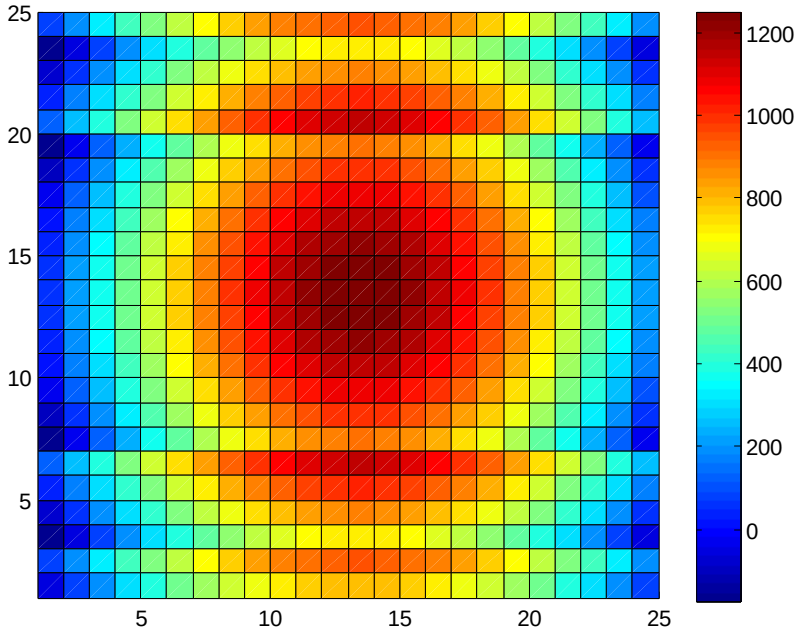

Figure 47 Surface phase distribution of the feed horn over the planar array

As can be seen from Figure 45 and Figure 46, *x*-directed and *y*-directed fields have amplitude values very close to each other in the edges of the array. Phase distribution due to the feed horn over the patches is shown in Figure 47. Phase change between adjacent patches in the middle is about 10° so the phase change can be ignored in the vicinity of the 13^{th} line, which is in the middle of the array, so it is advisable to construct an array for the 13^{th} line and copy between 11^{th}-15^{th} or 10^{th}-16^{th} lines. After this step, a new line can be synthesized and can be used for 2-3 lines both up and down.

3.4 Cosecant square beam synthesis by phase only synthesis method

In a reflectarray, to achieve cosecant square beam pattern, the phase only synthesis method is applied because the amplitude values cannot be changed. There are several different techniques using phase only synthesis method [36]. From those methods, genetic algorithm is chosen for this thesis.

For the synthesis of a cosecant square beam, phases of the patches are found by using the genetic algorithm in a MATLAB code [37]. In this algorithm, regardless of the patch shape, phase of every single patch element is evaluated under the assumption of plane wave incident on each patch so there is no amplitude taper over any individual element. Other assumption is that, since the microstrip patches have broad beam, there is no amplitude reduction after reflection in any angle of interest. Phase compensation is applied to all elements in the array, which is described in the next section. Also from Figure 45, amplitudes are chosen for the middle line, synthesis is performed and phases are obtained. These obtained phases are used for seven rows in the middle, i.e., for the lines numbered from 10 to 16 because there is no significant variation between amplitude values. Also synthesis process takes approximately 1 day so 1 week is needed to find the individual phases for the whole array. Then amplitude values of the 5^{th} row (from the middle) are taken and new synthesis is done. Those new phases applied to rows 7-9 and 17-19.

Phases of the individual patches for the center rows are given in Table 17. These values are raw phase values in degrees that should be modified and used in the reflectarray design.

Table 17 Phase values found from genetic algorithm code

1st patch	133.23	***8th patch***	85.04	***15th patch***	348.66	***22nd patch***	326
2nd patch	124.72	***9th patch***	68.03	***16th patch***	314.65	***23rd patch***	320.3
3rd patch	147.4	***10th patch***	42.52	***17th patch***	272.13	***24th patch***	311.8
4th patch	110.55	***11th patch***	48.19	***18th patch***	235.28	***25th patch***	257.95
5th patch	110.55	***12th patch***	22.68	***19th patch***	42.52		
6th patch	110.55	***13th patch***	14.17	***20th patch***	17		
7th patch	87.87	***14th patch***	11.34	***21st patch***	320.32		

3.4.1 Genetic algorithm based phase only synthesis method

In genetic algorithm, any dataset is called individual. These individuals are expressed with bits, which are thought to be chromosomes that give the characteristic of each individual. Those individuals form small groups, named subpopulation. Subpopulations are composed of the same number of individuals. In this group, individuals are used to produce new datasets, labelled as children. In this structure, mutation can be seen in some individuals' chromosomes rarely, which may change the characteristic drastically. Then these subpopulations form the complete population. The best individual, which means the best dataset that best fits the desired pattern, is chosen. Figure 48 illustrates the process.

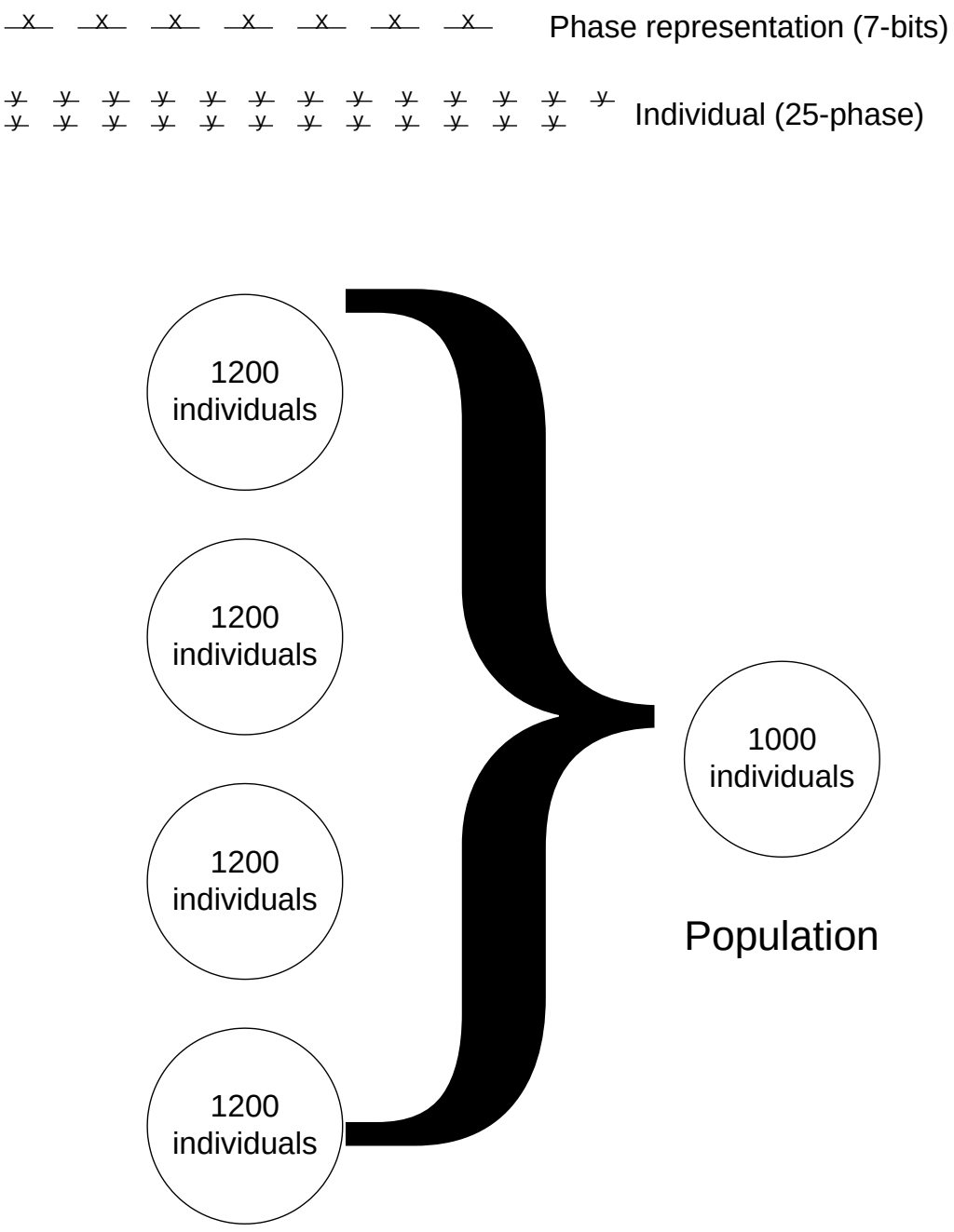

Figure 48 Genetic algorithm structure

In MATLAB code used in synthesis, each phase is represented with 7-bits. It means that 360° of complete phase is divided into 2^7 equal parts and has 2.8125° of resolution. For the unit cell chosen, since 0.263 mm error in patch

dimension in the center frequency causes 3° of phase deviation, this resolution seems to be enough for this application. As mentioned earlier, individuals represent datasets; in this synthesis, this dataset is the phase of 25-elements in the reflectarray. As a result, each individual contains 25 x 7 = 175 bits string. Next, for each subpopulation, 1200 individuals are chosen randomly by the code. There are four subpopulations thus total of 4800 individuals are chosen. These individuals are used to compute the radiation pattern and this pattern is compared with the predetermined pattern. This predetermined pattern is divided into some regions as shown in Table 18 and Figure 49.

Table 18 Synthesis code regions (numerically)

1st region	-90° - (-30°)	Far side lobe region in the left
2nd region	-30° - (-1°)	Near side lobe region in the left
3rd region	-1° - (1°)	Main beam increase region
4th region	1° - (5°)	Tip of cosecant square beam
5th region	5° - (20°)	Main cosecant beam region
6th region	20° - (36°)	Main cosecant beam region
7th region	36° - (38°)	Cosecant square decrease region to right hand side lobes
8th region	38° - (90°)	Far side lobes in the right

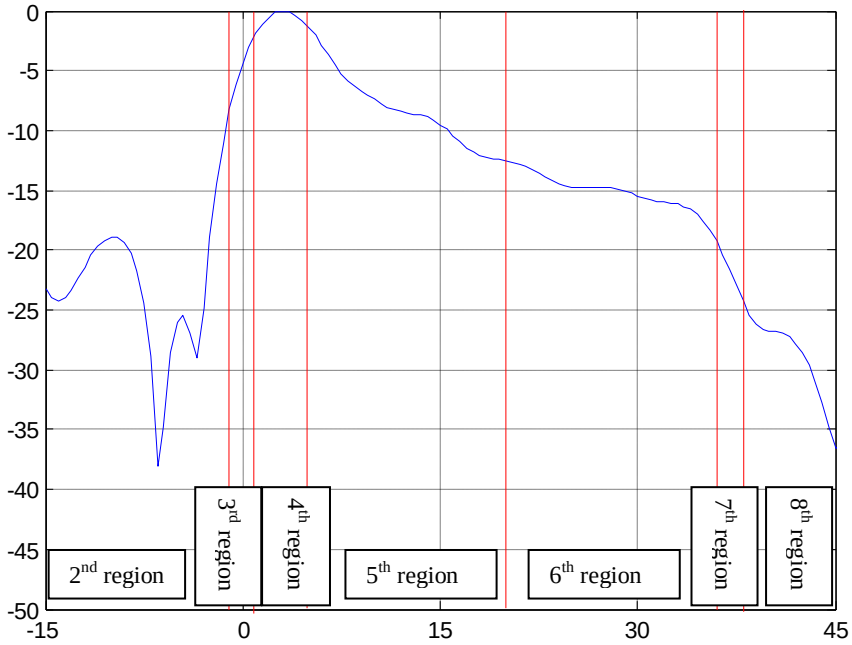

Figure 49 Synthesis code regions (graphically)

In Figure 49, there are three parallel lines with blue, cyan and black colours. These lines constitute a mask for the synthesis code. Cyan coloured line represents the desired pattern and other two represent the error in synthesis. In the synthesis code, this error is 1 dB and other two lines have 1 dB difference in any region with the desired line. This mask is important in 3rd, 4th, 5th, 6th and 7th regions. In other two regions, it is nearly impossible to synthesize the pattern in predefined mask so these two regions just limit the maximum side lobe level.

Three important genetic algorithm concepts, fitness, error and weights are defined as follows. Weights are used to arrange the regions according to their importance. In this synthesis, weights of 5th and 6th regions are relatively high with respect to other regions. Also at first, these two regions are united but since this region has high importance, a point between 5° and 36° is chosen and optimization is performed here. Error means that the total of differences of the amplitudes between the desired pattern and the synthesized pattern multiplied

by the weights in each angle. Generally, error is set to a very low value and it is not possible to reach this value. In this synthesis, this value is set to 0.01. Fitness represents the proximity of the desired pattern and the achieved pattern. This value is the inverse of corresponding error. For example, if the error values for three individuals are 50, 100 and 15, then the corresponding fitness values are 0.02, 0.01 and 0.06667. Higher fitness value shows that the synthesized pattern is closer to the desired pattern than the others. Next, best individuals denoted as elite selection are chosen in subpopulation and put in a pool, and using all individuals, including the best individuals, children are formed. These children have two randomly chosen parents from subpopulation. When two parents are picked, there is a number generated by the code between 0 and 1, and this value is compared with "the probability of crossover". This value is set to 0.8-0.9, because it is needed to mate parents but a small probability is introduced for non-mating. If crossover operation is selected, from those parents, one random bit and the bit string before this bit are selected from first parent and similarly one random bit and the bit string before this bit are selected from the second parent and these two strings are crossed over. This step is shown in Figure 50. If there are 360 individuals are preselected, 840 children are formed. Thus new subpopulation is composed of 1200 individuals. This process is done sub-iteration number times for all subpopulations. In the next step, equal number of individuals is taken from each subpopulations and population class is formed. By applying a number of times of iteration, forming children operation is performed. In this step, the best individual, in other words the one has best fitness, is chosen. This length of the whole process depends on both the loop iteration and iteration number. The individuals are found after all loop iterations are performed. These individuals are compared by their fitness and the best individual is chosen.

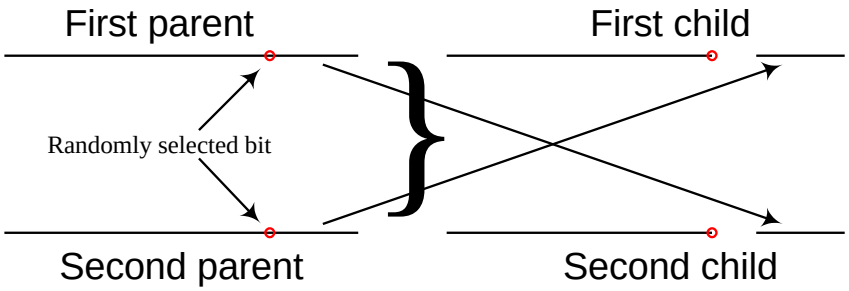

Figure 50 Children formation

As described above, all processes include probability. Also there is an additional probability process used in this code. It is called mutation. Mutation is done with a very small probability and inverts 4 bits' value (i.e. 1 to 0 or vice versa) for predetermined number of mutants. Mutants are selected randomly after each reproduction stage. At mutation stage, reproduced individuals are selected among subpopulations or population. These mutant numbers are determined at the beginning of the code. At this stage, the code randomly generates a number between 0 and 1, and if this value is smaller than the "probability of mutation", then mutation is done. Typically, this probability is set to a low value.

Table 19 Parameters used in genetic algorithm code

Error limit	0.01	Global mutant parent number	400
Loop iteration	20	Mutant bit number	4
Antenna number	25	Probability of mutation	0.2
Subpopulation density	1200	Global probability of mutation	0.3
Subpopulation number	4	Probability of crossover	0.8
Population density	1000	Elite selection	0.3
Sub iteration number	200	Amplitude bit number	1
Iteration number	400	Phase bit number	7
Selection threshold org	4.1	Phase upper value	2π
Mutant parent number	200	Phase lower value	0

3.5 Phase compensation

Reflectarrays are illuminated with a feed horn similarly as in reflector antennas, which radiate spherical waves. Since reflectarray is a flat structure, these spherical waves cause phase taper starting from the middle and achieve its peak at the edge of the array given in Figure 51. In other words, since the waves are spherical, because of the path difference from the phase center of the feed to the array elements, phases of incoming electric fields' to elements in the array are lagging depending on the position of elements in the array. Thus, the array design which is done assuming plane wave incidence must be modified. Graphical representation of these phenomena is shown in Figure 51.

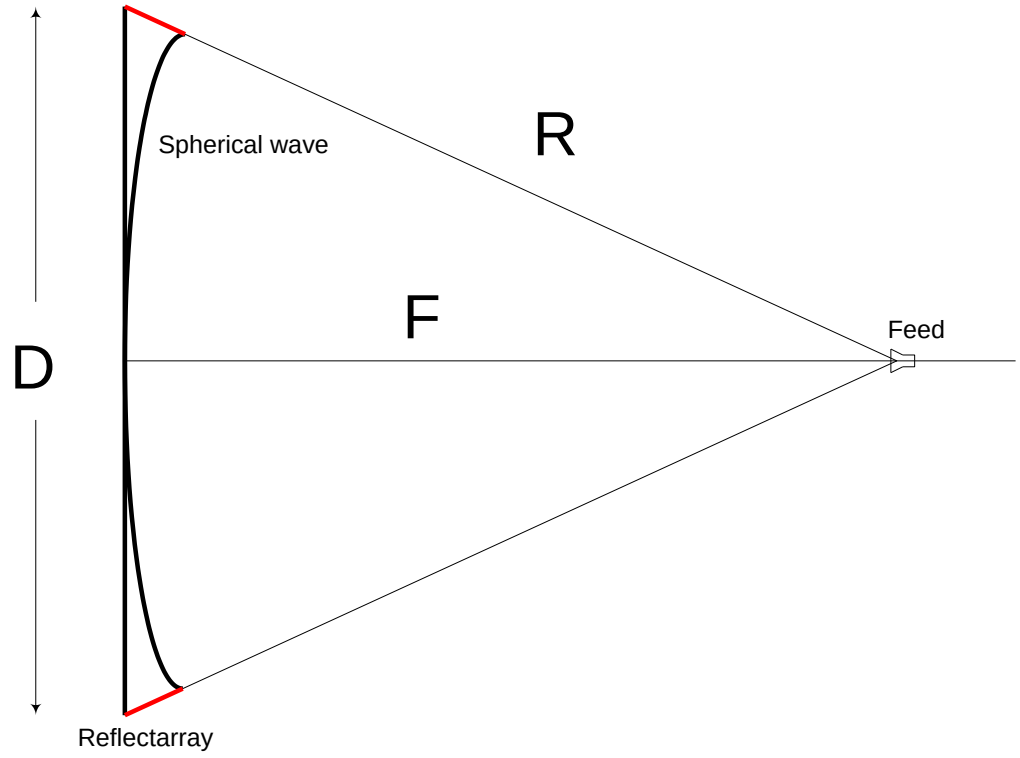

Figure 51 Reflectarray structure

Throughout the derivations, the phase in the middle of the array is the reference point. It is important to note that feed is located across the middle of the array.

In the beginning, maximum phase difference caused by the path difference which is the red line in Figure 51 should be found. Phase difference between any patch and the center element can be found by replacing the D in (7) with the distance of the observed patch to the center element

$$\varphi_{max} = k * \left(\sqrt{F^2 + \frac{D^2}{4}} - F \right) \tag{7}$$

where ϕ_{max} is the maximum phase that should be compensated, k is the wave number, F is the focal distance and D is the maximum antenna diameter. ϕ_{max} dependence on *F* and *D* are presented in Figure 52 and Figure 53, respectively. For 2D arrays, phase of each cell with a coordinate (x,y), if the center element is in the origin, is that:

$$\varphi_{max} = k * \left(\sqrt{F^2 + x^2 + y^2} - F \right) \tag{8}$$

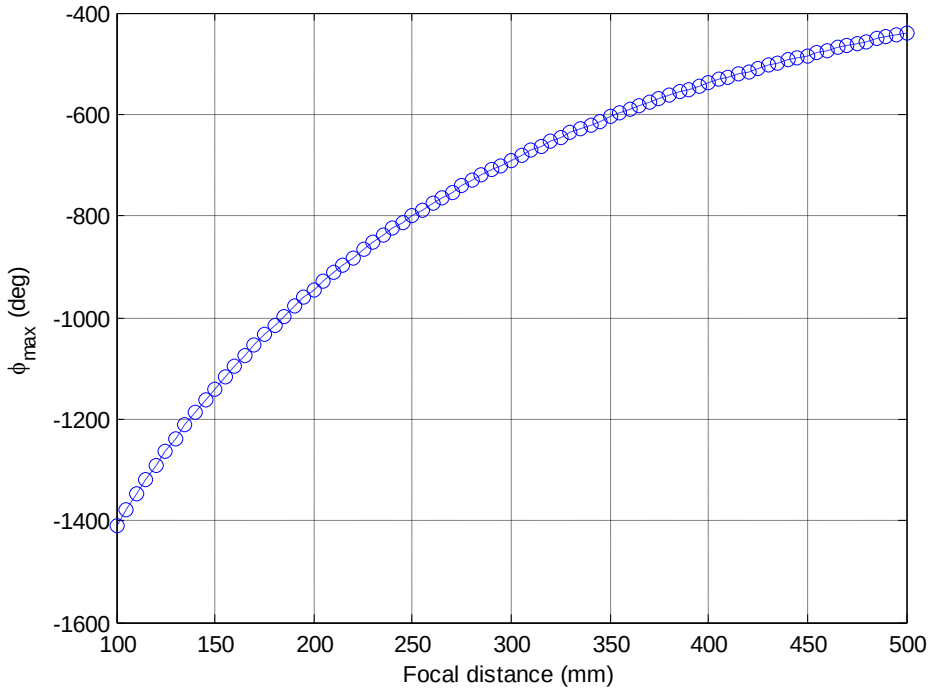

Figure 52 Effect of focal distance on ϕ_{max} (D=400mm)

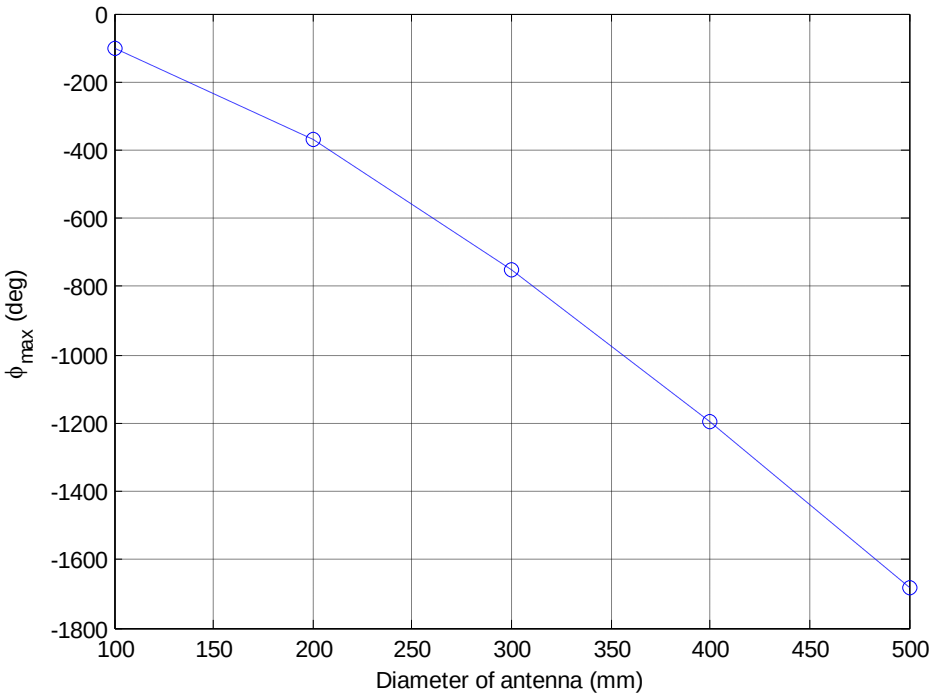

Figure 53 Effect of diameter (F=138 mm)

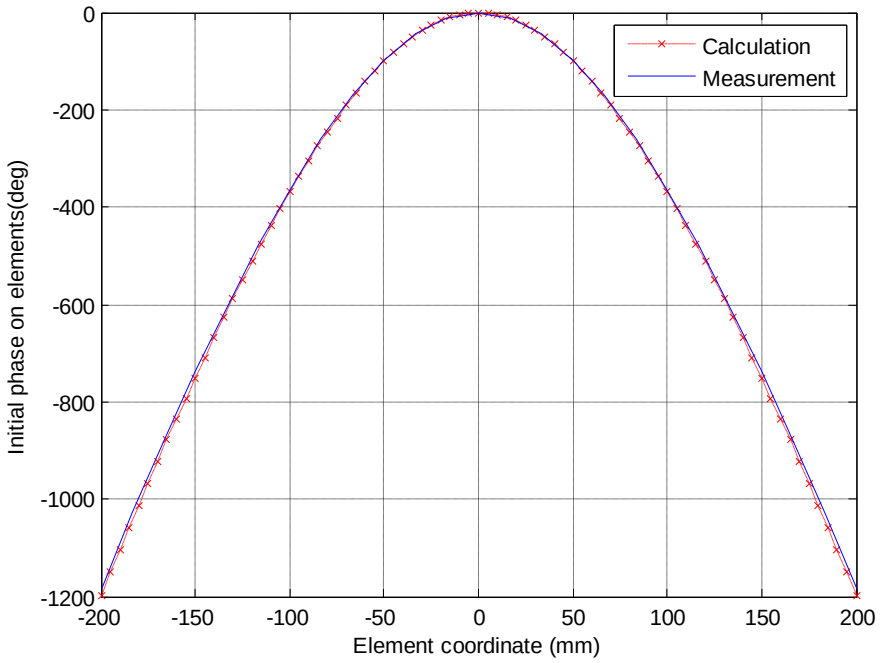

Figure 54 Phase variation that should be compensated over array location (F=138 mm)

From Figure 53, if the focal point remains constant, with increasing antenna diameter, ϕ_{max} increases. This is obvious because angle of incidence increases with higher *D*. In Figure 52, with constant antenna diameter and increasing focal length, ϕ_{max} decreases. This result is consistent with the previous one; if the diameter remains constant, far focal point means a decrease in the angle of incidence for elements at the edges of the array. Thus smaller phase difference is observed.

Since these parameters cause difficulties for optimizing the design, using $\frac{F}{D}$ ratio would be better. Modifying (7) results,

$$\phi_{max} = k * \left(\sqrt{1 + \frac{1}{4 * \left(\frac{F}{D}\right)^2}} - 1 \right) \tag{9}$$

(9) implies that high $\frac{F}{D}$ ratio reduces ϕ_{max}.

In wideband applications, ϕ_{max} may give intuition about bandwidth, as shown in following derivation.

$$\phi_{max} = \frac{2 * \pi * f}{c} * \left(\sqrt{1 + \frac{1}{4 * \left(\frac{F}{D}\right)^2}} - 1 \right) \tag{10}$$

In (10), if ϕ_{max} is evaluated for two frequencies namely f_1 and f_2, then bandwidth can be predicted within a given limit of ϕ_{max} difference.

Next step is to find the total phases that should be used in the reflectarray. To do so, phase values in Figure 54 and Table 17 should be combined. In Figure 54, calculated phase values are negative, which shows that incoming wave is incident upon the patch with some delay with respect to reference

patch. Thus, this lagging phase should be compensated for each patch and phase values in Table 17 should be applied to phases of corresponding patches.

3.6 Design method and simulations with results

Synthesis code is used to find the phases of one row with 25 elements. From Figure 45, it is concluded that adjacent rows of the center row are illuminated with nearly the same amplitude level. Thus, reflection phases for the center row, which are found with the phase only synthesis method, are used for the adjacent rows of the center row. Simulations are performed and it is seen that the results are better than the previous ones. Then it is continued to apply the same procedure, i.e., additional two rows are added, one in each side and simulations are made. Until the design with seven rows, reflectarray performance increases after the addition of rows in each step. Then two rows are added and the new design has nine rows. But the simulation results of seven rows reflectarray are better than the nine row reflectarray so it is concluded that, the change in amplitude levels for the last two rows are very critical. Thus one more synthesis is done. It should be noted that, in all steps phase compensation is applied. So new phase set is synthesized using the second amplitude set, which covers the amplitudes of the 6^{th} row from the center. Moreover, phase compensation is applied to this row and adjacent two rows in both side, forming the 5^{th}, 6^{th} and 7^{th} rows in each side with respect to the center row.

It is seen from Figure 43, horn antenna has nearly the same radiation pattern in the entire frequency band of operation. Thus, amplitudes of the electric field intensity over the patches at different frequencies remain nearly constant; only phase changes as a result of the spatial phase delay. As a consequence, main lobe peak level remains almost the same in the operation band but this phasing effect can be seen in lower-amplitude part of the main beam. If one can adjust the feed distance depending on the frequency, operating frequency band increases.

To find the patch dimensions, after phase compensation, required phase values are mapped to a phase region from 0° to 360°. Best fitted patch sizes are chosen from the phase design curve that provides required phase differences between adjacent elements. After selection of the patch sizes, full reflectarray including the feed horn is simulated by HFSS®.

In the reflectarray simulation, symmetry boundary is used in the YZ-plane because the array is electrically large and it will require super computers to perform full wave simulation. Simulation setup for the reflectarray in HFSS® is shown in Figure 55. Simulated far fields are plotted in Figure 56, Figure 57, Figure 58 and Figure 59 for different frequencies.

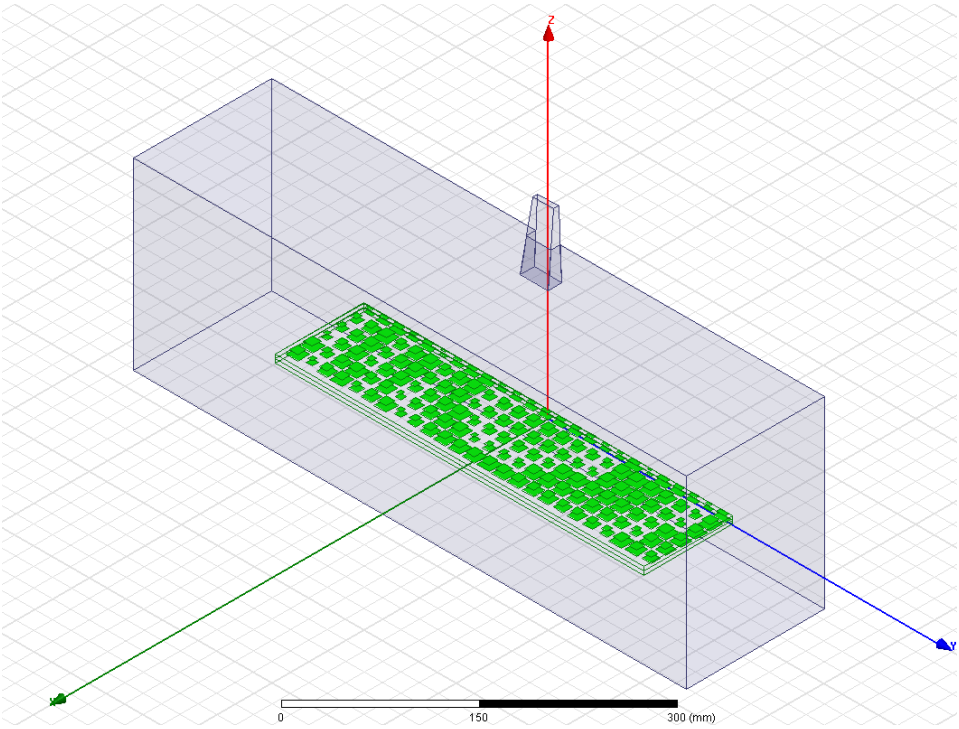

Figure 55 Simulated final design

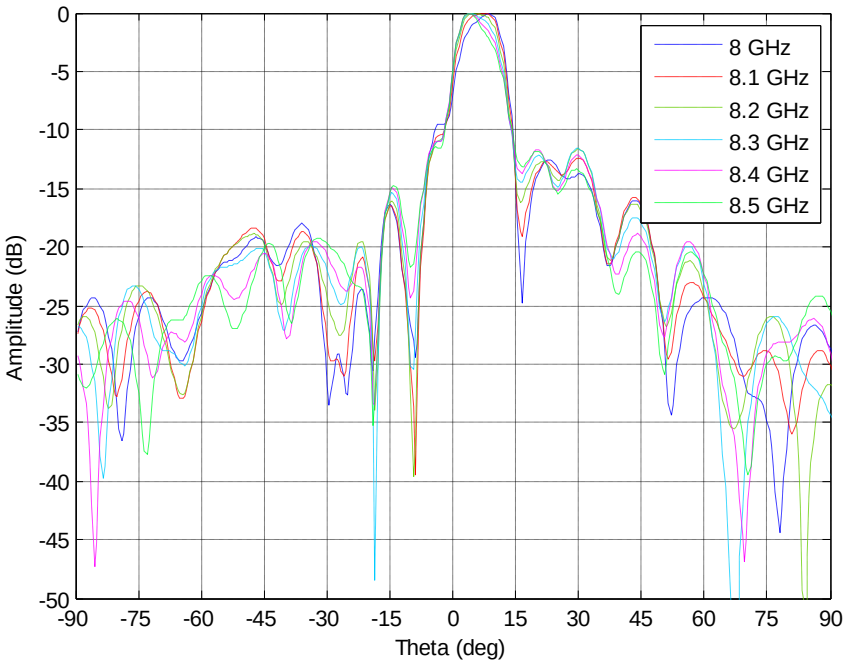

Figure 56 8-8.5 GHz cosecant square patterns

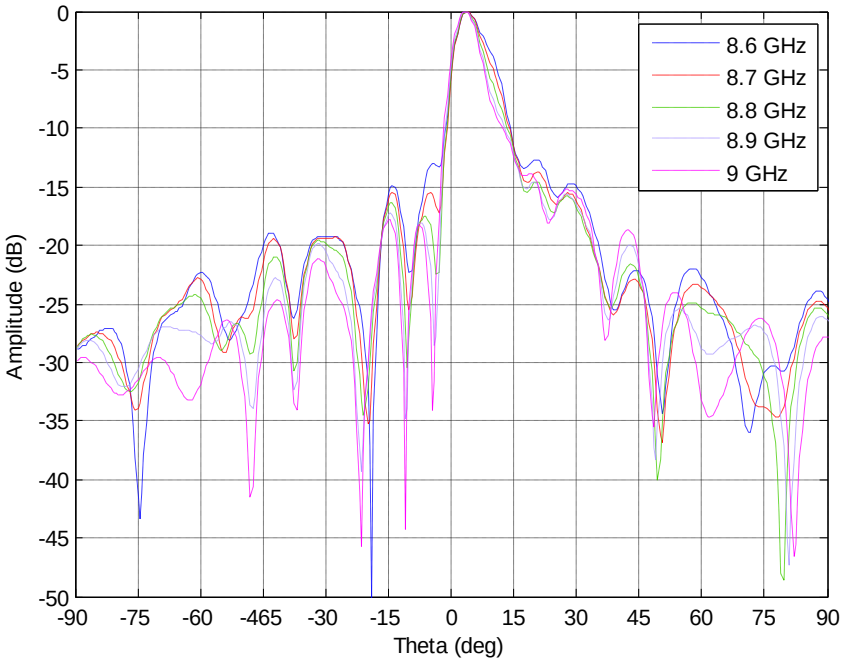

Figure 57 8.6-9 GHz cosecant square patterns

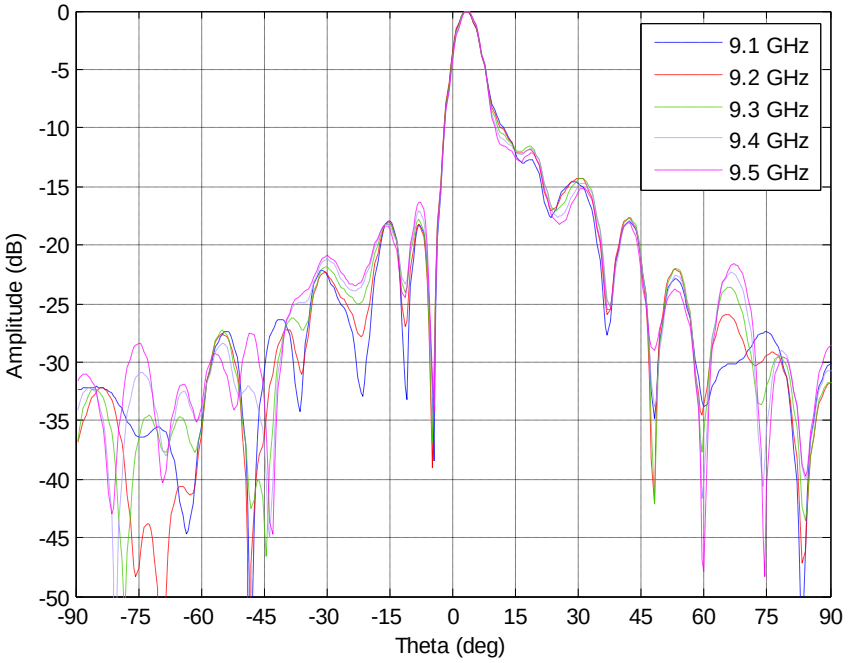

Figure 58 9.1-9.5 GHz cosecant square patterns

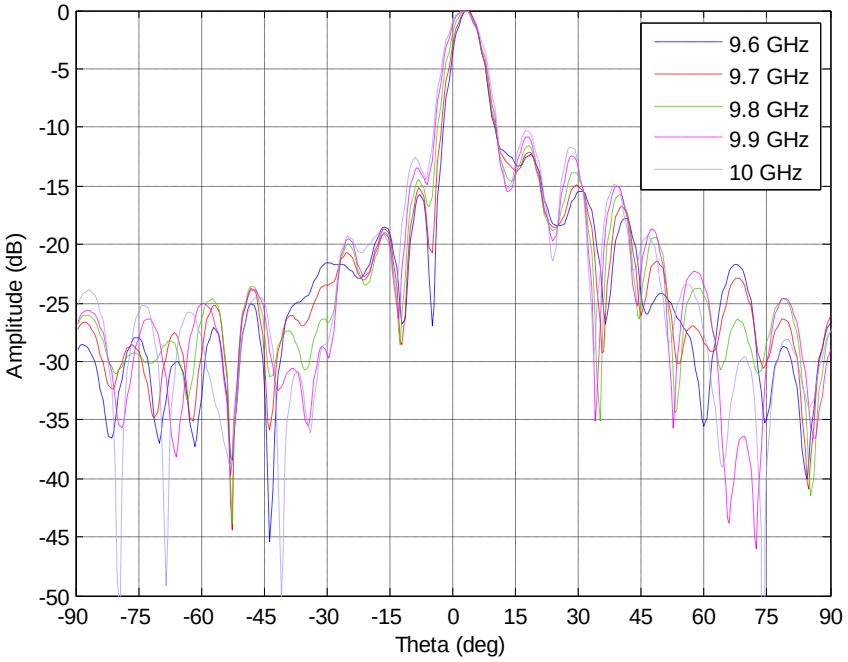

Figure 59 9.6-10 GHz cosecant square patterns

3.7 Design of a fixed rotated beam reflectarray

As another application, a reflectarray with a fixed rotated beam is designed. An array of the same dimensions and number of patches is aimed. This array is capable of rotating the beam to a fixed angle, 30° from broadside.

In array theory, to rotate a beam from broadside direction to a desired direction, progressive phase shift should be introduced. In Figure 60, this phase shift is applied to compensate the phase difference caused by |AC|, assuming the rays are parallel to each other. Thus,

$$k * d * \sin(\theta) = -\beta_p \tag{11}$$

formula is applied and progressive phase shift value (β_p) is found for 9.5 GHz. k, d, θ and β_p values are shown in Table 20.

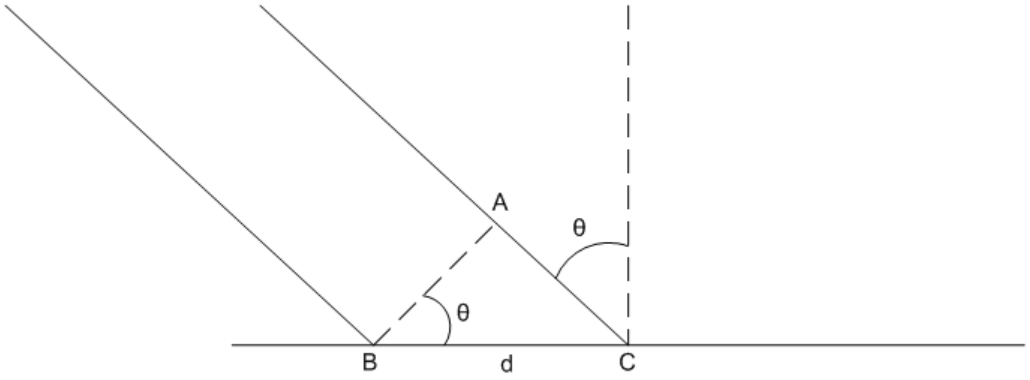

Figure 60 Progressive phase shift

Table 20 Progressive phase shift and beam rotation values for different frequencies

	9 GHz	9.5 GHz	10 GHz
$k = \frac{2 * \pi}{\lambda}$	10.8 °/mm	11.39 °/mm	12 °/mm
d	16 mm	16 mm	16 mm
β	91.14°	91.14°	91.14°
θ	31.8°	30°	28.3°

In this application, it is assumed that the progressive phase value is the same in all three frequency cases because this array is designed for the center frequency (9.5 GHz) and the phase differences for adjacent patches are adjusted for this frequency. That means, constant phase difference is applied to all patches, assuming the phase differences do not change critically when the frequency changes. Using the same design procedure, appropriate patch dimensions are selected using the phase design curve. Then full reflectarray is simulated. Simulation setup for this array is shown in Figure 61 and results are given in Figure 62. It is observed from Figure 62 that the main beam is shifted smaller than ±2.5° in the frequency band. The change in the spatial phase delay causes beam tilt but ±2.5° shift is tolerable in %10 frequency band.

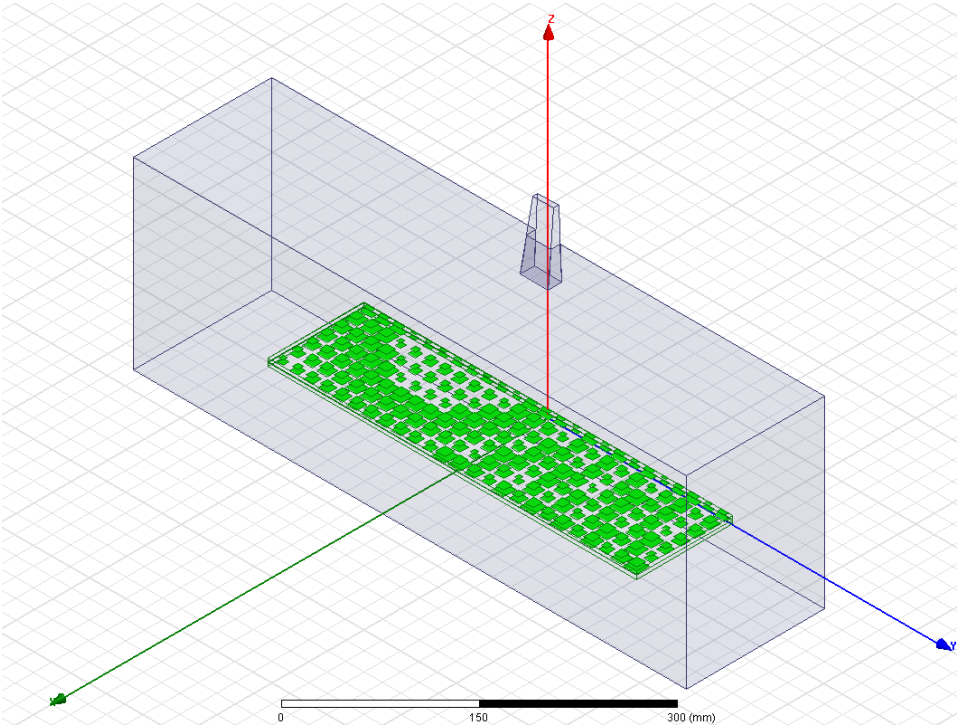

Figure 61 Simulation setup for 30° scan angle

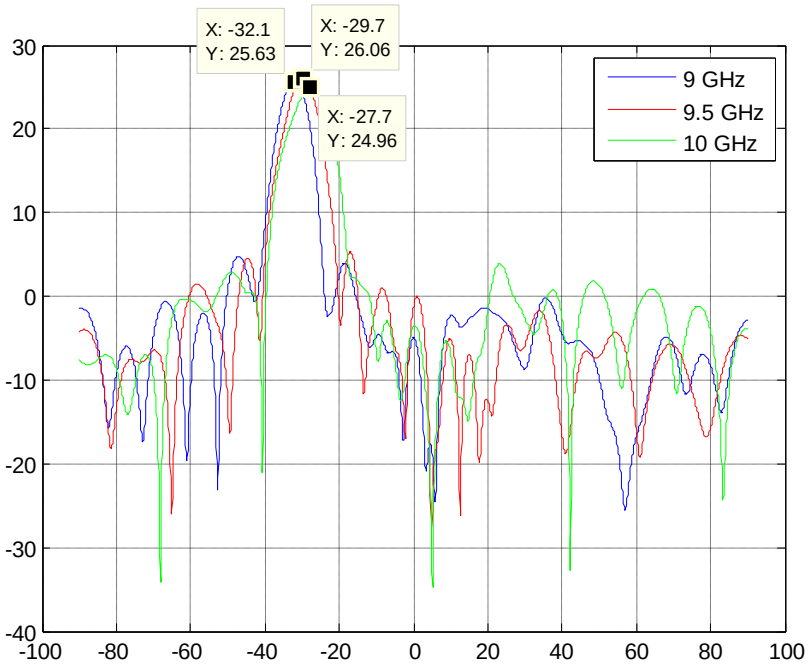

Figure 62 9-10 GHz pattern for 30° scan angle

3.8 Conclusion

Feed horn design is introduced in this chapter. Also results of the simulations and measurements are compared. Cosecant square beam synthesis code is explained briefly and required reflection phases are found. Using spatial phase distribution of the horn, phase compensation is performed and the reflectarray is designed and simulation results are presented.

CHAPTER IV

PRODUCTION OF THE REFLECTARRAY and MEASUREMENTS

4.1 Introduction

Stacked patch unit cell simulations for the suitable unit cell configuration is presented in Chapter II. Then simulations and measurements of the designed feed horn are given in Chapter III. Moreover, phase compensation concept is presented and the phases of each patch are found. Using the phases obtained from phase only synthesis method and phase design curve, the reflectarray is designed. Then this reflectarray is manufactured and measurements are performed. Measurement results compared with simulations are given in this chapter.

4.2 Production and measurements of the reflectarray

A 25 x 13 element reflectarray is designed in section 3.6. Feed antenna is produced in 5D CNC machine, which is capable of moving in x, y and z directions as well as ϕ and θ angles. Feed horn is produced as two separate pieces and these parts are connected via many screws.

4 mm foams are produced by trimming foams with 7 mm thickness. On the other hand, metallic patches on the thin dielectric layers are manufactured with photo-lithography technique. These materials are connected to each other with very thin double sided tape. In order to place and hold the feed antenna in its correct position, a metal support part is fabricated. This support part consists of

many smaller parts and these small parts are attached to each other via screws to adjust the feed horn position because of possible placement or manufacturing errors.

Produced reflectarray has been measured in Satimo Starlab spherical near field range of Aselsan Inc. Photographs of the measured reflectarray and Satimo Starlab spherical near field range are shown in Figure 63, Figure 64 and Figure 65.

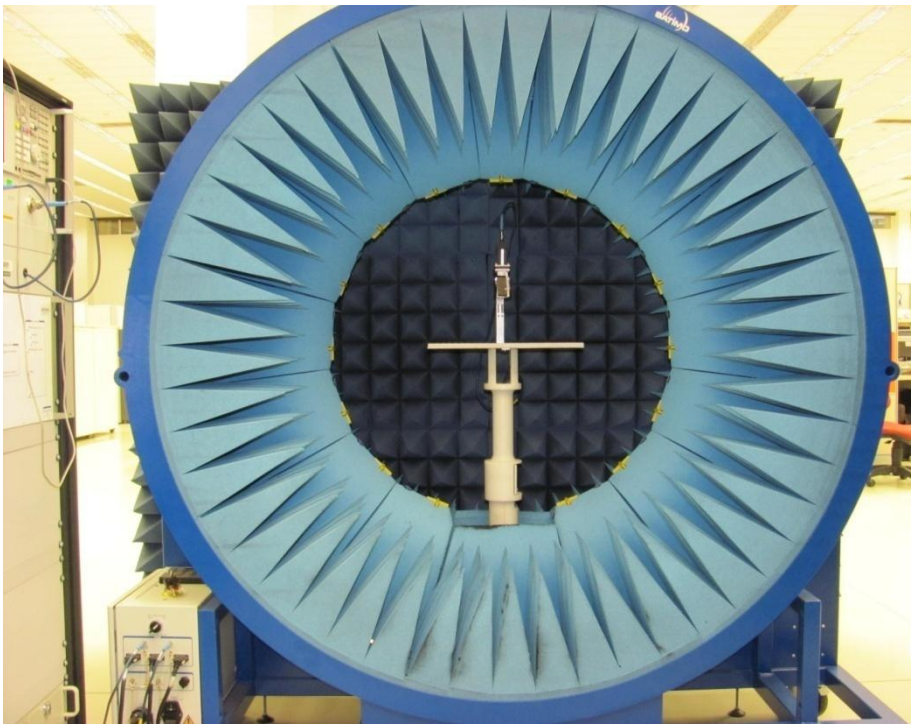

Figure 63 Satimo starlab spherical near field and reflectarray measurement setup-1

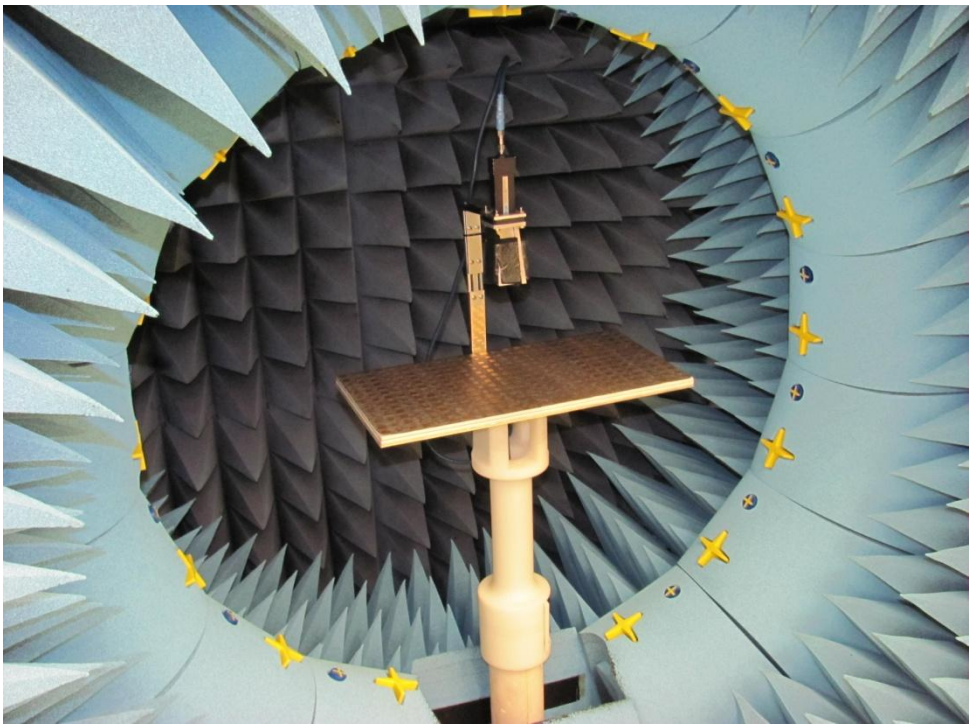

Figure 64 Satimo starlab spherical near field and reflectarray measurement setup-2

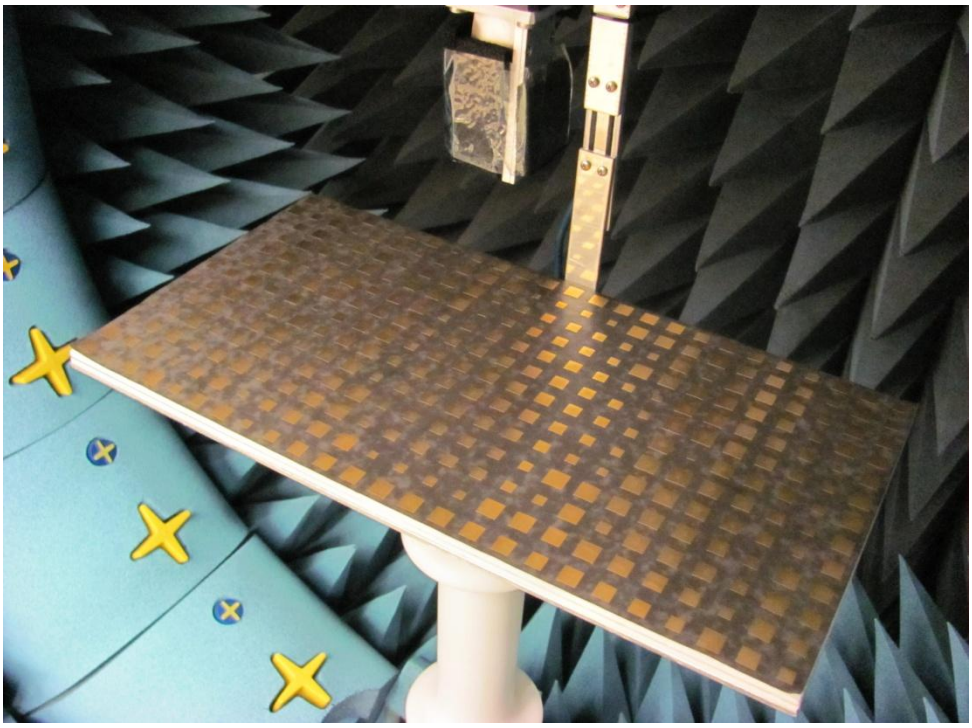

Figure 65 Satimo starlab spherical near field and reflectarray measurement setup-3

In this section, measurements in spherical near field range and simulation results are compared. For comparison, all patterns are normalized. Gain data is given in Table 21. Simulations and measurements are presented with 100 MHz steps, from 8.5 GHz to 10 GHz and are plotted in Figure 66 to Figure 97. Cross polarization levels for 9.2 GHz in azimuth and elevation cuts are given in Figure 97 and Figure 98 respectively.

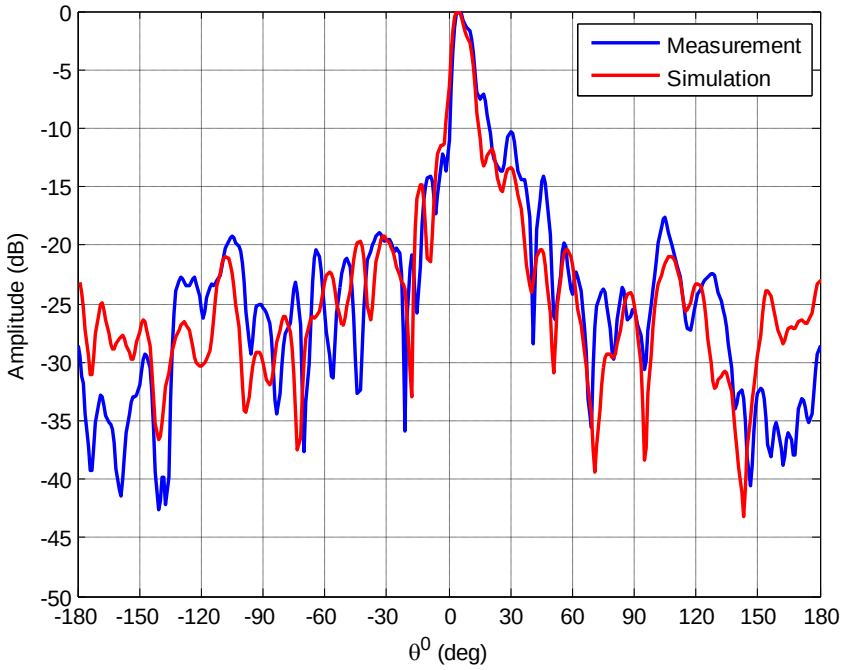

Figure 66 Normalized pattern of simulated and measured reflectarray at 8.5 GHz (azimuth cut)

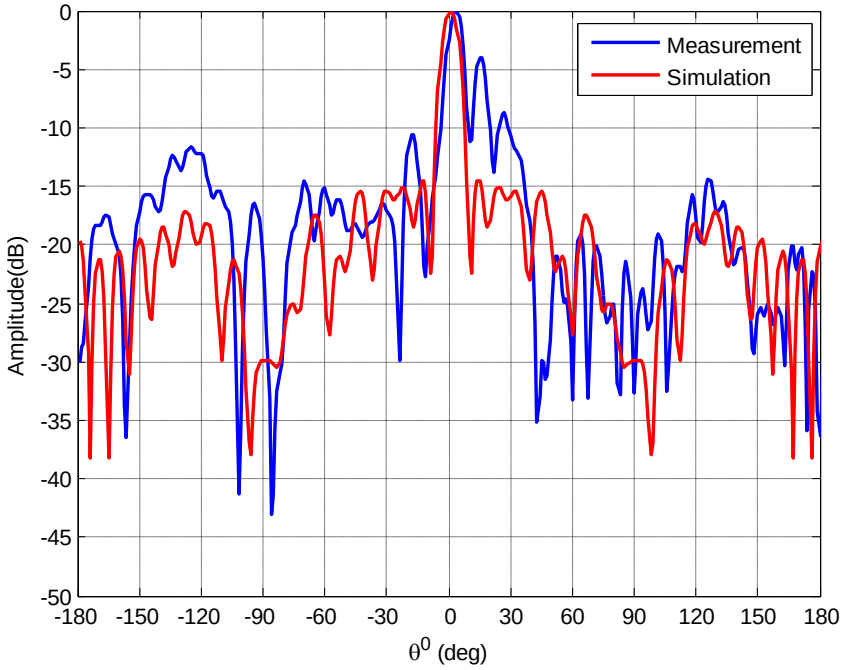

Figure 67 Normalized pattern of simulated and measured reflectarray at 8.5 GHz (elevation cut)

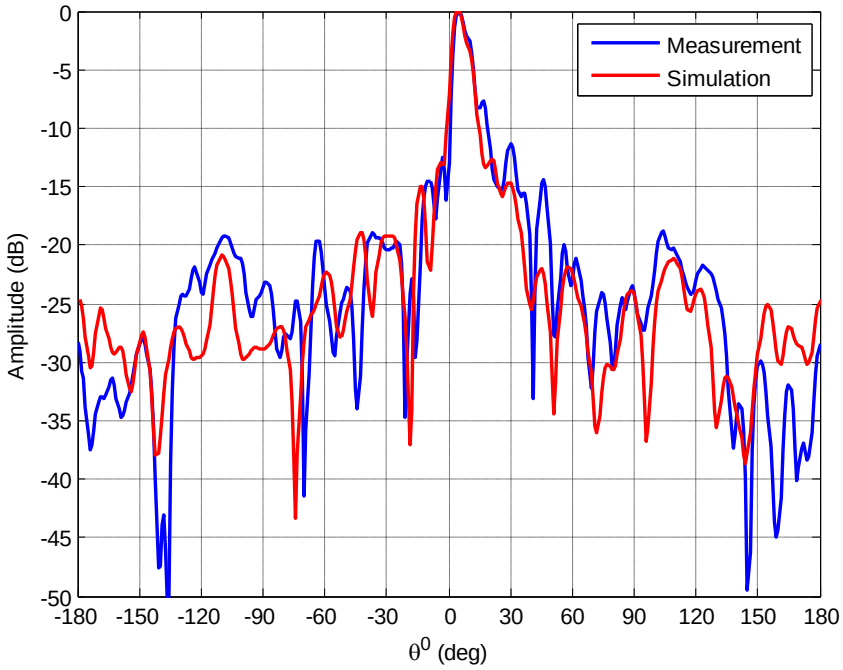

Figure 68 Normalized pattern of simulated and measured reflectarray at 8.6 GHz (azimuth cut)

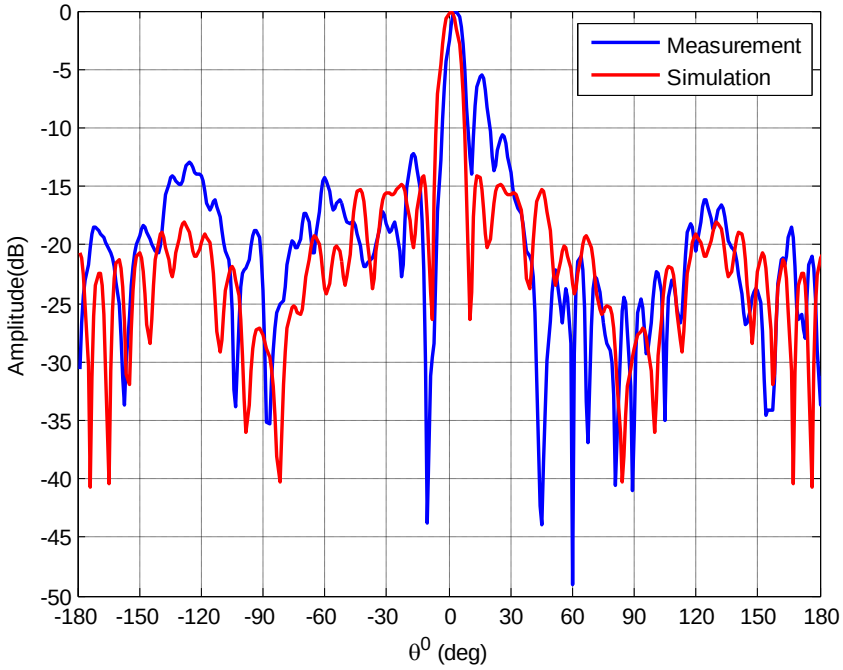

Figure 69 Normalized pattern of simulated and measured reflectarray at 8.6 GHz (elevation cut)

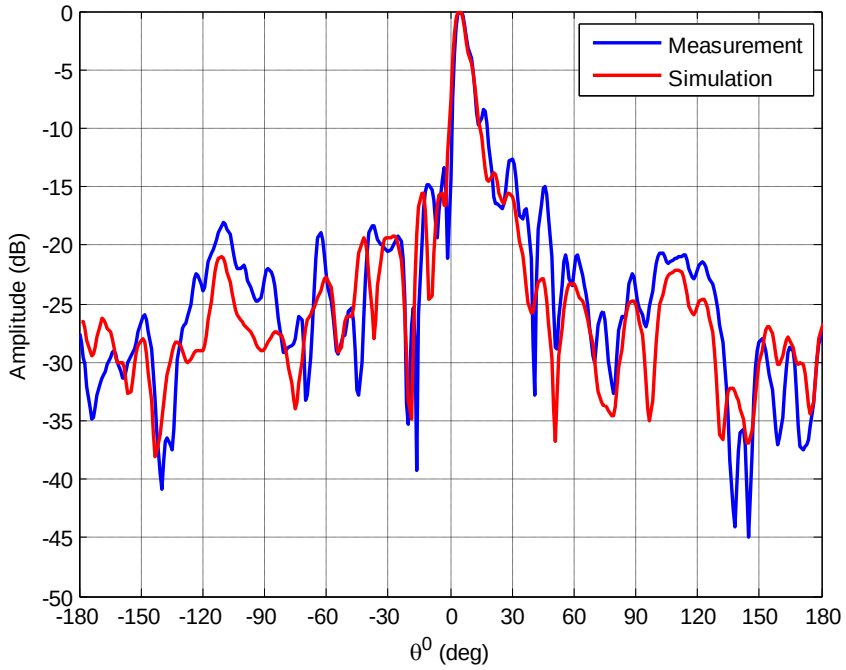

Figure 70 Normalized pattern of simulated and measured reflectarray at 8.7 GHz (azimuth cut)

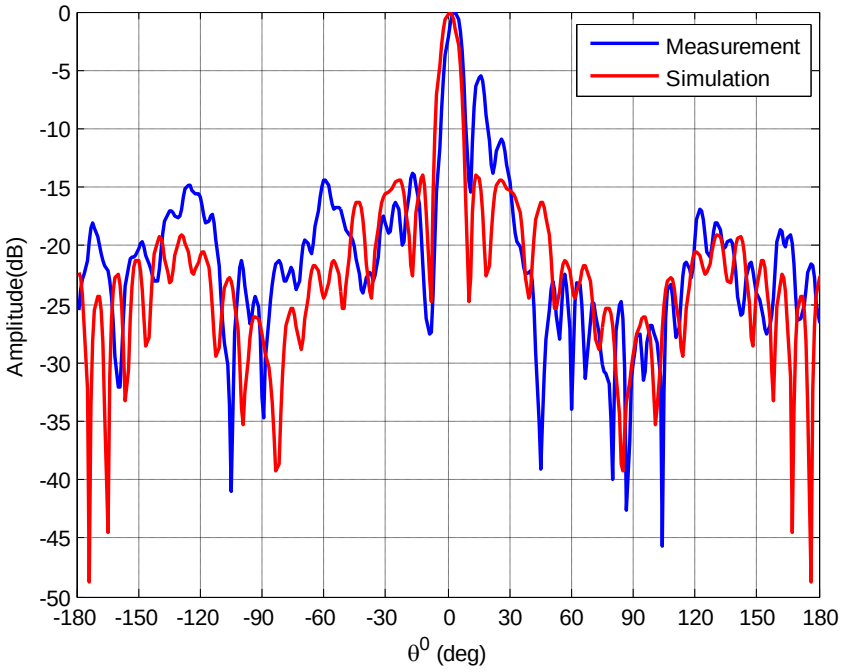

Figure 71 Normalized pattern of simulated and measured reflectarray at 8.7 GHz (elevation cut)

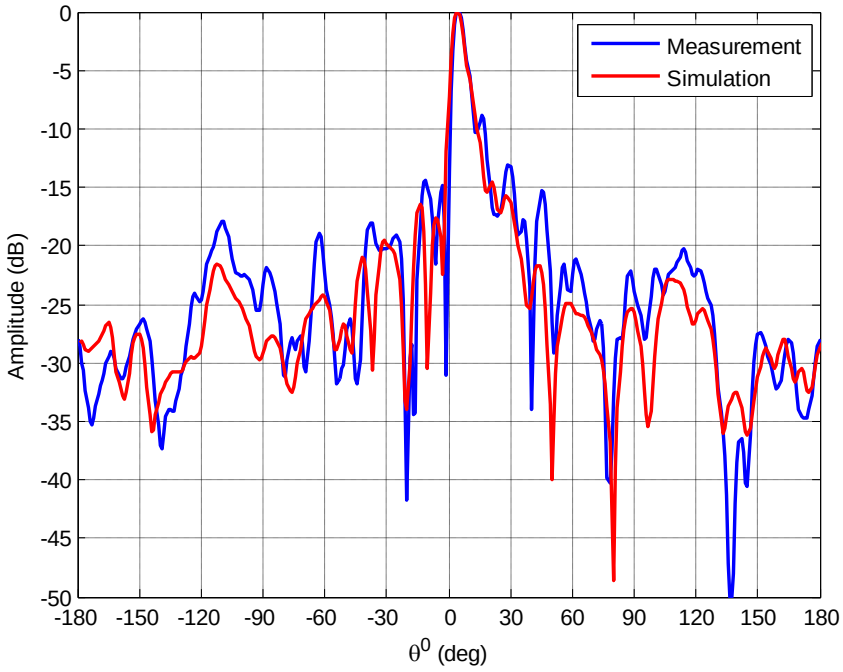

Figure 72 Normalized pattern of simulated and measured reflectarray at 8.8GHz (azimuth cut)

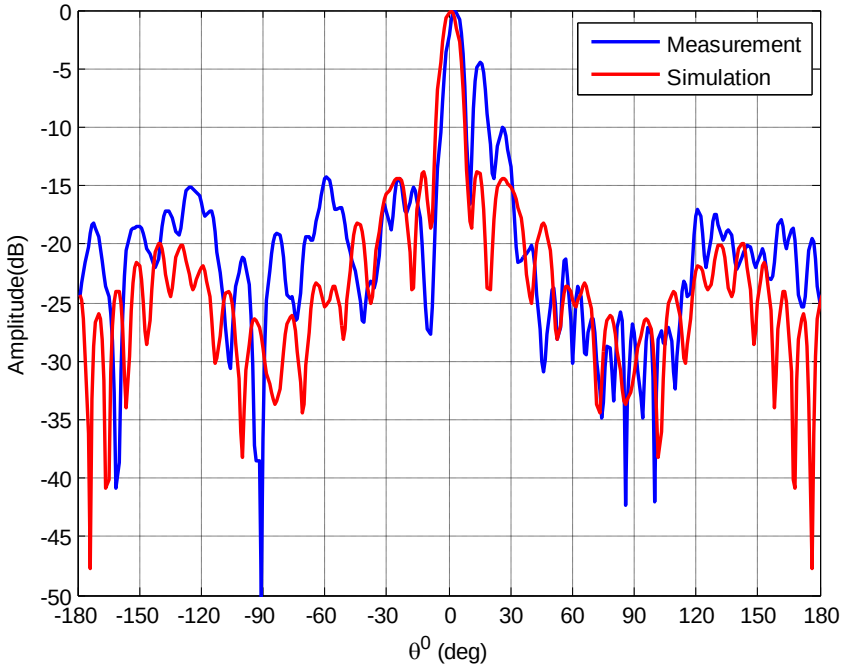

Figure 73 Normalized pattern of simulated and measured reflectarray at 8.8 GHz (elevation cut)

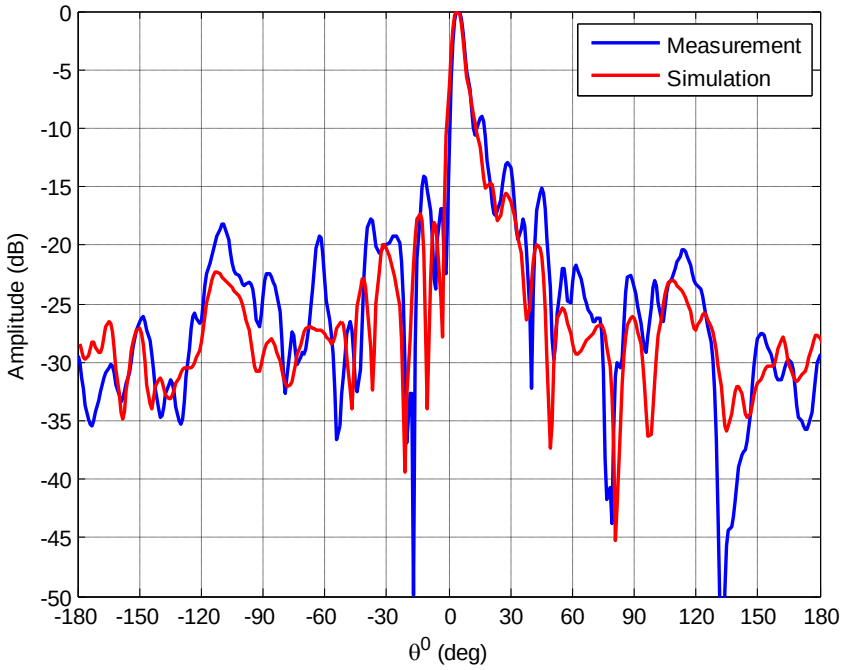

Figure 74 Normalized pattern of simulated and measured reflectarray at 8.9 GHz (azimuth cut)

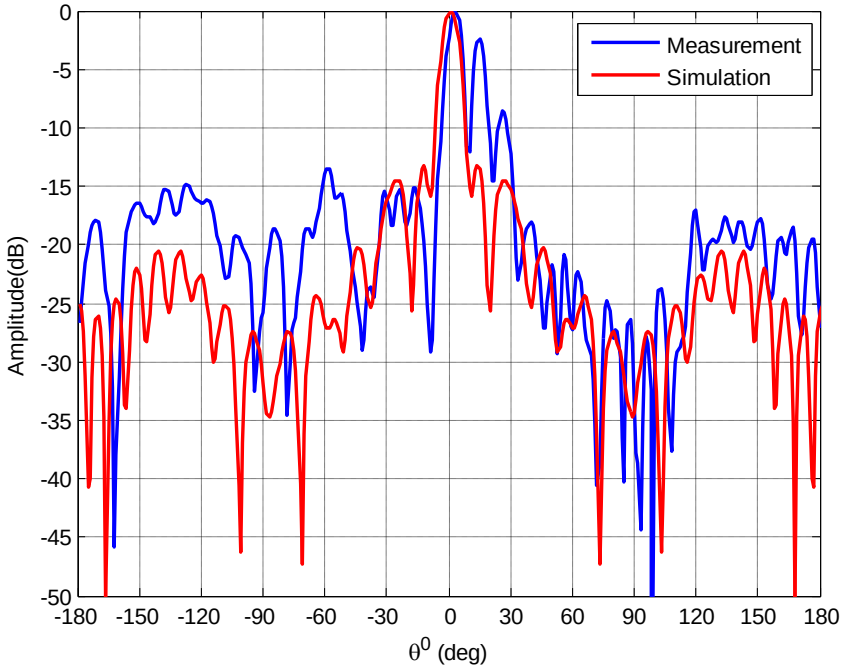

Figure 75 Normalized pattern of simulated and measured reflectarray at 8.9 GHz (elevation cut)

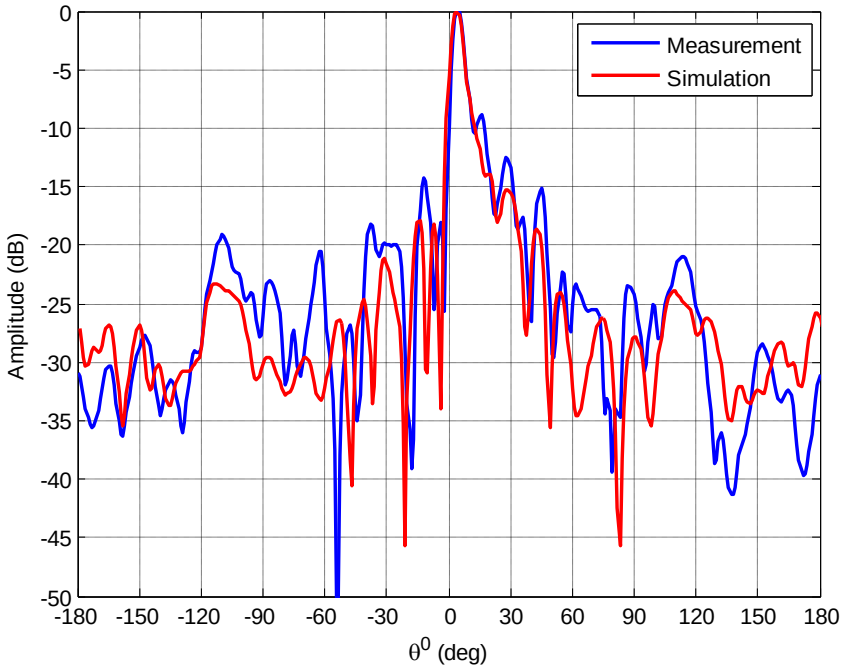

Figure 76 Normalized pattern of simulated and measured reflectarray at 9 GHz (azimuth cut)

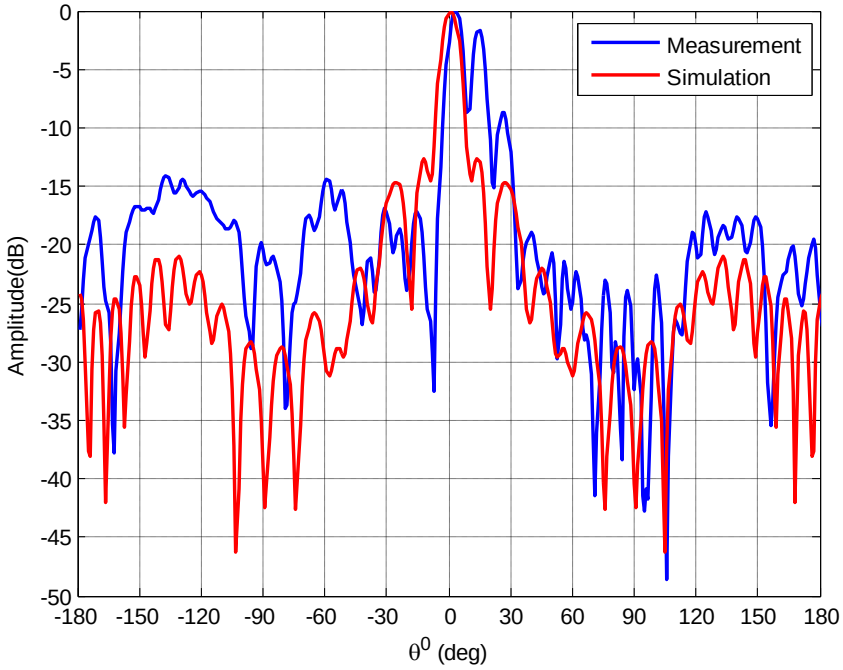

Figure 77 Normalized pattern of simulated and measured reflectarray at 9 GHz (elevation cut)

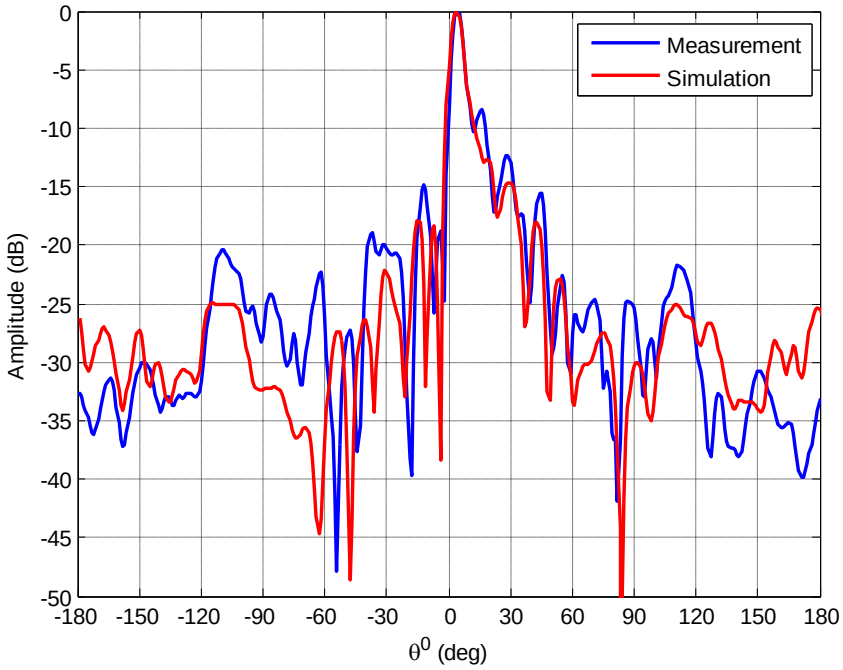

Figure 78 Normalized pattern of simulated and measured reflectarray at 9.1 GHz (azimuth cut)

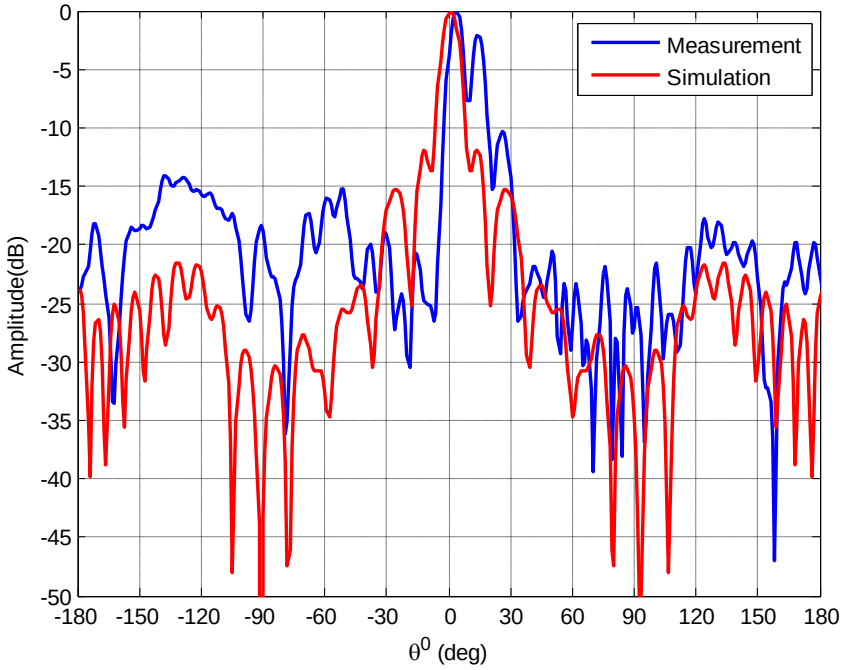

Figure 79 Normalized pattern of simulated and measured reflectarray at 9.1 GHz (elevation cut)

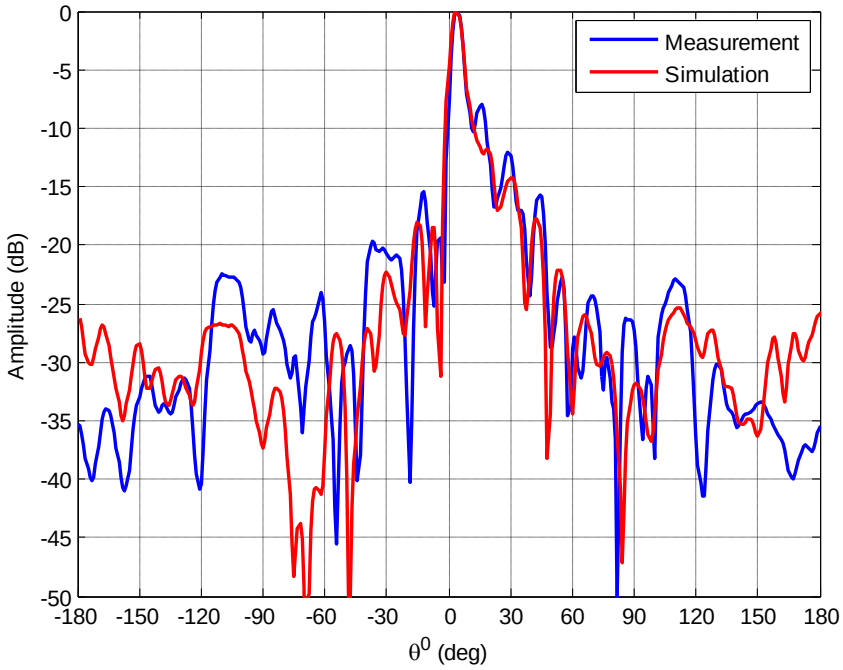

Figure 80 Normalized pattern of simulated and measured reflectarray at 9.2 GHz (azimuth cut)

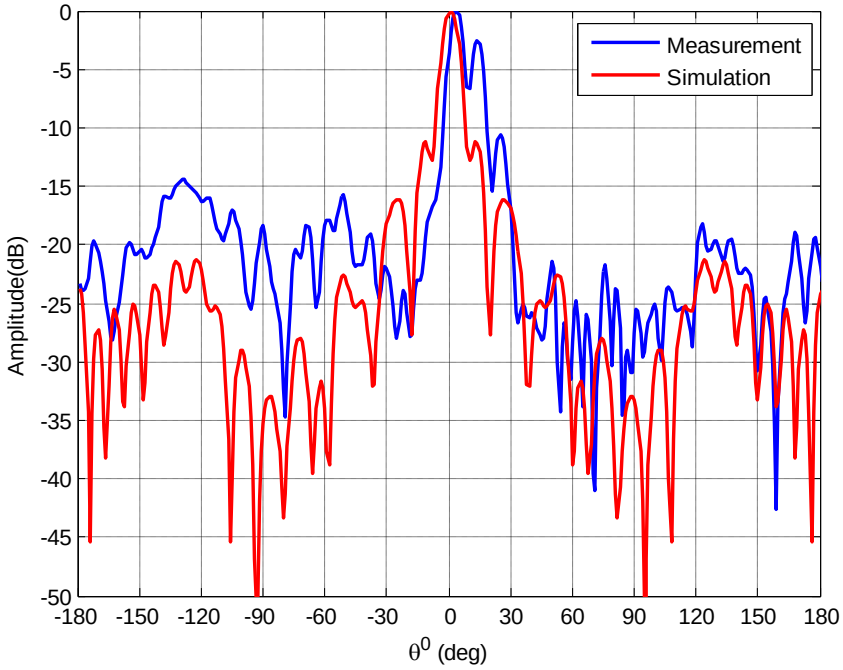

Figure 81 Normalized pattern of simulated and measured reflectarray at 9.2 GHz (elevation cut)

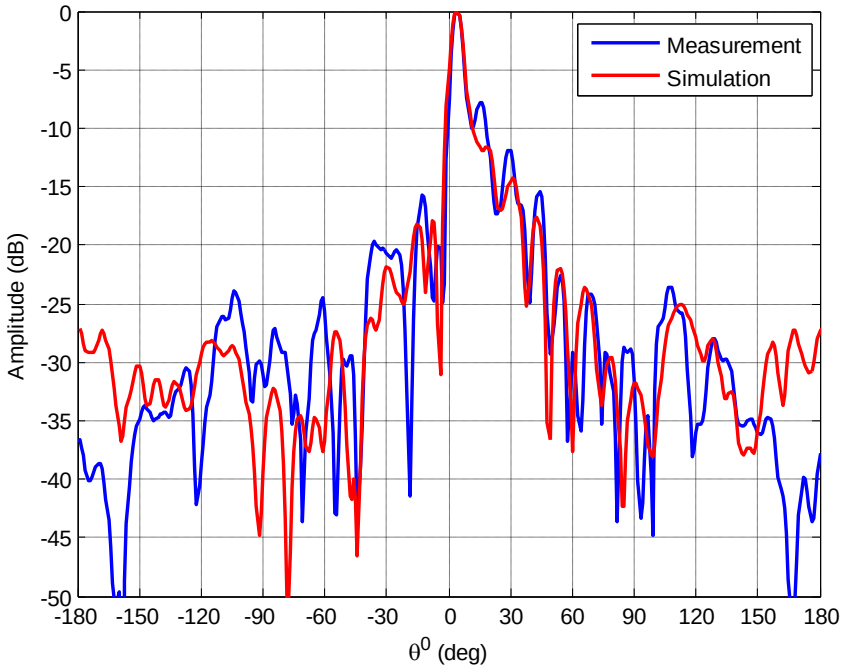

Figure 82 Normalized pattern of simulated and measured reflectarray at 9.3 GHz (azimuth cut)

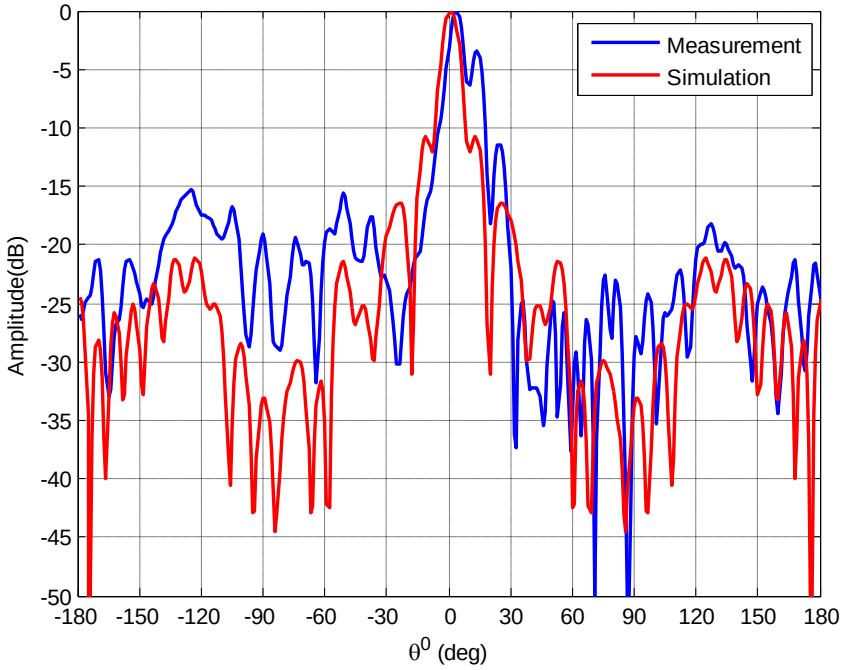

Figure 83 Normalized pattern of simulated and measured reflectarray at 9.3 GHz (elevation cut)

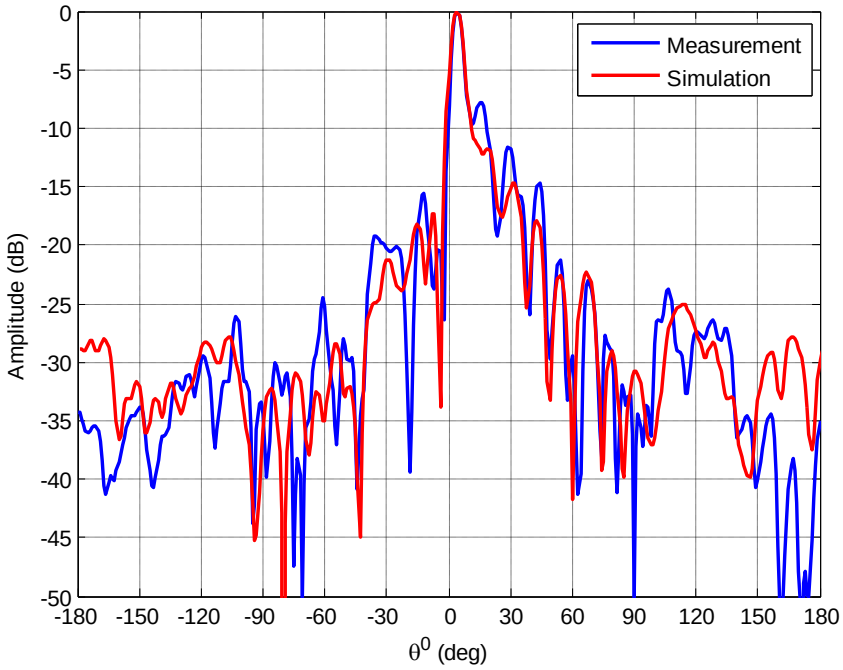

Figure 84 ***Normalized pattern of simulated and measured reflectarray at 9.4 GHz (azimuth cut)***

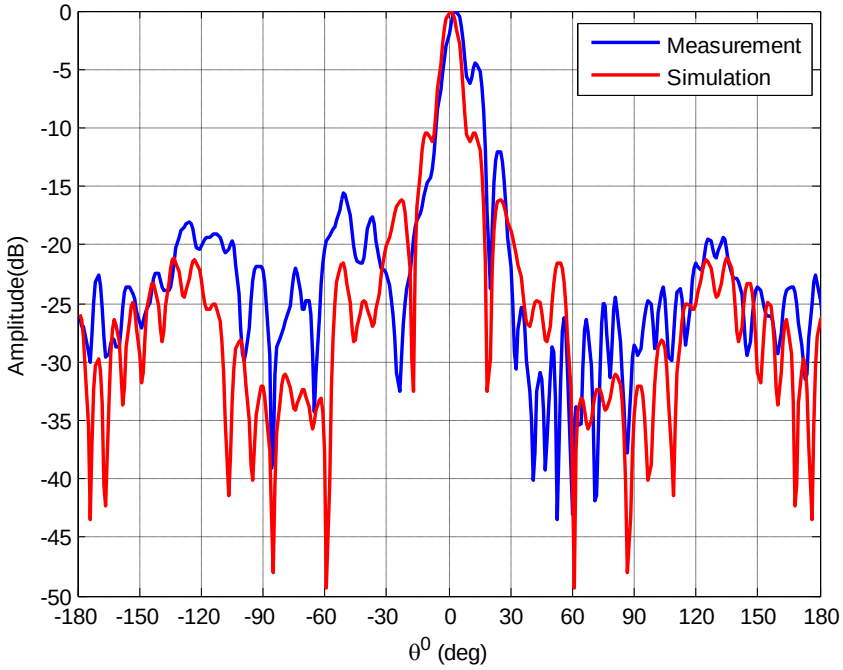

Figure 85 Normalized pattern of simulated and measured reflectarray at 9.4 GHz (elevation cut)

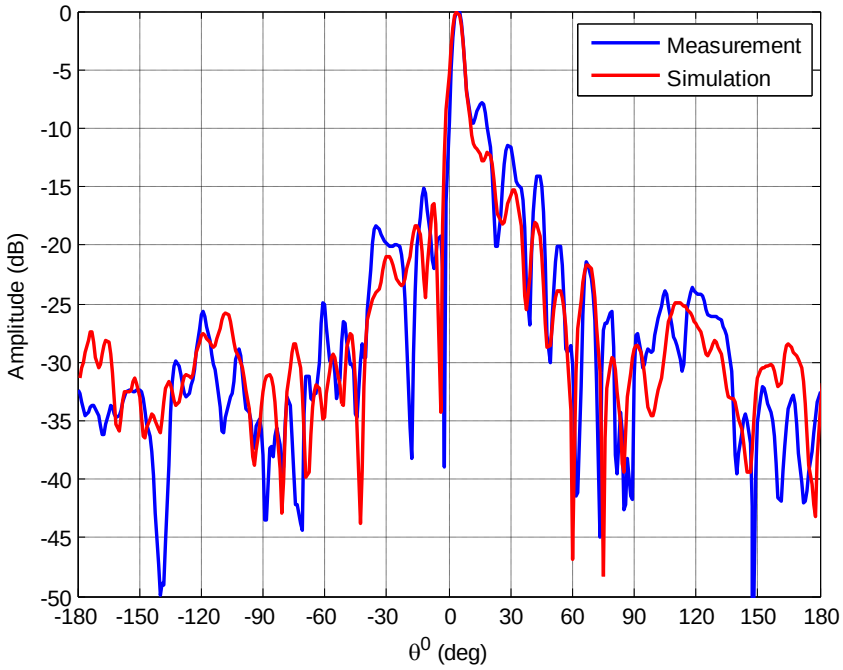

Figure 86 Normalized pattern of simulated and measured reflectarray at 9.5 GHz (azimuth cut)

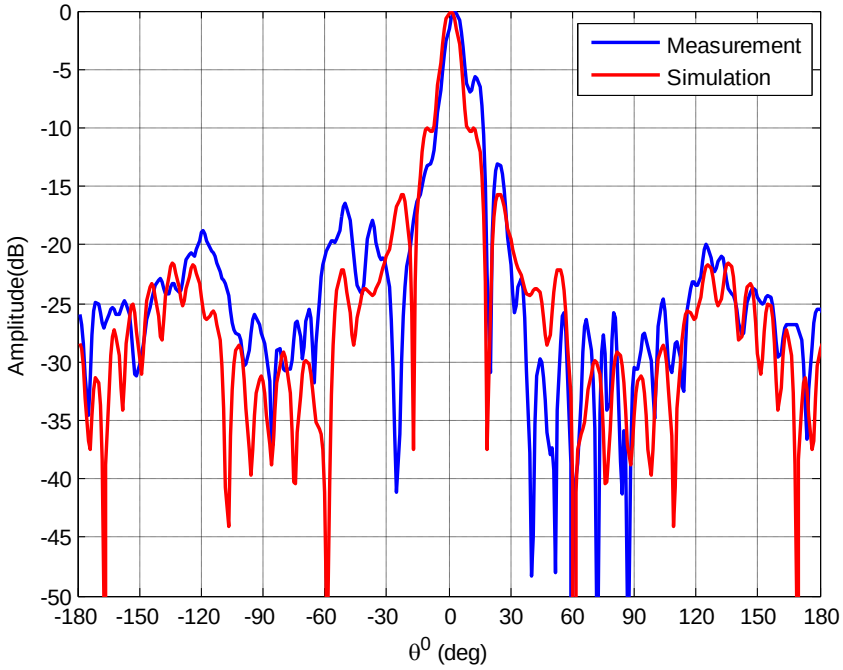

Figure 87 Normalized pattern of simulated and measured reflectarray at 9.5 GHz (elevation cut)

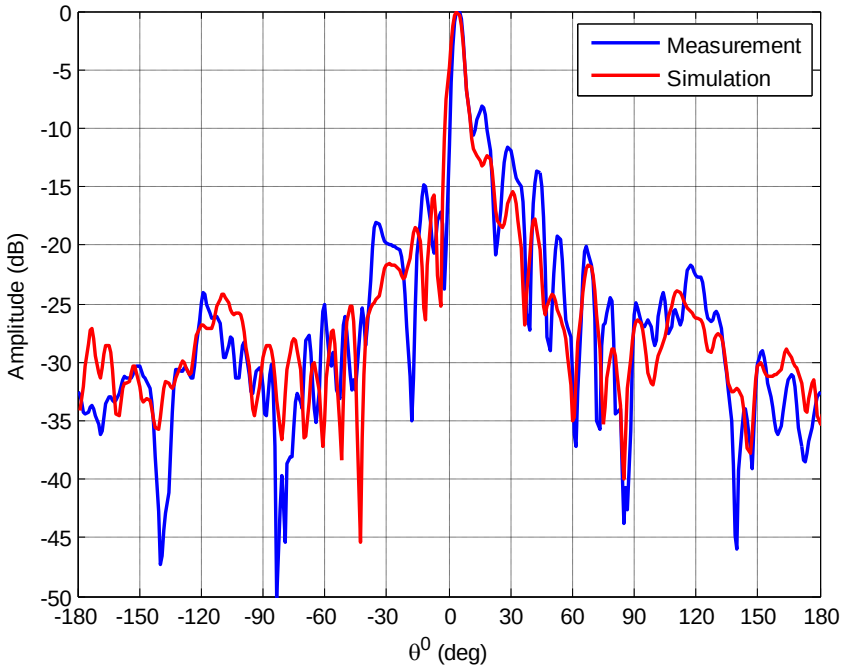

Figure 88 Normalized pattern of simulated and measured reflectarray at 9.6 GHz (azimuth cut)

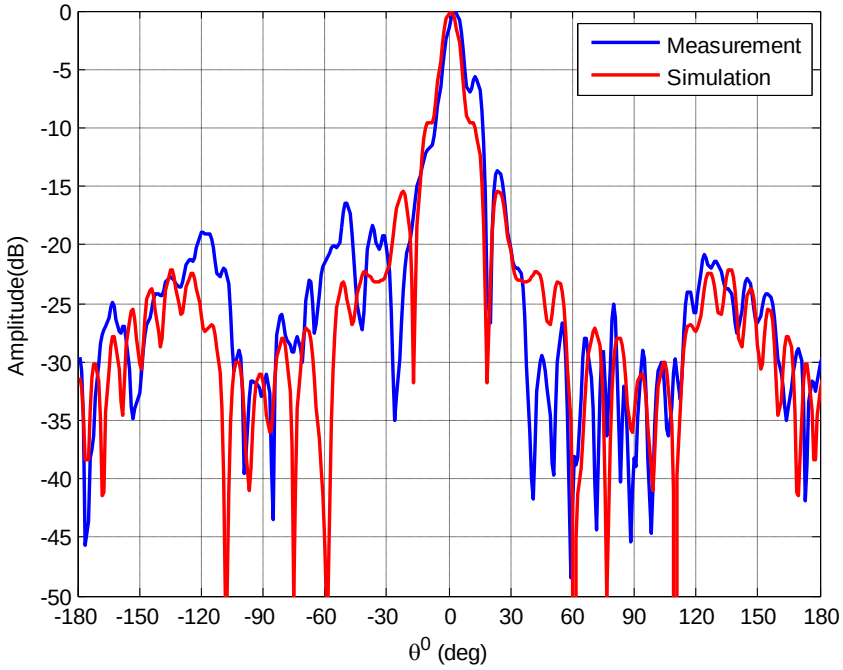

Figure 89 Normalized pattern of simulated and measured reflectarray at 9.6 GHz (elevation cut)

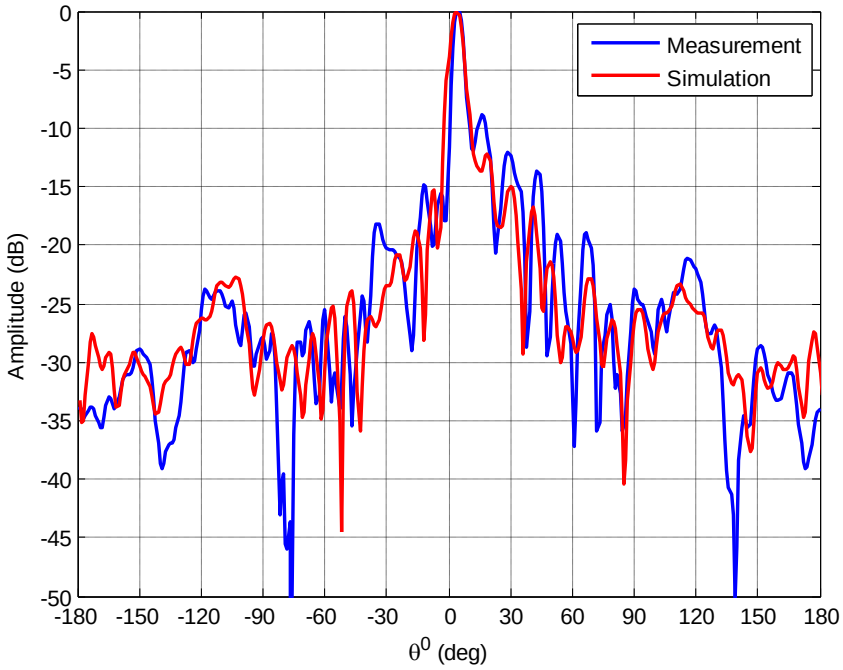

Figure 90 Normalized pattern of simulated and measured reflectarray at 9.7 GHz (azimuth cut)

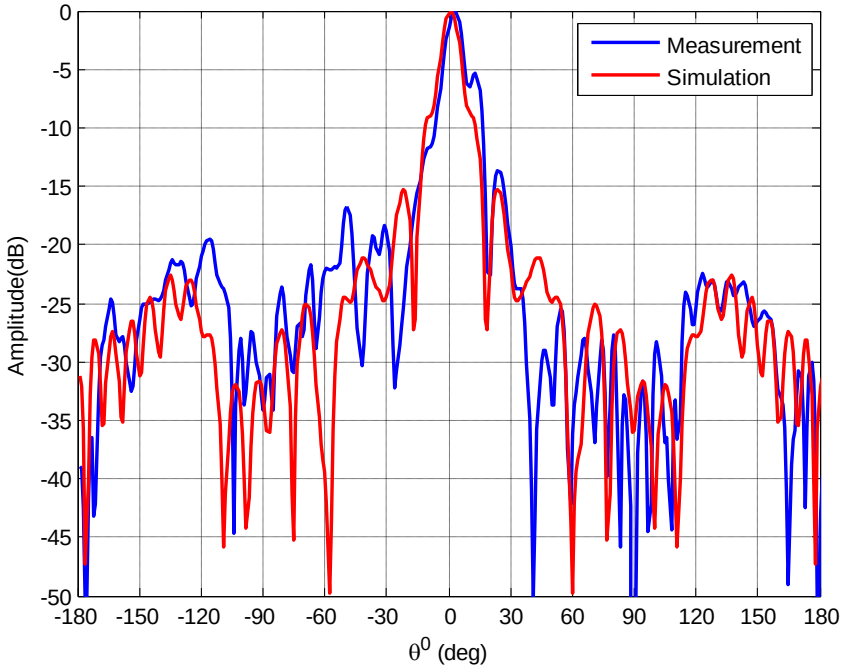

Figure 91 Normalized pattern of simulated and measured reflectarray at 9.7 GHz (elevation cut)

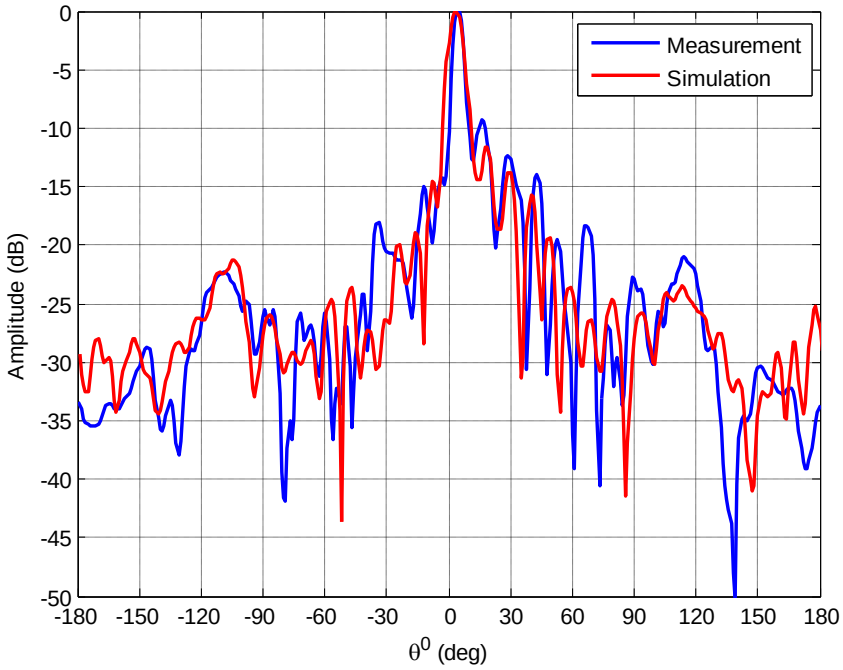

Figure 92 Normalized pattern of simulated and measured reflectarray at 9.8 GHz (azimuth cut)

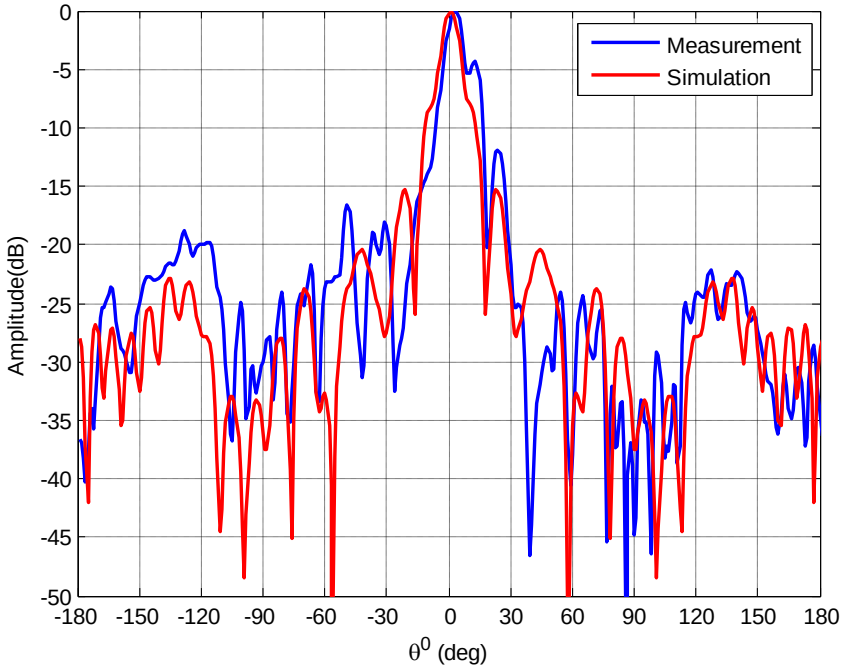

Figure 93 Normalized pattern of simulated and measured reflectarray at 9.8 GHz (elevation cut)

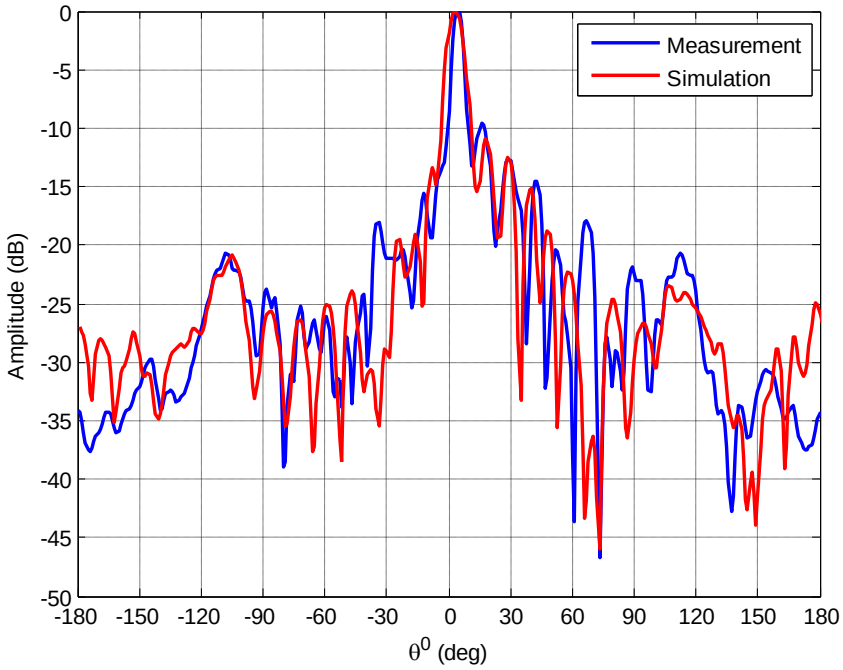

Figure 94 Normalized pattern of simulated and measured reflectarray at 9.9 GHz (azimuth cut)

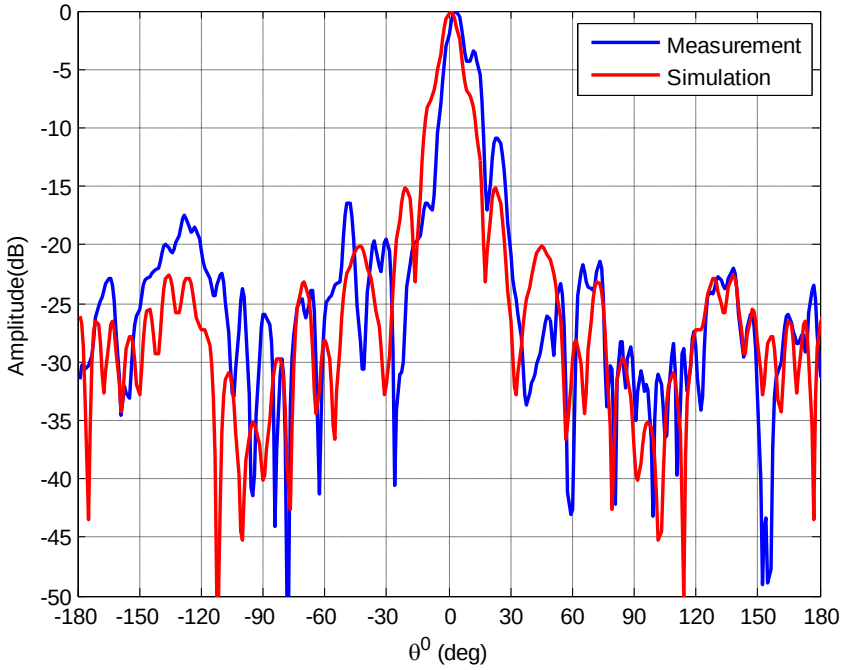

Figure 95 Normalized pattern of simulated and measured reflectarray at 9.9 GHz (elevation cut)

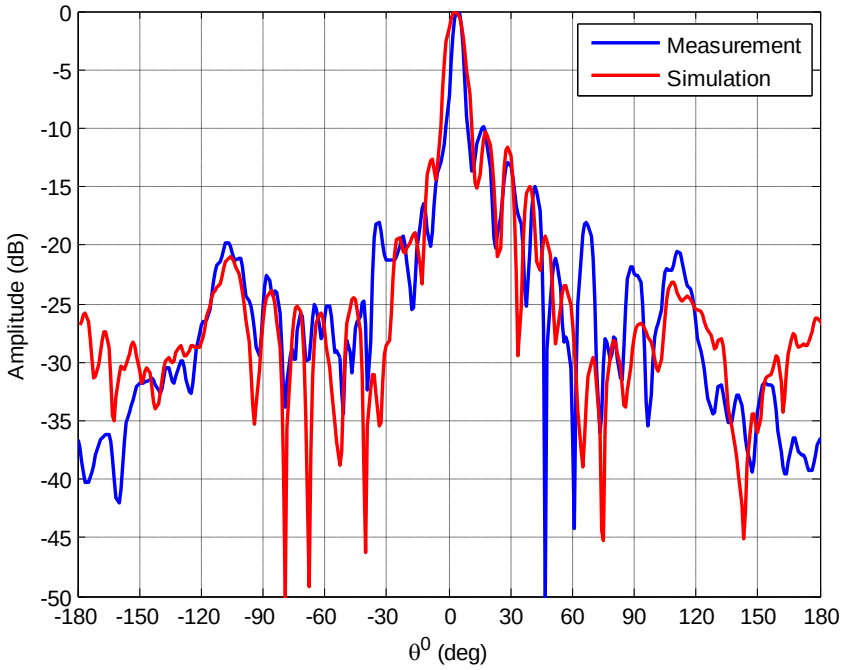

Figure 96 Normalized pattern of simulated and measured reflectarray at 10 GHz (azimuth cut)

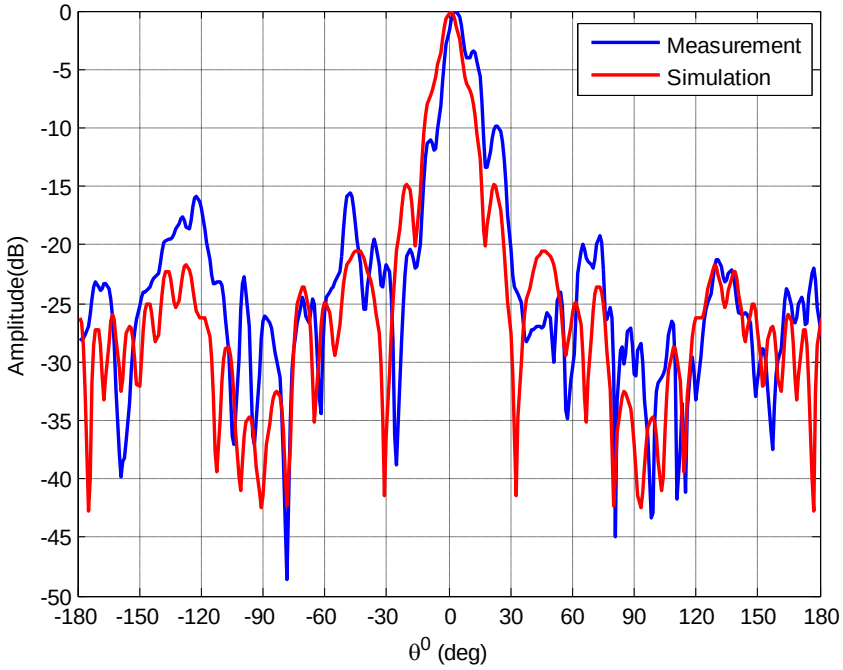

Figure 97 Normalized pattern of simulated and measured reflectarray at 10 GHz (elevation cut)

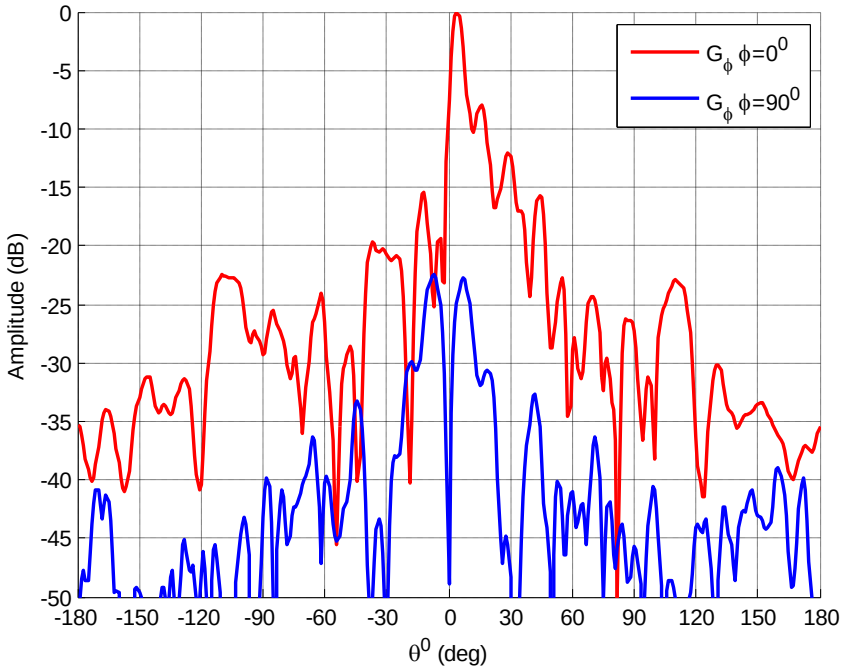

Figure 98 Cross polarization level of measured reflectarray at 9.2 GHz (azimuth cut)

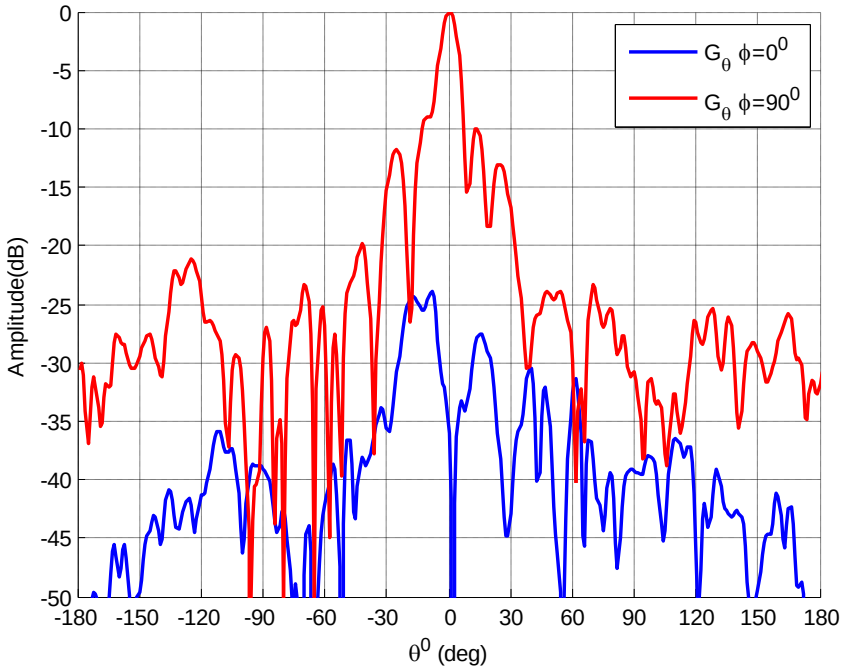

Figure 99 Cross polarization level of measured reflectarray at 9.2 GHz (azimuth cut)

Gain values of the reflectarray are given in Table 21.

Table 21 Gain of the reflectarray

Frequency (GHz)	Gain (dB, Measurement)	Gain (dB, Simulation)
8.6	20.77	22.9
8.7	21.5	23.4
8.8	22	23.8
8.9	22.4	24.1
9	22.8	24.3
9.1	22.4	24.4
9.2	22.3	24.6
9.3	22.5	24.8
9.4	22.6	24.9
9.5	21.9	24.9
9.6	21.3	24.6
9.7	21.2	24.2

In general, there is a good agreement between simulation and measurement results in azimuth cut; maximum of 5 dB amplitude difference can be seen between simulated and measured data in entire band. In elevation cut, measured radiation patterns are not symmetric. This is because of asymmetrical feed support structure. This part is not included in simulations so simulation results are symmetrical. In first configuration, feed supporting structure is as shown in Figure 63 - Figure 65. There is a notch seen in 22° in azimuth cut in measurements. Then, this configuration is simulated (including the feed supporting structure) same notch is seen in exactly in the same place. Thus, this structure is taken backwards about 15 cm and covered with absorber, shown in Figure 101. In the next measurements, this notch is disappeared as given in Figure 66-Figure 97.

Radiation patterns of sector -10 to 40 degrees are plotted to concentrate on the coseqant square part. Measurement and simulation results for the azimuth cut are compared in Figure 100 for verification purposes. It should be noted that

the cosecant square region is between 3° and 33°. When this region is examined, a good agreement is observed.

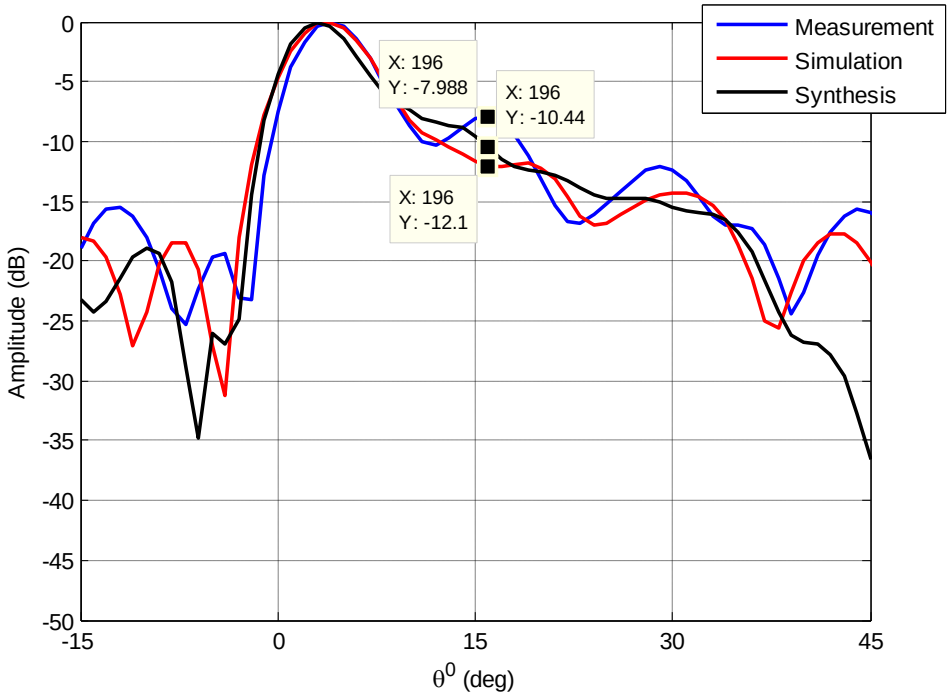

Figure 100 Normalized pattern of simulated and measured reflectarray at 9.2 GHz (azimuth cut)

Compared with the performance of wideband reflectarrays in literature [1]-[4], better performance is achieved with presented reflectarray. Thus, 8.6 – 9.7 Ghz band is seemed suitable to define bandwidth, and in percentage the bandwidth is nearly %12. Due to mutual coupling of the elements in the realized reflectarray, phase distribution on the reflectarray surface can be different than the required one. Thus, after synthesis procedure, dimensions of each stacked patch should be optimized to achieve the synthesized phase distribution. To achieve this, near field diagnostic tools can be combined with optimization algorithms. As an initial step, we try to determine the phase distribution of the reflected fields on the reflectarray surface by the simulations of full reflectarray. Similar study has been performed for single layer patch array in

[38]. However, the simulation results showed that this procedure appears to be not applicable for stacked patch configuration. This point is left as a future work.

Cross polarization levels for the array is lower than -25 dB in azimuth cut and -50 dB in elevation cut. These levels are given only for center frequency because those levels are not challenging.

For wideband operation, multifrequency phase only pattern synthesis tools should be used [36,37].

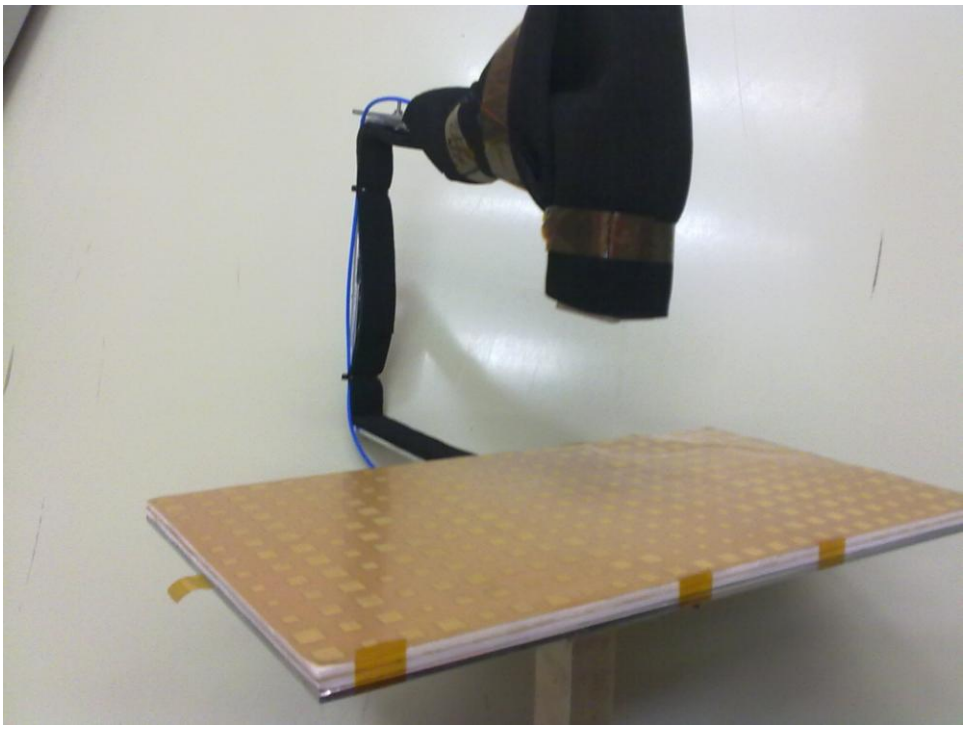

Figure 101 Modified and measured reflectarray configuration

CHAPTER V

CONCLUSION

In this thesis, X-band shaped beam reflectarray consisting of stacked patch elements with variable size patch as a phase shift mechanism is studied. Such reflectarrays can be used in space applications where contour beam and shaped beam are required for a substitute of conventional reflector antennas.

A 25 x 13 element reflectarray with cosecant square beam in azimuth and pencil beam in elevation is designed, manufactured and measured in this study. To design the reflectarray, first, appropriate unit cell dimensions are chosen with parametric study. Infinite array approach is used in the simulations and the phase design curve is obtained. Then, a feed horn in X-band is designed, manufactured and measured. In the next step, amplitude values of the radiated field on each element are determined and spatial phase delay caused by the feed is calculated for all elements. Amplitude values of the electric fields caused by horn illumination are input in a MATLAB code [37]. Phase only synthesis method is applied in the code. Reflection phases of each element are obtained under the assumption of plane wave is incident on each element. With the spatial phase delay and the reflection phase values on each element, phase compensation is presented. Using the compensated phases and phase design curve, patch dimensions are determined and the designed reflectarray is simulated. Besides, a fixed rotated pencil beam reflectarray is designed to investigate the effect of frequency change over radiation pattern. ±2.5° of beam squint is observed and it is concluded that the designed reflectarray is suitable for wideband applications. Designed shaped beam reflectarray is manufactured and the results are compared with simulations in 8.5 - 10 GHz band.

Differences in amplitudes are observed but considering the phase diversion caused by different frequencies, these effects are treated as acceptable. So a microstrip patch array with more than %10 bandwidth (8.6 – 9.7 GHz) is achieved compared with other shaped beam reflectarrays in the literature. Low cross polarization level is expected in unit cell simulations and below -22 dB X_{pol} level is achieved.

In the future, multifrequency phase only synthesis tools will be studied to achieve wideband operation. Also this synthesis will be adopted for 2D array synthesis.

REFERENCES

1. M. Arrebola, J. A. Encinar and M. Barba, “Multifed Printed reflectarray with three simultaneous shaped beams for LMDS central station antenna,” *IEEE Trans. Antennas Propagat.*, Vol. 56, No. 6, pp. 1518-1527, Jun. 2008.

2. E. Carrasco, M. Arrebola, J. A. Encinar and M. Barba, “Demonstration of a shaped beam reflectarray using aperture-coupled delay lines for LMDS central station antenna,” *IEEE Trans. Antennas Propagat.*, Vol. 56, No. 10, pp. 3103-3111, Oct. 2008.

3. A. Zeitler, *et al.*, “Folded Reflectarrays with shaped pattern for foreign object debris detection on runways,” *IEEE Trans. Antennas Propagat.*, Vol. 58, No. 9, pp. 3065-3068, Sep. 2010.

4. J. A. Zornoza , R. Leberer, J.A. Encinar and W.Menzel, “Folded multilayer microstrip reflectarray with shaped pattern,” *IEEE Trans. Antennas Propagat.*, Vol. 54, pp. 510-518, Feb. 2006.

5. J. A. Encinar , J. A. Zornoza, “Three-layer printed reflectarrays for contoured beam space applications,” *IEEE Trans. Antennas Propag.*, Vol. 52, pp. 1138-1148, May 2004.

6. D. M. Pozar, “A Shaped beam microstrip patch reflectarray,” *IEEE Trans. Antennas Propagat.*, Vol. 47, No. 7, pp. 1167-1173, Jul. 1999.

7. J. A. Encinar, *et. al.*, “Dual-polarization dual-coverage reflectarray for space applications,” *IEEE Trans. Antennas Propagat.*, Vol. 54, No. 10, pp. 2827-2837, Oct. 2006.

8. J. Huang, J. A. Encinar, *Reflectarray Antennas*. John Wiley & Sons, Inc., USA, 2008.

9. J. A. Encinar and J. A. Zornoza,”Broadband design of three-layer printed reflectarrays,” *IEEE Trans. Antennas Propagat.*, Vol. 51, No. 7, pp. 1662-1664, Jul. 2003.

10. D. M. Pozar and T. A. Metzler,”Analysis of a reflectarray antenna using microstrip patches of variable size,” Electron. Lett., Vol. 29, No. 8, pp. 657-658, Apr. 1993.

11. D. Berry, R. G. Malech and W. A. Kennedy, "The reflectarray antenna," *IEEE Trans. Antennas Propagat.*, Vol. AP-11, pp. 645-651, Nov. 1963.

12. J. Huang and A. Feria, “Inflatable microstrip reflectarray antennas at X and Ka-band frequencies,” *IEEE AP-S Symposium*, Orlando, Florida, pp. 1670-1673, Jul. 1999.

13. H. R. Phelan, “Spiralphase reflectarray for multi target radar,” *Microwave Journal*, Vol. 20, pp.67-73, Jul. 1977.

14. C. S. Malagisi, “Microstrip disc element reflect array,” Electronics and Aerospace Systems Convention, pp. 186-192, Sep. 1978.

15. J. Huang, “Bandwidth study of microstrip reflectarray and a novel phased reflectarray concept,” *IEEE AP-S/URSI symposium*, Newport Beach, California, pp. 582-585, Jun. 1995.

16. J. Huang and R. J. Pogorzelski, ”Microstrip reflectarray elements having variable rotation angles,” *IEEE Symposium*, Vol. 2, pp. 1280-1283, Jul. 1997.

17. B. Strassner, C. Han and K. Chang, “circularly polarized reflectarray with microstrip ring elements having variable rotation angles”, *IEEE Trans. Antennas Propagat.*, Vol. 52, No. 4, pp. 1122-1125, Apr. 2004.

18. R. E. Munson and H. Haddad, “Microstrip reflectarray for satellite communication and RCS enhancement and reduction,” U.S. patent 4,684,952, Washington, D. C., Aug. 1987.

19. J. Huang, ”Microstrip reflectarray,” *IEEE AP-S/URSI symposium*, London, Canada, pp. 612-615, Jun. 1991.

20. E. Carrasco, M. Barba and J. A. Encinar, “Reflectarray element based on aperture-coupled patches with slots and lines of variable length,” *IEEE Trans. Antennas Propagat.*, Vol. 53, No. 3, pp. 820-825, Mar. 2007.

21. D. M. Pozar and T. A. Metzler, “Analysis of a reflectarray antenna using microstrip patches of variable size,” *Electronics Letters*, pp. 657-658, Apr. 1993.

22. A. Kelkar, “FLAPS: conformal phased reflecting surfaces,” *Proc. IEEE National Radar Conf.*, Los Angeles, California, pp. 58-62, Mar. 1991.

23. Y. T. Gao and S. K. Barton, “Phase correcting zonal reflector incorporating rings,” *IEEE Trans. Antennas Propagat.*, Vol. 43, pp. 350-355, Apr. 1995.

24. F. C. E. Tsai and M. E. Bialkowski, “Designinng a 161-element Ku-band microstrip reflectarray of variable size patches using an equivalent

unit cell waveguide approach," *IEEE Trans. Antennas Propagat.*, Vol. 51, No. 10, pp. 2953-2962, Oct. 2003.

25. J. A. Encinar,"Design of two-layer printed reflectarray using patches of variable size," *IEEE Trans. Antennas Propagat.*, Vol. 49, pp. 1403-1410, Oct. 2001.

26. O. Bayraktar, "Beam Switching Reflectarray with RF MEMS Technology," MS., Institute of Natural Sciences, Middle East Technical University, Ankara, 2007.

27. M. R. Chaharmir, J. Shaker, M. Cuhaci, and A. Ittipiboon, "Broadband reflectarray antenna with double cross loops," *Electronic Letters*, Volume 42, Issue 2, pp. 65-66, Jan. 2006.

28. L. Li, et al., "Novel broadband planar reflectarray with parasitic dipoles for wireless communicarion applications," *IEEE Antennas and Wireless Propagat. Letters*, Vol. 8, pp. 881-885, 2009.

29. H. Hasani, M. Kamyab and A. Mirkamali, "Broadband reflectarray antenna incorporating disk elements with attached phase-delay lines," *IEEE Antennas and Wireless Propagat. Letters*, Vol. 9, pp. 156-158, 2010.

30. Ansoft HFSS®, accessed 20 October 2011, <http://www.ansoft.com/products/hf/hfss/>.

31. K. S. Yee, "Numerical solution of initial boundary value problems involving Maxwell's equations in isotropic media," *IEEE Trans. Antennas Propagat.*, Vol. AP-14, pp. 302-307, May 2003.

32. F. C. E. Tsai and M. Bialkowski, "Designing a 161-Element Ku-band microstrip reflectarray of variable Size patches using an equivalent unit cell waveguide approach," *IEEE Trans. Antennas Propagat.*, Vol. 51, pp. 2953-2962, Oct. 2003.

33. M. Bozzi, S. Germani and L. Perregrini, "Performance comparison of different element shapes used in printed reflectarrays," *IEEE Antennas and Wireless Propagat. Letters*, Vol. 2, pp. 219-222, 2003.

34. M. E. Bialkowski, K. H. Sayidmarie, "Investigations into phase characteristics of a single-layer reflectarray employing patch or ring elements of variable size," *IEEE Trans. Antennas Propagat.*, Vol. 56, pp. 3366-3372, Nov. 2008.

35. C. A. Balanis, *Antenna Theory*. John Wiley & Sons, Inc., Hoboken, NJ, 2005.

36. E. Ercil, "A new approach to phase only synthesis method in phased array antennas," *URSI National Conference*, 2010.

37. E. Yıldırım, "Beam synthesis by genetic algorithm code", Aselsan Inc., 2011.

38. H. Rajagopalan, Y. Rahmat-Samii, "Reflectarray antennas: an intuitive explanation of reflective phase behaviour," *General Assembly and Scientific Symposium XXXth URSI*, Aug. 2011

APPENDIX-1

Single Layer Unit Cell Parametric Study

In order to make comparison between single layer and multi layer unit cells, parametric study of single layer unit cell is done. This unit cell has 16 mm x 16 mm length and width, same with two layer structure, patch is square, but 4 mm thick foam is used, which is the half height of the stacked patch structure. Patch dimension is swept from 6 mm to 15.5 mm with 0.5 mm steps. Periodic boundary conditions and infinite array approach are used in the simulations. Magnitude and phase responses of the unit cell are shown in Figure-Appx 1 and Figure-Appx 2 respectively.

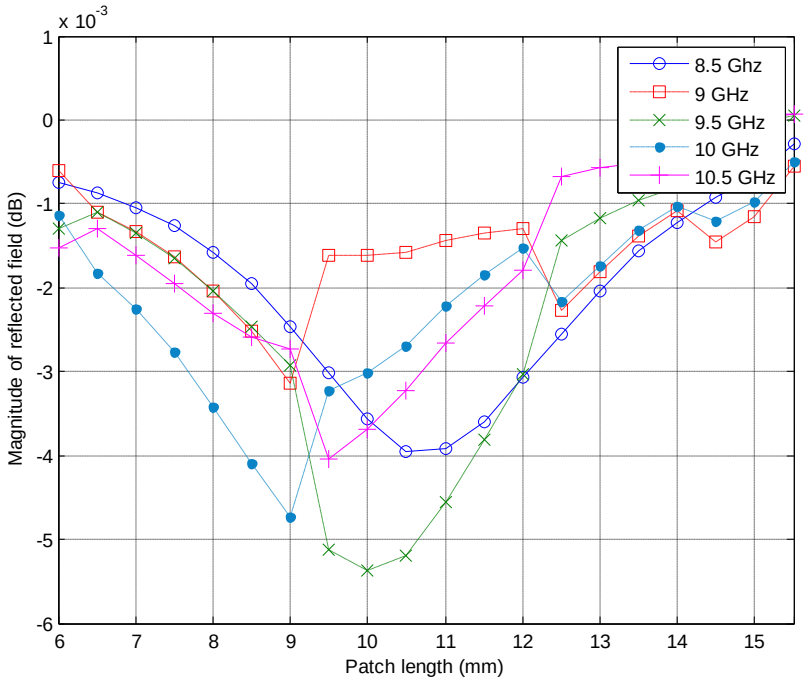

Figure-Appx 1 Magnitude of reflecting field in single layer unit cell (normal incidence)

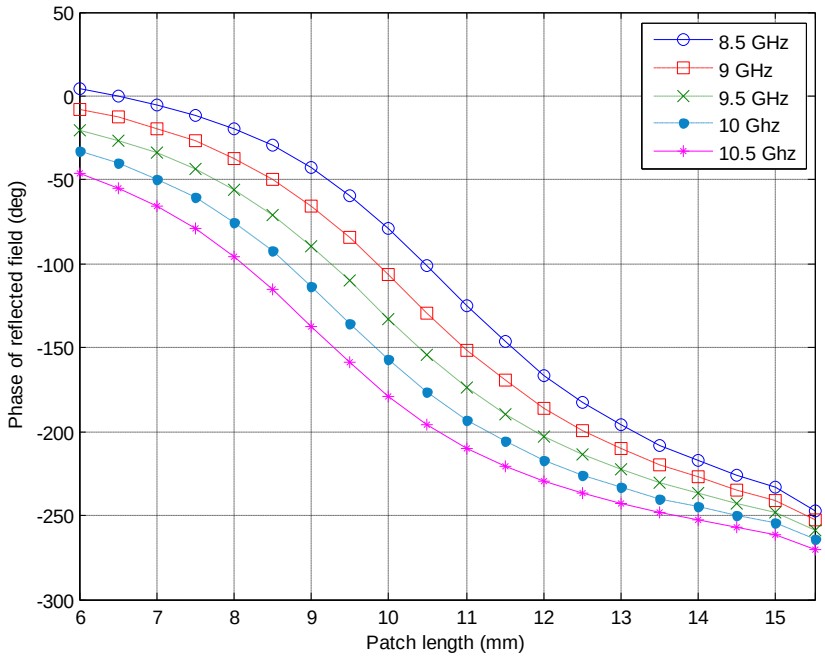

Figure-Appx 2 Phase of reflecting field in single layer unit cell (normal incidence)

Performance parameters are defined [33] to compare the performances of different element shapes in reflectarrays. These parameters are briefly discussed in chapter 2 and are used for evaluating the performance of the unit cell in each of the parametric study step. Here, performance parameters for single layer substrates with the same unit cell dimension but with different dielectric height are discussed. Sensitivity and maximum range of reflection phase values are shown in Figure-Appx 3 and Figure-Appx 4 respectively. With increasing the dielectric height, R is decreasing, as in Figure-Appx 3. From Figure-Appx 4, it is concluded that increase in dielectric height results decrease in sensitivity.

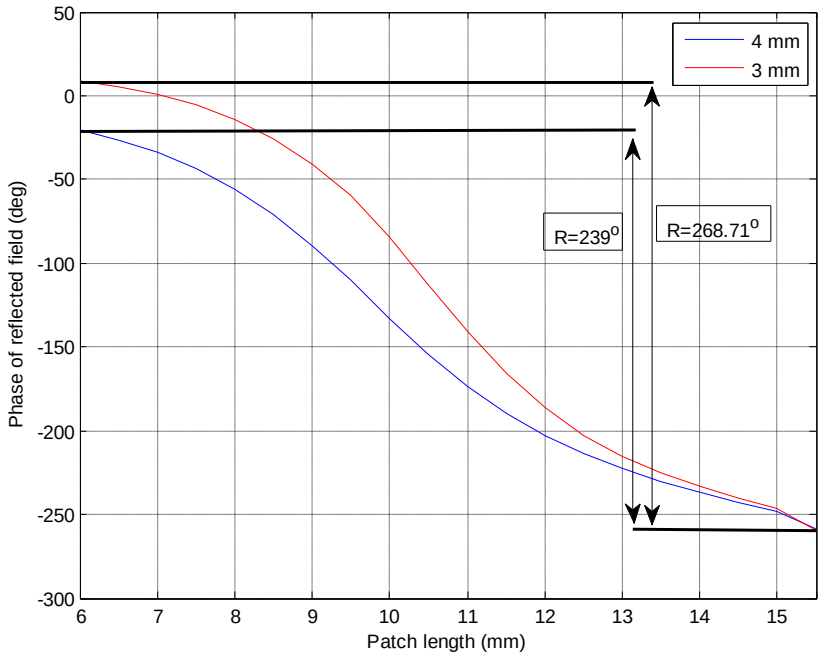

Figure-Appx 3 Effect of thickness over maximum range of the reflection phase in single layer configuration at 9.5 GHz (normal incidence)

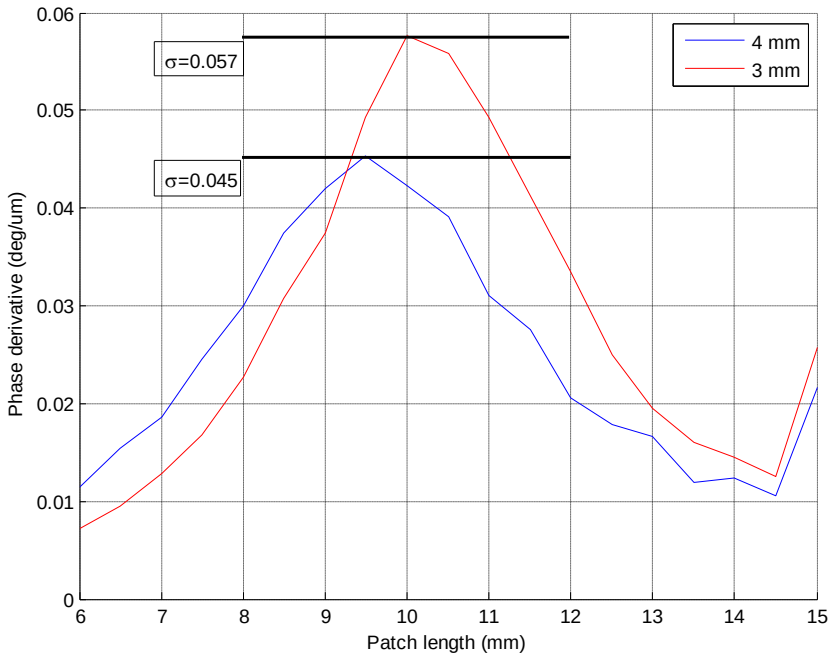

Figure-Appx 4 Effect of thickness over sensitivity in single layer configuration at 9.5 GHz (normal incidence)

Figure-Appx 5 and Figure-Appx 6 presents the bandwidth of single layer unit cell structures with 4mm and 3mm substrate heights respectively. Comparisons are made assuming 9.5 GHz is the center frequency. In both graphs, phase differences between center frequency and 8.5 GHz and 10.5 GHz are shown. Phase difference values are higher in Figure-Appx 6 compared to Figure-Appx 5, so that it can be concluded that bandwidth of unit cell with 4mm substrate is wider than the unit cell with 3mm substrate. This is because, threshold value (in this study, 45° is assumed) is closer to the phase differences of unit cell with 4mm dielectric thickness. In other words, f_1 value is closer to 8.5 GHz and f_2 value is closer to 10.5 GHz in first case compared with the second.

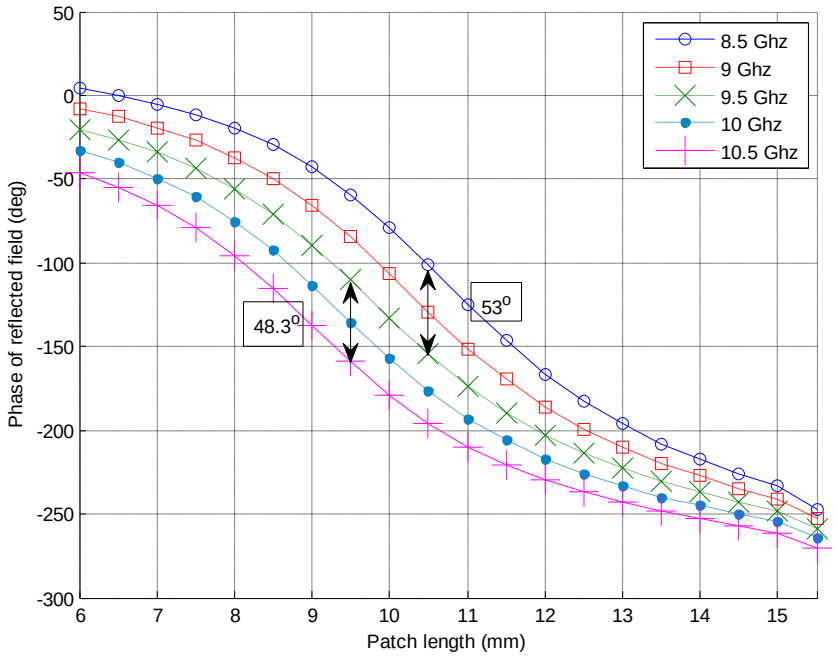

Figure-Appx 5 Bandwidth of a single layer unit cell with 4 mm dielectric thickness at 8.5-10.5 GHz band (normal incidence)

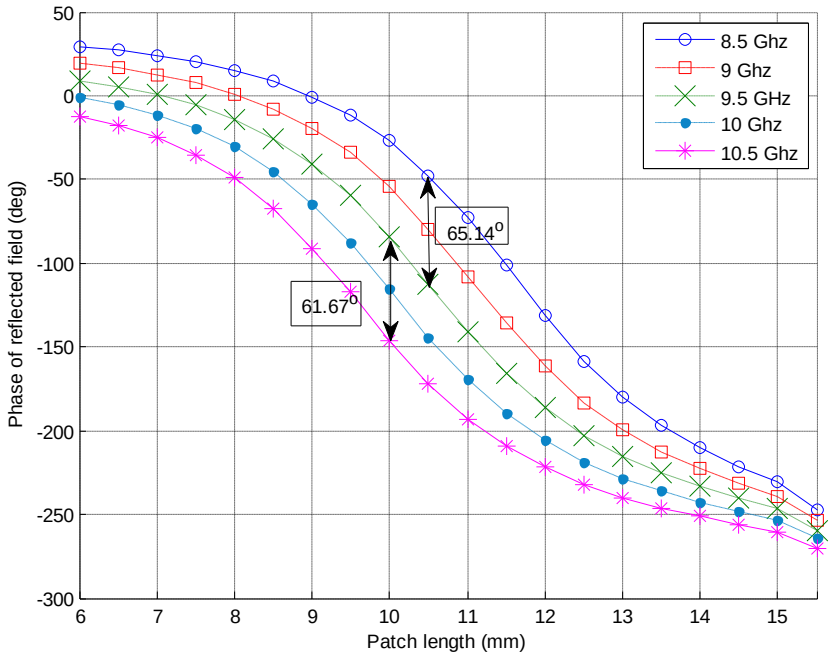

Figure-Appx 6 Bandwidth of a single layer unit cell with 3 mm dielectric thickness at 8.5-10.5 GHz band (normal incidence)